

Instituto Tecnológico y de Estudios Superiores de Monterrey

Campus Monterrey

School of Engineering and Sciences



Wavelets for Spindle Fault Diagnosis in High Speed Machining

A thesis presented by

George Francisco Batallas Moncayo

Submitted to the

School of Engineering and Sciences

in partial fulfillment of the requirements for the degree of

Master of Science

In

Manufacturing Systems

Monterrey, Nuevo León, December 4th 2017

Instituto Tecnológico y de Estudios Superiores de Monterrey

Campus Monterrey

School of Engineering and Sciences

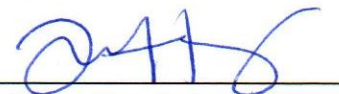
The committee members, hereby, certify that have read the dissertation presented by George Francisco Batallas Moncayo and that it is fully adequate in scope and quality as a partial requirement for the degree of Master of Science in Manufacturing Systems.



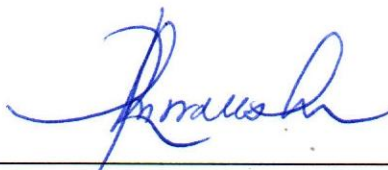
Dr. Rubén Morales Menéndez
Tecnológico de Monterrey
Advisor



Dr. Antonio Jr. Vallejo Guevara
Tecnológico de Monterrey
Committee Member



Dra. Diana Hernández Alcántara
Universidad de Monterrey
Committee Member



Dr. Rubén Morales Menéndez
Dean of Graduate Studies
School of Engineering and Sciences

Monterrey, Nuevo León, December 4th 2017

Declaration of Authorship

I, George Francisco Batallas Moncayo, declare that this dissertation titled, *Wavelets for Spindle Fault Diagnosis in High Speed Machining* and the work presented in it are my own. I confirm that:

- This work was done wholly or mainly while in candidature for a research degree at this University.
- Where any part of this dissertation has previously been submitted for a degree or any other qualification at this University or any other institution, this has been clearly stated.
- Where I have consulted the published work of others, this is always clearly attributed.
- Where I have quoted from the work of others, the source is always given. With the exception of such quotations, this dissertation is entirely my own work.
- I have acknowledged all main sources of help.
- Where the dissertation is based on work done by myself jointly with others, I have made clear exactly what was done by others and what I have contributed myself. Notwithstanding, there are three sections we made together in partnership with my fellow student *Silvia Cristina Villagómez Garzón*. So, long paragraphs belong to us and we notice they will be used in both dissertations. These sections are: The introductory text in Chapter 1, the Table 2.1 and the proposed methodology.



George Francisco Batallas Moncayo
Monterrey, Nuevo León,
December 4th 2017

@2017 by George Francisco Batallas Moncayo
All rights reserved

Dedication

Este trabajo lo dedico principalmente a mi familia, por haberme enseñado a ser una mejor persona día tras día, por todas las alegrías y por cuidarme a pesar de la distancia.

A mi padre, por enseñarnos a mi y a mis hermanos a ser campeones e inculcarme desde pequeño que con esfuerzo todo se puede.

A mi madre, que por medio de su amor, paciencia y ternura ha convertido todos los momentos negativos en oportunidades de reflexión.

A mis hermanos, con quienes he compartido los momentos mas grandiosos de mi vida y que han sido la base principal de mi fortaleza.

A mi sobrina, quien me impulsa a salir adelante y seguir cambiando este mundo para hacerlo mejor para ella.

A mis amigos que me han llenado de risas y experiencias, por enseñarme que la amistad no conoce fronteras, los llevaré muy dentro de mi corazón.

Finalmente, dedico a Dios y a la Virgen María por las oportunidades que me han brindado y las diversas lecciones de vida que me han permitido llegar a este punto tan importante de mi formación profesional.

Acknowledgements

I thank to *Tecnológico de Monterrey* for giving me an important scholarship during my studies, in particular to the Automotive Consortium research group. Thanks to CONACyT for the financial support which contributed to continue my studies without any inconvenience.

I would like to thanks to my thesis advisor, Dr. Rubén Morales Menéndez for his important suggestions, remarkable willingness to help and its patience. His support has been important to achieve this work and the papers derived from this thesis.

In a very special way, I wish to express my deepest thanks to my committee members Dr. Diana Hernández Alcántara for her significant advices and Dr. Antonio Jr. Vallejo for his insightful comments to complete this thesis.

I want to thank to my colleague Cristina Villagómez for her support and her friendship that made this work educational and rewarding.

I would like to express my deepest gratitude to the Mexican people for sharing with me their history, their culture and their gastronomy, México will always be my second home.

Agradezco al *Tecnológico de Monterrey* por brindarme una importante beca durante mis estudios, en particular al grupo de investigación del Consorcio Automotriz. Gracias al CONACyT por el apoyo financiero que me permitió continuar mis estudios sin ningún inconveniente.

Me gustaría agradecer a mi asesor de tesis, Dr. Rubén Morales Menéndez por sus importantes sugerencias, notable disposición para ayudarme y su valiosa paciencia. Su apoyo ha sido importante para lograr este trabajo y los artículos derivados de la misma.

De manera muy especial, deseo expresar mi más profundo agradecimiento a los miembros de mi comité de tesis: la Dra. Diana Hernández Alcántara por sus importantes consejos y al Dr. Antonio Jr. Vallejo por sus profundos comentarios para completar esta tesis.

Quiero agradecer a mi compañera Cristina Villagómez por su apoyo y su amistad que hicieron que este trabajo fuera educativo y gratificante.

Quiero expresar mi más profundo agradecimiento al pueblo mexicano por compartir conmigo su historia, su cultura y su gastronomía, México siempre será mi segundo hogar.

Wavelets for Spindle Fault Diagnosis in High Speed Machining

By

George Francisco Batallas Moncayo

Abstract

The spindle of machining centers must provide high rotational speed, transfer torque and power to the cutting tool during continuous periods of time. The constant forces generate faults in its components where the most important are the shaft and bearings. As the fault increases, it affects other components and may lead to a catastrophic damage and a production stoppage.

The maintenance strategies have been evolving in order to prevent irreversible damages. Over the last years, great progress has been made in the condition-based maintenance, particularly in the vibration analysis, where the vibration signature can be associated with the fault.

In recent years, several signal processing techniques have been introduced to extract the features from vibration signals. The *WT* has caught the attention of the scientific community by its characteristics and its limitless number of wavelets. In this thesis a methodology based on the *WT* is proposed to detect faults in spindle. The approach is capable of extracting the bearing characteristic frequencies related to the fault from the resonance frequency and the low frequencies information associated with shaft faults.

The implemented method contemplates the latest advances in the literature to detect robustly the type of the fault, it is focused on industrial environment where the faults are usually tainted by noise from other machines or by errors in the acquisition. The method is applied to different types of bearing faults to demonstrate its effectiveness and robustness when detecting faults at early stages.

In the three studied cases the proposed methodology got several properties; for the *CWRU* signals the characteristic fault frequency peak got an increase from 6 to 32% compared with the traditional methods; when the signal is tainted by *Gaussian* noise, the method works more effectively, since in these cases the increase percentage reaches up to 57%. Similarly, in the *IMS* database the characteristic frequency peak increases from 6 to 70%. Finally, in the machining center database there was not an increment but the method acts as filter which eliminates the undesired frequencies.

Experimental results indicate the proposed approach is reliable to detect bearing and shaft faults. It also has a superior diagnosis performance compared to traditional methods in extracting fault features. The method removes most of the noise and can be used in future works as preprocessor.

Contents

1	Introduction	3
1.1	Motivation	4
1.2	Problem Description	5
1.3	Research Question	6
1.4	Solution Overview	6
1.5	Main Contribution	7
1.6	Disertation	7
2	State of the Art	9
2.1	Research on bearings faults using wavelets	9
2.2	Research on unbalance using wavelets	12
2.3	Theoretical Background	16
2.3.1	Wavelet Transform	16
2.3.2	Rolling element bearings	18
2.3.3	Shaft	19
3	Theoretical Proposal	21
3.1	Proposed Methodology	21
4	Experimental System	31
4.1	Case studies	31
4.1.1	CWRU Bearing Data Center	31
4.1.2	<i>IMS</i> Bearing Data	32
4.1.3	GROB 550 recorded data	33
5	Results	35
5.1	Introduction	35
5.2	Method Results	35
5.2.1	Shaft faults: GROB 550 data set	35
5.2.2	Bearing Faults case 1: <i>IMS</i> dataset	35

5.2.3	Bearing Faults case 2: <i>CWRU</i> database	38
5.3	Discussions	40
5.3.1	Shaft faults: GROB 550 data set	40
5.3.2	Bearing Faults (case 1: <i>IMS</i> database)	40
5.3.3	Bearing Faults (case 2: <i>CWRU</i> database)	42
5.4	Comparison	43
5.4.1	Shaft faults: GROB 550 data set	43
5.4.2	Bearing Faults case 1: <i>IMS</i> Dataset	43
5.4.3	Bearing Faults case 2: <i>CWRU</i> Database	46
6	Conclusions	49
6.1	Summary	49
6.2	Contributions	50
6.3	Publications	50
6.4	Future Work	51
	Bibliography	53
A	Acronyms Definition	57
B	IMS Data selection	59
B.1	Identification and categorization of the bearing faults	60
B.2	Initial considerations	61
C	Parameters Selection	65
C.1	Wavelet Transform	65
C.1.1	Computing time	66
C.1.2	Frequency Resolution	66
C.2	Statistical method	69
C.3	Threshold	75
D	Additional Results	85
D.1	<i>IMS</i> Data	86
D.2	<i>CWRU</i> Data	89
E	Published papers	93
F	Developed Programs	97
	Curriculum Vitae	103

List of Figures

2.1	Third level decomposition using <i>DWT</i>	17
2.2	Third level decomposition using <i>WPT</i>	17
3.1	Methodology flowchart	22
3.2	Signal pre-processing	23
3.3	Best Tree	24
3.4	Time domain and FFT of the signal	24
3.5	Shaft faults	25
3.6	Generation of the <i>KR</i> employing wavelet coefficients	27
3.7	Threshold application for <i>KR</i> indicator	28
3.8	Hilbert envelope applied to a signal with 50 Hz and 1,000 Hz	28
3.9	Bearing faults behavior in the frequency spectrum	29
4.1	CWRU Bearing test rig.	32
4.2	<i>IMS</i> bearing test rig.	33
4.3	<i>GROB 550</i> acquisition system	33
5.1	<i>GROB</i> signals after the application of the proposed methodology	36
5.2	<i>IMS</i> signals after the application of the proposed methodology showing sidebands and shaft speed harmonics	37
5.3	<i>IMS</i> signals after the application of the proposed methodology	38
5.4	<i>CWRU</i> signals after the application of the proposed methodology	39
5.5	<i>RE</i> signal with offset removal	41
5.6	Signal with $UB=26.1$	44
5.7	<i>OR</i> fault signal (<i>IMS</i> database)	45
5.8	<i>IR</i> fault signal (<i>IMS</i> database)	45
5.9	<i>IR</i> fault signal (<i>IMS</i> database)	46
5.10	<i>OR</i> fault signal (<i>CWRU</i> database)	46
5.11	<i>IR</i> fault signal (<i>CWRU</i> database)	47
5.12	<i>OR</i> fault signal with <i>SNR</i> (<i>CWRU</i> database)	47
5.13	<i>OR</i> fault and $SNR=1$ (<i>CWRU</i> database)	48

6.1	Comparison of the characteristic fault frequency amplitude between the proposed Methodology and the enveloped- <i>FFT</i>	50
B.1	<i>Kurtosis</i> values for the bearing with <i>IR</i> at the end of its useful life. a) Channel 5, b) Channel 6	60
B.2	<i>Kurtosis</i> values for the bearing with <i>OR</i> fault at the end of its useful life	60
B.3	<i>Kurtosis</i> values for the bearing with <i>RE</i> fault at the end of its useful life. a) Channel 7, b) Channel 8	61
B.4	Frequency spectrum of the signal envelope of a signal at the beginning of the tests	62
B.5	Considered signals from <i>IMS</i> database	63
C.1	Scale-Frequency relation of the <i>MW db44</i>	67
C.2	Frequency range for each <i>DWT</i> coefficient of a signal sampled at 12,000 Hz	67
C.3	Frequency range for each <i>WPT</i> coefficient of a signal sampled at 12,000 Hz	67
C.4	<i>OR</i> fault decomposition	68
C.5	Frequency spectrum for a noise-free signal with an outer race fault	71
C.6	Statistical parameter applied to an <i>OR</i> fault signal	72
C.7	Statistical parameter applied to an <i>OR</i> fault signal with a <i>SNR</i> = 1 and two sinusoidal signals of 300 Hz and 50 Hz	72
C.8	Comparison of the different indicators	74
C.9	Parameters applied to an <i>OR</i> fault signal	75
C.10	Parameters applied to an <i>IR</i> fault signal	76
C.11	Parameters applied to an <i>RE</i> fault signal	77
C.12	Statistical parameter applied to an <i>OR</i> fault signal with a <i>SNR</i> = 1 and two sinusoidal signals of 300 Hz and 50 Hz	78
C.13	Statistical parameter applied to an <i>IR</i> fault signal with a <i>SNR</i> = 1 and two sinusoidal signals of 300 Hz and 50 Hz	79
C.14	Statistical parameter applied to an <i>IR</i> fault signal with a <i>SNR</i> = 1 and two sinusoidal signals of 300 Hz and 50 Hz	80
C.15	Execution time of the different indicators	81
C.16	Different thresholds applied to <i>OR</i> signal decomposition at 6 th level	81
C.17	Relation energy-node with different thresholds	82
D.1	Harmonics and sidebands location in an <i>IMS</i> signal with <i>RE</i> fault	85
D.2	Harmonics and sidebands hidden in an <i>IMS</i> signal with <i>RE</i> fault	86
F.1	<i>WPT</i> 2D scalogram function	98
F.2	<i>WPT</i> 3D scalogram function	98

List of Tables

2.1	Comparison between some machining researches using <i>WT</i> approach	13
4.1	<i>CWRU</i> Bearing Defect frequencies (multiple of running speed in Hz)	32
4.2	<i>IMS</i> Bearing defect frequencies (multiple of running speed in Hz)	33
4.3	<i>GROB 550</i> Bearing defect frequencies (multiple of running speed in Hz)	34
A.1	Acronyms Definitions	57
B.1	<i>IMS</i> bearing bata structure	59
B.2	Number of the selected tests	61
C.1	Decomposition time of each <i>WT</i>	66
C.2	Index (x) results for several thresholds and different signals	83
C.3	<i>Pareto</i> principle check for the <i>CWRU</i> database with the threshold average.	83

Chapter 1

Introduction

Industrial development and customers demands have increased the need to pursue high-quality products at low cost while ensuring safety during manufacturing. For this reason, machine maintenance strategies have evolved from corrective over preventive to condition-based maintenance, for which real-time fault diagnosis and prognosis are needed [Yan *et al.*, 2014]. Therefore, all efforts must be focused in preventing breakdowns in machines; thus, spindles must be monitored. A failure in the spindle can be catastrophic, leading to costly machine downtime, affecting the productivity in the company.

Rolling element bearings are one of the foremost cause of faults in a machine tool spindle, they are the most critical and vulnerable components in the mechanical transmission. According to statistics, approximately 30% of mechanical failures in rotating machinery are due to the fault of rolling bearings, [Cui *et al.*, 2016]. Hence, the bearing faults diagnosis has been gaining importance due to its detrimental effect on machines reliability.

During bearing operation, localized faults or wear produce successive periodic impacts when rollers pass over the defect and causes wideband impulses. The strength and period of these impulses depend on the shaft speed, the type of fault (location) and the bearing geometry. Vibration signal analysis is one of the most effective techniques for analyzing impulses to detect and diagnostic faults for a successful maintenance program.

Nevertheless, there are several difficulties in signal analysis for fault detection. The foremost problem to deal with are the characteristics of the damage bearing signals, they are nonlinear and non-stationary. Another issue to solve is that the signature of a defective bearing can be undercovered by noise, and low frequency effects; also, as defect frequency is typically small it is not easily noticed. It also needs to be consider that, in an initial stage of wear, the vibration signal shows up distinct peaks in the frequency domain, but after wear develops along the surface, the signal becomes more like random noise and can not be easily detected [Chancey *et al.*, 2002]. A bearing is composed by four components: inner race, outer race, rolling elements and a cage, a fault may occur in any of these components; among other difficulties, the outer race defects are

clear in the spectra, but the inner race and are not easily detected.

To cope with these problems many research have been developed, and a wide variety of techniques have been introduced. Traditional approaches (conventional time domain and frequency domain analysis) are not useful as they tend to average out transient effects. Some defects such as unbalance, eccentricity and bent shaft or bowed rotor can display similar time traces with impulses of similar amplitude and frequency; therefore, defects can not be isolated. Also, the complexity and non-stationary characteristics of signals carrying out with a large amount of noise make bearing faults very difficult to detect with these traditional methods.

Signals have a vast information, but they are often tainted by noise. The ability that signal processing techniques should have is to split close frequencies in real data. Due to the high frequency nature of defect bearings impulses, it is required to handle bearing damage with a high frequency signal analysis.

1.1 Motivation

The automated machining centers work at a constant, uniform and continuous production 24/7 while maintaining the good finish of the piece. The implementation of this type of machines leads to raise the production with the lowest material waste and the higher efficiency.

Among the principal components in a machining center, the spindle is one of the most important, it supports the tools and transmit the rotary motion from the motor to the shaft, as consequence, during the machining process the spindle is exposed to different loads which may produce long-time faults in any of its components. The unexpected breakdown can lead to severe part damage and costly machine downtime, as result the overall production logistic and productivity is affected. Therefore, increasing the useful life of the spindle is one of the principal goals in the manufacturing industry.

There are several logistic solutions to increase the life of a component, the traditional maintenance strategies such as the run-to-break and preventive maintenance are being replaced by the *Condition Based Monitoring (CBM)*. In the run-to-break, the machines work until a fault occurs, this fault can have catastrophic results in the machined part or even in the rest of the components. Preventive maintenance presents a time variable, in which the maintenance of the equipment is carried out at regular intervals, can be handled correctly and the catastrophic failure is reduced, but there are many repairs and there is much component replacement which brings to new equipment costs. The *CBM* also called predictive maintance does not have the problems of the previous ones, but it needs monitoring techniques to predict and calculate the level of damage in the equipment.

The condition monitoring must be online without stopping the production, thus it means the information must be extracted from the exterior avoiding dismantling the machine. There are several methods to achieve this goal, some of them are the oil and vibration analysis. The oil

analysis need some days to obtain results; but with the vibration analysis, it is possible to detect immediately the characteristics of the signal. Additionally, many processing techniques can be applied to extract the desire fault characteristic.

When determining the type of fault that exists inside the spindle, it will be possible to make a particular maintenance to the damaged part, and even it will be possible to know the estimated life time.

1.2 Problem Description

The signal gathered externally in the condition monitoring is often submerged in structural vibrations of the entire machine system, these interfering signals and the background noise make it difficult to detect the faults in spindle. The noise taints the signal and they might have a higher magnitude than the vibration from the faulty component studied. Therefore, the noise can affect the information and can lead to incorrect conclusions.

The problem increases when the detection is desired in early stages of the fault, the amplitude is low and could be weaker than the noise. The signal processing method must be capable of detecting faults in noisy signals; therefore, a proper signal processing method is needed.

Traditional methods have several limitations and new methods evolved in the last decade have presented acceptable results; these new signal processing techniques include: *Short Time Fourier Transform (STFT)*, *Wavelet Transform (WT)*, *Hilbert-Huang Transform (HHT)*, *Wigner-Ville Distribution (WVD)* and *Statistical Signal Analysis (SSA)*.

In the literature, there are several research studies in the detection field which applies these new methods, most of them are only designed to identify some of the defects occurring in the spindle, as a consequence, despite the arduous investigations, the perfect method for detecting the entire set of faults in the machining center with a 100% of efficiency still does not exist. The research in the topic indicates the condition monitoring must detect where the fault occurs and the magnitude of the problem.

As the principal element which fail is the bearing, a crack on any of its components: inner race, outer race, rolling element and cage could decrease the useful life of the spindle. In the case of the shaft, if exist an unbalance or a misalignment not only could cause damage in the rest of the components, but also in the machined piece.

1.3 Research Question

Based on a brief *State-of-the-Art* review, the following hypothesis are proposed:

- i Defects in bearings can be diagnosed using only vibration analysis.
- ii Unbalance and misalignment in the shaft can be diagnosed using only vibration analysis.
- iii Wavelet Transform analysis leads to an efficient transient detection because of its diverse characteristics.
- iv Faults can be diagnosed at early stages despite having a lot of noise.
- v Shaft and bearing faults diagnosis can be implemented in a same methodology.

1.4 Solution Overview

The *WT* has been applied to industrial vibration analysis, it has the benefits of both time and frequency analysis because its window is changeable. In the processing of non-stationary signals, it presents better performance than the traditional *Fourier* analysis, [Kankar *et al.*, 2011]. Additionally, unlike the Fourier transform, *WT* has an infinite set of possible basis functions and it is more efficient dealing with time-frequency analysis even when compared with the *Fast Fourier Transform (FFT)*, [Lauro *et al.*, 2014].

The *WT* decomposes the signal in terms of wavelets, they have some characteristics that differ from a traditional wave. The wavelet is a mathematical oscillation that begins at zero and moves between positive and negative polarity until it returns back to zero, as a consequence it has a finite energy, comparable to the behavior expected in a real shock.

Wavelets are additionally used in denoising, they have the characteristic of denoise a signal in both time and frequency domains simultaneously through the use of certain threshold values called hard and soft thresholding, [Randall, 2011].

There are several types of *WT*, the most used in literature are: the *Continuous Wavelet Transform (CWT)*, the *Discrete Wavelet Transform (DWT)*, the *Wavelet Packet Transform (WPT)* and the *Second Generation Wavelet Transform (SGWT)*, each one of them has been used widely for fault diagnosis of rotary machines; but, there is still no evidence which a method is better than the others.

It is possible to observe the potential advantages of this signal processing method. In this thesis will be used the *WT* to identify the different types of spindle faults at diverse case studies including *High Speed Machining (HSM)*.

1.5 Main Contribution

The proposed technique in this thesis has the following contributions:

- i New methodology for fault diagnosis with a satisfactory effectiveness.
- ii This new method identifies in one single step bearing and shaft defects.
- iii Unbalance, Misalignment, Mechanical Looseness, Outer Race, Inner Race and Rolling Element faults are detected.
- iv The method distinguishes among different levels of unbalance conditions.
- v It detects early stage bearings faults.
- vi The method has good results by reducing environmental noise.

1.6 Disertation

This thesis document is structured as follows:

Chapter 2 presents the *State of the Art* from the first investigations in vibration analysis until the development of the *WT* for machine health diagnosis, while it is presented the evolution of the signal processing methods for condition monitoring. Additionally, an overview for the *WT* theory is also presented, so that the unfamiliar readers gets used to this concept.

Chapter 3 describes the main contribution of this work, it introduces the proposed methodology with a detailed description of each part.

Chapter 4 introduces three case studies used for validate the methodology: the *IMS* database, the bearing dataset recovered from the *CWRU* and the machining center database for *HSM* vibration analysis.

Chapter 5 shows the results by the proposed methodology and compare them with the results obtained by traditional methods.

Chapter 6 presents the conclusions, highlights the obtained contributions, shows published articles during this research work and introduces future works.

Chapter 2

State of the Art

Since 1939, the relation between vibration signals and machine condition has been investigated [Rathbone, 1939]. By 1960 it was recognized that periodic monitoring avoids machine failures, in the next decade *FFT* analyzers were applied on machine vibration; from 1980s the technology of the accelerometers and digital computers improved, obtaining a better performance in the efficiency and effectiveness of the results, [Randall, 2011].

The recent improvements in this field include: small acquisition systems with higher performance, different monitoring techniques, and new processing methods. As the literature indicates a trend in the use of *WT* for detecting machinery faults, the present review of *State of the Art* introduces the diverse investigations in wavelets for both: bearing and shaft faults.

2.1 Research on bearings faults using wavelets

As bearings are the principal reason for rotary machine breakdowns, there are numerous investigations about the vibration signal on its elements. From recent works, there is a trend to improve the effectiveness in fault detection, in the case of the *WT* for bearing fault detection this factor is influenced by some characteristics such as: the mother wavelet, the type of faults and the classifiers.

Most typical faults in bearings are produced by local faults, they may appear in the following elements: *Inner Race (IR)*, *Outer Race (OR)*, *Rolling Element (RE)*, *Cage (C)*.

As the amplitude of the shock depends on the element where occurs the fault, the order for detection stays as follows: *OR*, *IR* and *RE* where the first is the easiest to identify and *RE* fault is the more difficult because of the lower amplitude generated by the fault. [Zhang and Gao, 2004] proved that the *WT* could identify the *OR* and *IR* fault unlike the Fourier transform, which only could identify *OR* faults, later it was expanded to *UB* in the shaft [Zhang *et al.*, 2005]. Finally, [Zhang *et al.*, 2006] got improvements for their method using envelope and analytic wavelet, as result, it was possible to detect *RE* faults.

The effective *Mother Wavelet (MW)* is still unknown, the investigations are divided in computational efficiency and relation between the wavelet and the real vibration. [Rafiee *et al.*, 2010] made a research about the ideal wavelet for gear and bearing diagnosis, this research group examined 324 *MW* concluding that the *Daubechies 44 (db44)* has the most similar shape for bearings and gears; but it is not the proper function for all process because this type of wavelet demands a lot of computational resources.

The use of *Artificial Neural Network (ANN)* has been propagated to automatically detect the type of fault; [Paya *et al.*, 1997] reports results of 96% in detecting *IR* faults using the *CWT* and *ANN* with back propagation.

[Yan and Gao, 2011] also used *ANN* in two study cases, the achieved effectiveness were 96.6% and 91%. According to the author, the best suited wavelet is the *Biorthogonal 5.5*, but they did not present experimental results for this statement. [Pandya *et al.*, 2012] also used *rbio5.5* in his method, which includes energy *Kurtosis* and *ANN*, with these considerations, the results show an efficacy of 93% in the classification of the *IR*, *OR* and *RE* fault damage.

By the other hand, [Chandel and Patel, 2013] concluded that combining the *ANN* and the *WT* with *Daubechies 10 (db10)*, the classifier is capable to obtain results of up to 100%. The study establishes that the *Daubechies MW* have great benefits on accuracy for detecting faults in bearings, and among them, with the *db10* the computational cost can be reduced. In other investigations, the use of the *Markov* models as classifier had made it possible to catalog the *IR*, *OR* and *RE* faults with a 99% of performance [Purushotham *et al.*, 2005].

[Kankar *et al.*, 2011] presented a procedure for bearing fault diagnosis to detect: *IR*, *OR*, *RE* and combined faults using machine learning techniques. The authors analyse different methods to detect which one is better for bearing diagnosis. They concluded that the *Complex Morlet* is the best suited for bearing diagnosis followed by the *Daubechies 44 (db44)*. The use of the *Complex Morlet* and *Support Vector Machine (SVM)* correctly classifies the faults with a 100% performance.

Wavelets have other applications in the field of signal processing one of them is in denoising. Applying a threshold in the decomposed signal eliminates noise. [Cui *et al.*, 2016] proposed a method which first reduces the noise and afterwards processes the signal. The steps are: denoising the vibration signal using wavelet, extract the characteristics in both time and frequency domain; finally it is detected the fault using the *Grey Correlation Method (GCM)*. The results are close to 100% for *IR*, *OR* and *RE* faults.

The *WT* is a reversible transform, which means, after the decomposition, the original signal can be recovered. This property could be applied to all the *WT* such as the *CWT*, *DWT* and *WPT*. Additionally, the same characteristic allows to recovered a signal with the selected wavelet coefficients which allows to remove the not desired peaks on the signal. [Zhu *et al.*, 2009] used this property in their method, the *CWT* is selected to decomposed the original signal into the corresponding scale-space coefficients. Later, the coefficients are processed with a non-parameter test of *Gaussianity*

which detects the transients; finally, the coefficients without important information are removed and the signal is reconstructed, this methodology eliminates the *Gaussian* noise.

[Tse and Leung, 2010] applied the same principle, the signal was decomposed with a *Reassignment Wavelet Transform (RWT)*, an improved method to the traditional *CWT*. Then, in each frequency it is calculated the Kurtosis and *RMS*. The coefficients with the highest *Kurtosis x RMS* value are selected to reconstruct a signal with only the bearing faults.

To achieve a better performance, the scientific community has combined different processing methods in the same signal. [He *et al.*, 2009] fused wavelet filters and sparse shrinkage, the authors explain this method allows to have a better signal with a considerably reduced noise. [Kedadouche *et al.*, 2016a] presented a method that combines *Empirical Wavelet Transform (EWT)* and *Operational Modal Analysis (OMA)* to extract the frequency related to the fault. According to the study, the obtained envelope spectrum from the scheme (*EWT- OMA*) has superior performance than applying only *EWT*.

[Li *et al.*, 2017] analysed a method for bearing fault detection on early stages of failure using *Q Factor Wavelet Transform (QFWT)* and the *Intrinsic Characteristic-scale Decomposition (ICD)*. According to the authors, in both studied cases were obtained good results for detecting *OR* and *IR* faults. Also, they presented the computational time of the method and established that the used *WT* has better and faster results than *EMD*.

[Liu, 2012] shows a method for fault detection in bearings using *Exponential Moving Average (EMA)* filtering for eliminating the noise in the signal, and consequently it is used the *Shannon Wavelet Spectrum (SWS)* to detect the frequency of the fault. The *EMA* generates a threshold, from this point it is selected the upper values and later the denoised signal is processed with a *SWS*.

[Kedadouche *et al.*, 2016b] presented a comparison between the *Ensemble Empirical Mode Decomposition (EEMD)*, the *Empirical Mode Decomposition (EMD)* and the *EWT*. Additionally, it is presented a selection method of the *Intrinsic Mode Function (IMF)* in the *WT*, using the index selection variable. According to the authors, *EWT* can reduce the computational time by 95.96 % as compared with the *EMD* method and 98.91 % compared with the *EEMD* method. Additionally, the *EWT* has shown a better efficacy to decomposed a signal unlike the *EEMD* which overestimates the number of components.

[Law *et al.*, 2012] showed a technique for detecting important information of the signal with the use of *WPT* and *HT*. The method was applied to vibration signals to detect changes depending on the applied force. With the obtained information in the signal analysis, [Khanam *et al.*, 2014] presented a methodology for estimating the size in the *OR* fault using the *Sym5* wavelet. It is presented that the *Sym5* is the best suited for detecting size faults due its wavelet form, that represents the begin and ending of the ball when pass through the fault.

2.2 Research on unbalance using wavelets

Another important component of the spindle is the shaft, this element has the function of transmitting torque and rotation from the rotor to the cutting tool. It is subjected to constant loads and continuous movement, which affect the life of the shaft; Additionally, the wrong use of the machining center, such as an incorrect programming may generate cracks on it. The waviness caused by shaft misalignment or knocking in the process cause damage in the cutting process, in the quality of the machining and originates faults in the rest of the components, such as, bearing damage, wear of the holders and errors in the rotor and stator.

The critical faults which may occur in the shaft are: *UnBalance (UB)*, *MisAlignment (MA)*, *Oil Whipping (OW)*, *Shaft Crack (SC)*, *Mechanical Looseness (ML)*, *Rotor Stator Friction (RSF)* and *Rub Impact (RI)*.

Over several decades, faults in high speed machining has been studied, the importance lies in distinguish a normal signal from a faulty one even when exist small changes in the amplitudes. The technique used by [Peng *et al.*, 2007], combines the *Wavelet Transform Modulus Maxima (WTMM)* (a variance in the *CWT* which detects local maxima in the wavelet coefficients) and the Lipschitz exponent also known as *Holder* exponent. The method is implemented for detecting *UB*, *OW*, *MA*, *RI* and classifies them according to the singularity of the signal.

In [YanPing *et al.*, 2006], the authors proposed a method to characterize the shaft status using parameters extracted from wavelet coefficients of the *CWT*, which are obtained with the *Wavelet Grey Moment (WGM)* and first-order *Wavelet Grey Moment Vector (WGMV)* where the second one is implemented when the *WGM* shows overlapped results. The studied faults were normal *signal (NS)*, *UB*, *MA*, *OW*, *SC*, *ML* and *RSF*. The results of the method were compared with the *FFT* and suggest the presented method by the authors can detect all the studied faults unlike *FFT* which only detected *NS*, *UB*, *OW* and *ML*.

[Chen *et al.*, 2013] also reaffirmed that *WT* have better results than *FFT*. The *DWT* and the *Power Spectral density (PSD)* were implemented to determine the *UB* in a vertical simulated spindle. According to the study, the method can achieve a greater identification accuracy than *FFT*, by using lower sampling frequency and additionally, the storage space gets reduced and the processing speed is improved.

Table 2.1: Comparison between some machining researches using *WT* approach

<i>References</i>	<i>Defects</i>	<i>Case Study</i>	<i>Technique</i>	<i>Additional Analysis</i>	<i>Classifier and efficiency</i>
[Mori <i>et al.</i> , 1996]	<i>OR</i>	Test rig 660 RPM	<i>DWT</i> <i>MW</i> : Daubechies	Does not apply	Maximum Value of coefficients
[Paya <i>et al.</i> , 1997]	<i>IR</i>	Test rig 470-4230 RPM	<i>CWT</i> <i>MW</i> : Db4	Does not apply	<i>ANN</i> & Back-Propagation 96%
[Tse <i>et al.</i> , 2001]	<i>IR, OR, RE</i>	Test rig 1200 RPM	<i>CWT</i> <i>MW</i> : Gaussian	Does not apply	Visual
[Nikolaou and Antoniadis, 2002]	<i>IR, OR</i>	Simulation / Test Rig 1500 RPM	<i>WPT</i> <i>MW</i> : Db12	Energy of coefficients	Visual
[Prabhakar <i>et al.</i> , 2002]	<i>IR, OR</i>	Vibration Tester 1800 RPM	<i>DWT</i> <i>MW</i> : Db4	<i>RMS</i> and Kurtosis, <i>FFT</i>	Visual
[Tse <i>et al.</i> , 2004]	<i>IR, OR</i>	Simulation / Test Rig 1398 RPM	<i>EWA</i> <i>MW</i> : Multiple	Does not apply	Visual
[Shi <i>et al.</i> , 2004]	<i>IR, OR, RE</i>	Test Rig 1020 RPM	<i>CWT</i> <i>MW</i> : Gaussian	Shannon Entropy	Visual
[Purushotham <i>et al.</i> , 2005]	<i>IR, OR, RE, CO</i>	Test rig 1300 RPM	<i>DWT</i> <i>MW</i> : Db2	<i>MFCC</i>	<i>HMM</i> 99%
[Yan and Gao, 2005]	<i>OR</i>	Test rig 1200 RPM	<i>WPT</i> <i>MW</i> : Harmonic	<i>FDC</i>	<i>MLP, RBF</i> 99%, 100%
[Zhang <i>et al.</i> , 2006]	<i>IR, OR, UB, CO</i>	Test Rig 1200-8400 RPM	<i>AWT</i> <i>MW</i> : C. Morlet	<i>Envelope Spectrum</i>	Visual
[Zhu <i>et al.</i> , 2009]	<i>IR, OR, RE</i>	Simulation / Test Rig 1430 RPM	<i>CWT</i> <i>MW</i> : Morlet	<i>K-S</i>	Does not apply
[He <i>et al.</i> , 2009]	<i>IR, OR</i>	Simulation / Test Rig 1500 RPM	<i>CWT</i> <i>MW</i> : Morlet	<i>SCS</i>	Does not apply

Table 2.1: Comparison between some machining researches using wavelet approach (Continued)

<i>References</i>	<i>Defects</i>	<i>Case Study</i>	<i>Technique</i>	<i>Additional Analysis</i>	<i>Classifier and efficiency</i>
[Rafiee <i>et al.</i> , 2010]	<i>IR, RE, C</i>	Test Rig 1420 RPM	<i>CWT</i> <i>MW</i> : Analyzed: 324, Best: Db44	Variance, Standard Deviation, Kurtosis and 4th Central Moment	Does not apply
[Tse and Leung, 2010]	<i>IR, OR, RE</i>	Test Rig 1400 RPM	<i>CWT</i> <i>MW</i> : Morlet	Kurtosis and RMS	Does not apply
[Kankar <i>et al.</i> , 2011]	<i>IR, OR, RE, CO</i>	Test Rig 250-2000 RPM	<i>CWT</i> <i>MW</i> : Analyzed: 7, Best: Complex Morlet	MSEC, Kurtosis, Skewness, Standard Deviation.	<i>SVM</i> 100%
[Wang <i>et al.</i> , 2011]	<i>IR, OR, RE</i>	Simulation / <i>CWRU</i> Web Data 1796 RPM/ Test Rig 1496 RPM	Transient Modeling <i>MW</i> : Laplace, <i>HW</i> , Single-Side	Correlation Filtering	Automatic Estimation
[Yan and Gao, 2011]	<i>OR</i>	Test Rig 900-1500 RPM / 2000 RPM	<i>WPT</i> <i>MW</i> : Biorthogonal 5.5.	Kurtosis, Energy and PFA	<i>ANN</i> 93%
[Liu, 2012]	<i>IR, OR, RE</i>	<i>CWRU</i> Web Data 1796 RPM/ Test Rig 1500-1920 RPM	Shannon Wavelet Spectrum.	<i>EMA</i>	Visual
[Pandya <i>et al.</i> , 2012]	<i>IR, OR, RE</i>	Test Rig 1000-6000 RPM	<i>WPT</i> <i>MW</i> : Rbio5.5	Kurtosis, Energy, MSEC	<i>ANN</i> 93%
[Chandel and Patel, 2013]	<i>IR, OR, RE</i>	<i>CWRU</i> Web Data 1796 RPM	<i>DWT</i> <i>MW</i> : db10	Variance, Variance of autocorrelation	<i>ANN</i> 100%
[Cui <i>et al.</i> , 2016]	<i>IR, OR, RE</i>	<i>CWRU</i> Web Data 1796 RPM	Adaptive Wavelet Decomposition	Time-frequency features, ITD	Grey relational analysis 100%
[Kedadouche <i>et al.</i> , 2016b]	<i>OR</i>	Test Rig 600 RPM	<i>EWT</i>	Does not apply	Visual
[Li <i>et al.</i> , 2017]	<i>OR, IR</i>	Test Rig 1800 RPM	Q-factor <i>WT</i>	Does not apply	Visual

Table 2.1: Comparison between some machining researches using wavelet approach (Continued)

<i>References</i>	<i>Defects</i>	<i>Case Study</i>	<i>Technique</i>	<i>Additional Analysis</i>	<i>Classifier and efficiency</i>
[YanPing <i>et al.</i> , 2006]	<i>UB, MA, ML</i>	Test rig 0-10000 RPM	<i>CWT</i> <i>MW</i> : Morlet	<i>WGM</i> and <i>WGMV</i>	Numerical
[Chen <i>et al.</i> , 2013]	<i>UB</i>	Simulation 110 RPM	<i>DWT</i> <i>MW</i> : Db10	<i>PSD</i>	Visual
[Peng <i>et al.</i> , 2007]	<i>UB,MA</i>	Test rig 3000 RPM	<i>CWT</i>	<i>WTMM</i> and the Lipschitz exponent	Numerical

The investigation indicates the fault detection in *HSM* is an area of opportunity because most analyzes are focused on detecting faults at low speeds. Furthermore, the researchers have different points of view when choosing the type of *MW* and *WT*, for that reason there is no tendency to say which one is the optimal for the problem.

2.3 Theoretical Background

2.3.1 Wavelet Transform

The *WT* is mathematical tool that converts a signal in time domain into a series of wavelets located in a time-frequency domain.

The wavelets have finite energy with zero mean value and its oscillation is brief, so they differ from the sinusoidal waves used in the *FT*. When the wavelet can be dilated and shifted keeping its shape is called *MW*, this property allows the *WT* generates a desire response in both time and frequency domain.

Continuous Wavelet Transform

The *CWT* of a signal $x(t)$ can be performed through a convolution operation between the signal $x(t)$ and complex conjugate of a family of wavelets, [Yan *et al.*, 2014]. Mathematically, it is similar to the *FT*, except the *Fourier* analysis uses sines and cosines as base functions and the *WT* replace them with wavelets. One of the main disadvantages that the continuous transform presents is the redundant information, because of the change of the scale and translation parameters.

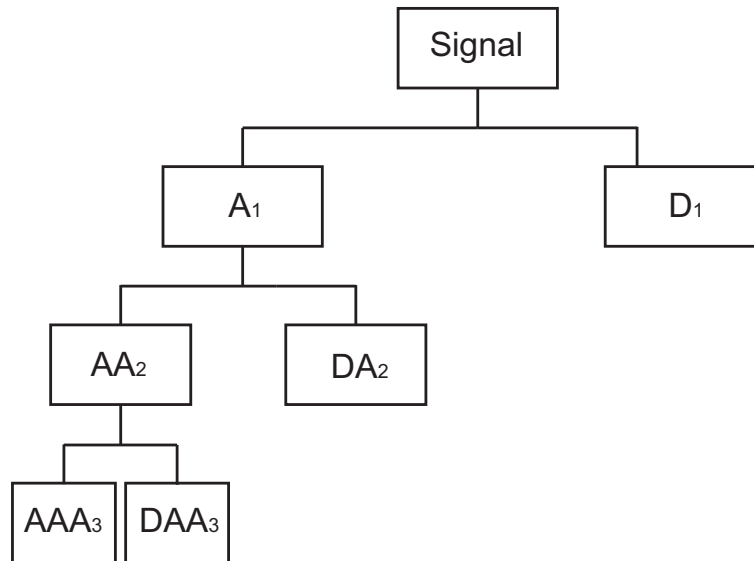
The scale can be approximated to frequency by the following relation:

$$F_a = \frac{F_c}{a \cdot \Delta} \quad (2.1)$$

where a is a scale, Δ is the sampling period, F_c is the center frequency of a wavelet in Hz, F_a is the pseudo-frequency corresponding to the scale a , in Hz.

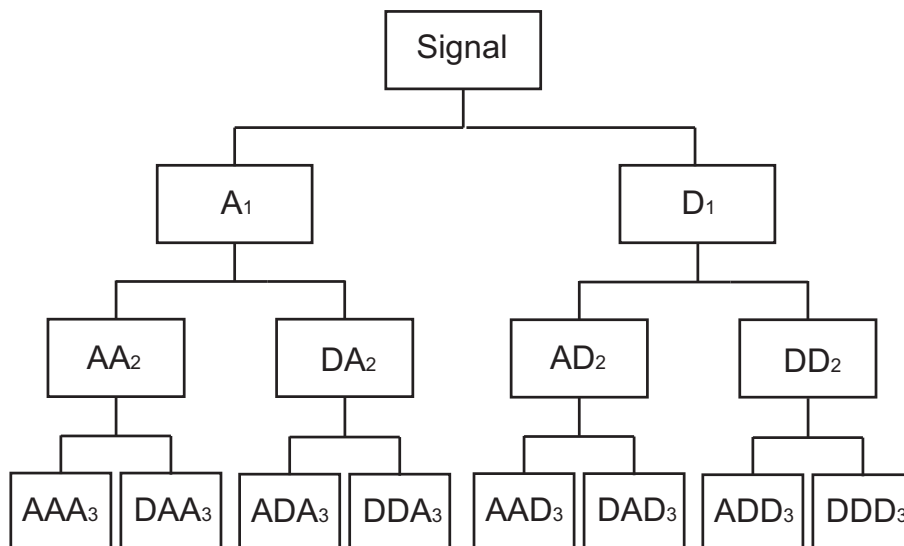
Discrete Wavelet Transform

The *DWT* acts as a pair of wavelet filters after the decomposition; it is obtained the approximation coefficients, which represents the low frequency of the signal and the detail coefficients that correspond to the high frequency. For next level analysis the new decomposition starts from the approximation coefficients found previously, as result this only allows decompose the low frequencies as the level increases, an illustration of its behavior is seen in the Fig. 2.1 where A and D are the *Approximation* and *Detail* coefficients and the next coefficients are the decomposition of the previous ones, but the detail coefficients (D) are not longer decomposed.

Figure 2.1: Third level decomposition using *DWT*.

Wavelet Packet Transform

The *WPT* can be seen as an extension of the *DWT*, where the detail coefficients are also analyzed and decomposed, which gives a same resolution in both low and high frequencies. The Fig. 2.2 demonstrate even the detailed coefficients are decomposed for each level, consequently each coefficient acts as a pass band filter with the same frequency range as the rest of the coefficients located in the same level. The computational cost increases in comparison to the *DWT*, but it is lower than the *CWT*.

Figure 2.2: Third level decomposition using *WPT*.

Additional variations of WT

There are others WT, among them are the *Second Generation Wavelet Transform (SGWT)*, *Wavelet Transform Modulus Maxima (WTMM)*, *Q factor Wavelet Transform (QFWT)* and *Empirical Wavelet Transform (EWT)* in which the transform builds adaptive wavelets and it is not necessary a MW selection.

2.3.2 Rolling element bearings

As bearings wear out, several faults may unleash. The principal faults affecting bearings are classified as distributed and local flaw. Distributed faults are divided in: surface roughness, waviness, misaligned races and off-size rolling elements. On the other hand, local faults are splitted into: cracks, pits and spalls on the rolling surface, [Prabhakar *et al.*, 2002]. The theoretical fault frequencies can be computed based on the geometry of the bearing [Randall, 2011]:

$$\begin{aligned}BPFO &= \frac{nf_r}{2} \left(1 - \frac{d}{D} \cos \alpha\right) \\BPMI &= \frac{nf_r}{2} \left(1 + \frac{d}{D} \cos \alpha\right) \\BSF &= \frac{Df_r}{2d} \left(1 - \left[\frac{d}{D} \cos \alpha\right]^2\right) \\FTF &= \frac{f_r}{2} \left(1 - \frac{d}{D} \cos \alpha\right)\end{aligned}$$

where n is the number of balls or rollers, f_r is the rotational speed, d is the ball or roller diameter, D is the average diameter between *OR* and *IR*, and α is the contact angle. The *BPFO* is the Ball Pass Frequency of Outer ring, *BPMI* is the Ball Pass Frequency of Inner ring, *BSF* is the Ball Spin Frequency and the *FTF* is the Fundamental Train Frequency.

There are four stages for bearing deterioration: (1) during the initial stage, the finish of the components in the bearing begin to deteriorate and produces ultrasonic frequency responses approximately in 20-60 kHz, [Scheffer and Girdhar, 2004], (2) in the second stage, the pits generate the ringing of the bearing at its frequency resonance and the harmonics appear in frequencies lower than 20 kHz, (3) in the third stage the pits spread along the raceway, emerge new peaks in the bearing fault frequencies and some harmonics, as the fault is considerable dangerous to the bearing it is recommended to replace the bearing because the remaining bearing life can be 1 h to 1% of its average life and (4) the fourth stage corresponds to a severe bearing condition. The amplitudes of the generated frequencies in the previous stages, the component 1x RPM and the random noise in high frequencies increase. By this time, the bearing is heated and produces a lot of noise, by its erratic behavior the coupling elements as the shaft could be damaged.

In this thesis are analyzed faults located in the *IR*, *OR* and *RE*. Defects in the cage are obviated because there are not recorded signals with cage faults in any of the data set studied.

2.3.3 Shaft

The shaft faults be detected by looking at the frequency spectrum and evaluating the speed harmonics. For this thesis, the focus will be limited to *UB*, *MA* and *ML* because they are the most common faults among the previously mentioned.

UB also called imbalance is the most common problem for rotating machines. It is said, the shaft is out of balance when its center of mass (inertia axis) does not match to its center of rotation (geometric axis), it causes a moment that affect the machine, [Mais, 2002].

There are three types of *UB*: static, couple and dynamic *UB*; any of them can be diagnosed by evaluating the speed frequency. Usually, the *UB* will not cause much damage to machines, but when the *UB* becomes serious, it will lead other destructive faults [Peng *et al.*, 2007].

MA occurs when the components are not aligned along their centerline, it can appear as angular and parallel or a combination of both. Its appearance causes the bearing to carry a higher load than the allowed in its design specification, which may cause bearing faults due to early fatigue.

The *ML* or pedestal looseness as the name implies is caused by the near components looseness or by a cracked frame structural.

To observe the behavior in a visual way for each one of the faults presented previously, please revise the Chapter 3 in the shaft fault section.

Chapter 3

Theoretical Proposal

A proposal for fault detection in the bearing system(*IR, RE, OR*) and shaft(*UB, MA, ML*) of a spindle is presented.

3.1 Proposed Methodology

The proposed method detects bearing and shaft faults by combining the benefits of the *WT* and some statistical techniques, Fig 3.1. To process the signal, *MATLAB* software was used with the *Wavelet Toolbox* version 2017a. The steps are the following:

Initial Signal Preprocessing

1. Acquire Signal

The signal comes from an accelerometer located on one side of the spindle, this signal must have a sampling frequency high enough so the desired fault frequencies can be detected.

2. Preprocess the signal

The signal might be embedded in heavy background noise; therefore, the signal should be preprocessed to reduce the background noise and errors of the measurement systems, [Lei, 2016]. It must be removed the trend and the mean of the signal, because the characteristic frequencies are tainted.

An illustration is presented in the Fig. 3.2, when the signal has an offset (also named mean) the direct component causes a fluctuation of a signal around $x = 5$ rather than $x = 0$, Fig. 3.2a. The undesired component produces a peak at 0 Hz, which does not carry any favorable information. Similarly, the trend (function associated with time t) influences the signal, Fig. 3.2e and 3.2f by generating an impulse at 0 Hz which opaques the other frequency and make it difficult to detect the important frequency. The

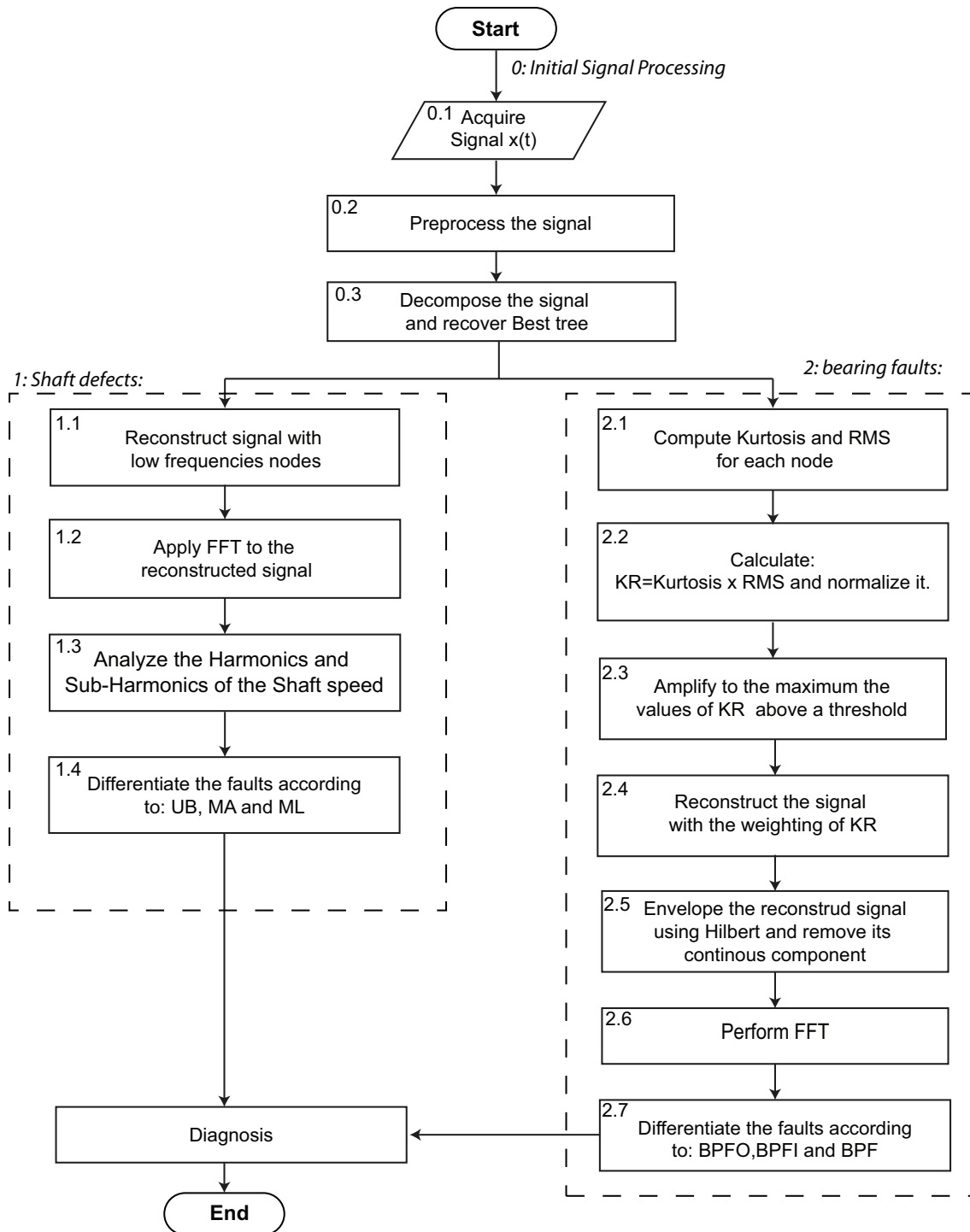


Figure 3.1: Methodology flowchart

trend and the mean can easily be eliminated without affecting the useful information as seen in the Fig. 3.2c and 3.2g.

3. Decomposition the signal and recover best tree

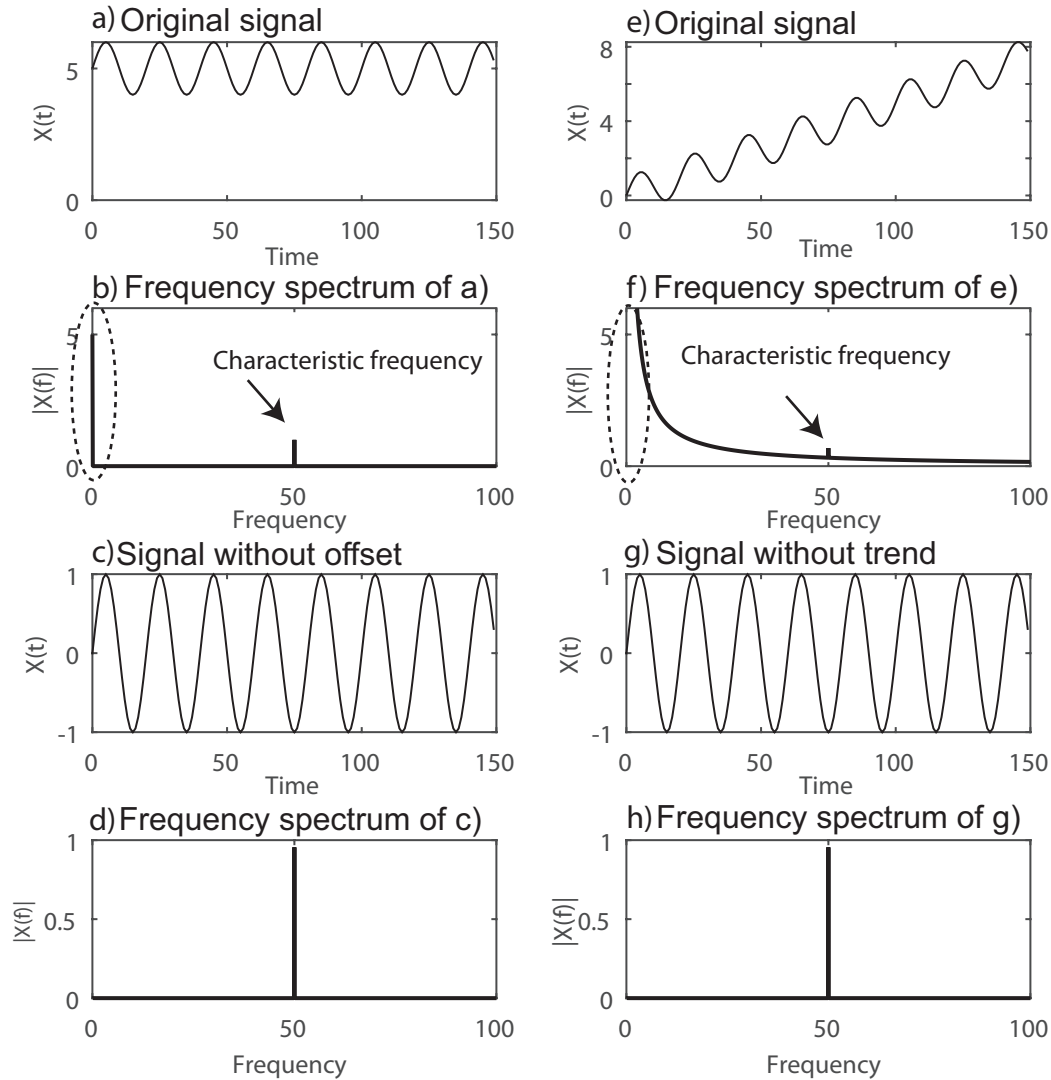


Figure 3.2: Signal pre-processing

The signal is decomposed with the *WPT* by its benefits, *section C.1 Appendix C*, it returns the wavelet coefficients organized in an energy-time-frequency array. There are 2^{level} coefficients with the same frequency range. For the bearing fault detection it is used the best tree which is computed based in the calculation of the entropy to detect which node from all the levels have the coefficients with more information. Figure 3.3 indicates the best tree of a signal decomposed until a third level.

The decomposition depends on the type of studied fault, the *Discrete Meyer* wavelet is used for detecting *OR*, the *Daubechies 45* for *RE* faults and the *Daubechies 41* for *IR* faults. These *MW* were selected based on a criterion named *Shannon Entropy*.

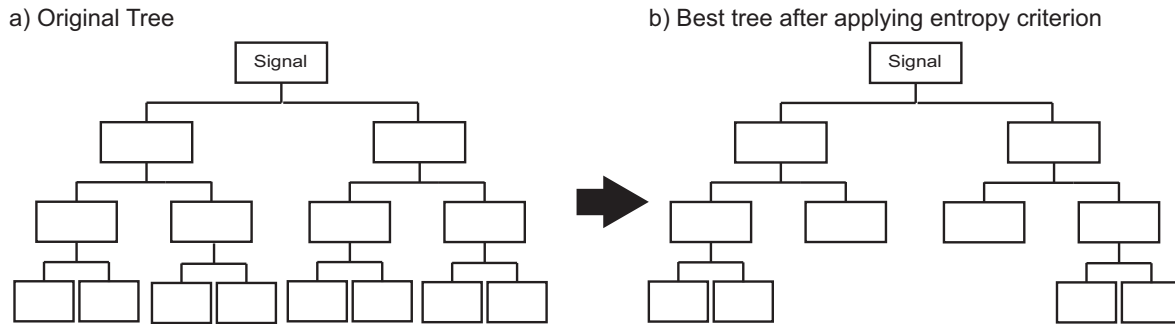


Figure 3.3: Best Tree

Shaft defects:

1. Reconstruct signal with low frequencies nodes

The corresponding nodes to the range from the first five harmonics are separate for shaft faults analysis, [Scheffer and Girdhar, 2004]. Reconstructing the signal using the low frequency nodes, generates a low pass filter effect, where the generated peaks by the faults in the bearings are eliminated, leaving behind only the information of the speed and its harmonics.

2. Apply FFT to the reconstructed signal

The *FFT* is a high-efficient algorithm for computing the signal in frequency domain, it is capable of executing the *Discrete Fourier Transform (DFT)* quickly. The transform returns a frequency-domain graph, which shows how much of the signal changes over a range of frequencies, Fig. 3.4.

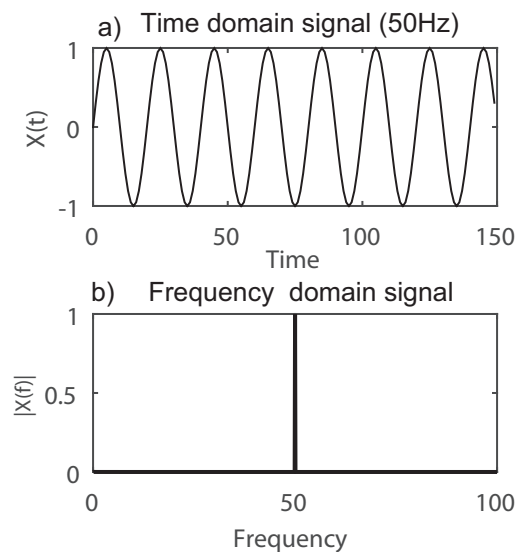


Figure 3.4: Time domain and FFT of the signal

3. Analyze the harmonics, subharmonics of the shaft speed

All the peaks which appear in the frequency spectrum are analyzed by taking into consideration their amplitude and the number of harmonics and subharmonics of the shaft speed (1X RPM).

4. Differentiate faults

The peaks are compared with the following criterion, [Mais, 2002]:

- When the 1X amplitude is higher than normal amplitude means *UB* is present in the system; the footprint is obtained by running the acquisition system with balanced components.
- To diagnose *MA* is necessary to compare the 1X and 2X speed amplitude. Normally, when the 2X amplitude is below 50% of 1X, the couplings are in an acceptable state of *MA*, if the 2X amplitude is located at a range of 50% to 150% of 1X, it is probable that coupling damage will occur. When the 2X amplitude is greater than 150% indicates a severe *MA*.
- If the $\frac{1}{2}X$ and its multiples have magnitudes greater than 20% the *ML* is present Fig.3.5 .

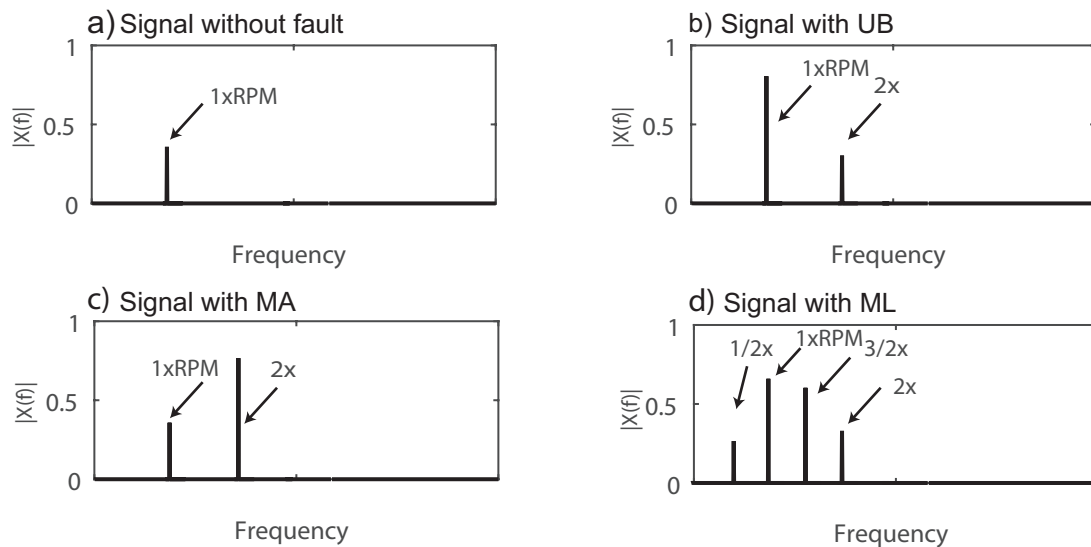


Figure 3.5: Shaft faults

For all the cases, an initial signal is required, with no fault and all spindle components must be working correctly.

Bearing faults:

1. Compute Kurtosis and RMS

The bearing fault excites low and high frequencies; therefore, for the analysis are considered all the generated nodes in the best tree. The *Kurtosis* and *RMS* are computed for each node separately, because of its characteristics *section C.2 (Appendix C)*.

Kurtosis gave a measure of the impulsiveness of a signal as a function of frequency [Randall, 2011]. However, the Kurtosis value could wrongly increase due the random impacts caused by noises.

RMS is commonly used as a destructive indicator, so in terms of machinery, it can be used as a health indicator of the machine. In the same way, it can be applied to each frequency band, it can return the intensity of a signal according to the frequency.

2. Compute KR

For each resulting node from the tree, the *KR* ($Kurtosis \times RMS$) is obtained with the product of the Kurtosis by the RMS, Fig. 3.6.

The result generates an amplitude arrangement of the *KR* amplitude versus the number of nodes, where nodes with high values have more information of the fault.

3. Amplify KR values above a threshold

Having the right indicator, the reconstruction will be based on these results, where it will depend on the weighting of the *KR* values. The problem lies on the fact the reconstruction of the maximum harms its surroundings since only one has weighting of 1; but, as shown in the Fig. C.5 *Appendix C*, a single node may not contain the entire information of the fault, and that is why it is proposed the *KR* values that surpass a threshold are increased to the maximum value and the values below remain unchanged. The procedure is shown in the Fig 3.7, the selection of the threshold is presented in the *section C.3, Appendix C*.

4. Signal reconstruction

The signal reconstruction is based on a ponderation given by the *KR*; the nodes with the maximum value of *KR* are entirely reconstructed, meanwhile the nodes based on low values are reconstructed with the percentage of the *KR* value against the maximum. The *WT* allows to reconstruct the signal from its coefficients by applying an inverse procedure. The input for the *Inverse Wavelet Transform (IWT)*, are the coefficients in each node, the result gives n signals with different ranges of frequency that posteriorly are added to have a modified signal where the noise is reduced.

5. Hilbert envelope

By using the *Hilbert* envelope, the high frequencies disappear and the defect frequency becomes more visible. As example, the signal in the Fig. 3.8 is composed by two frequencies: at 50 Hz and 1,000 Hz. The new signal (dotted line) envelopes the original, which eliminates the high frequency component without the use of a filter. In most

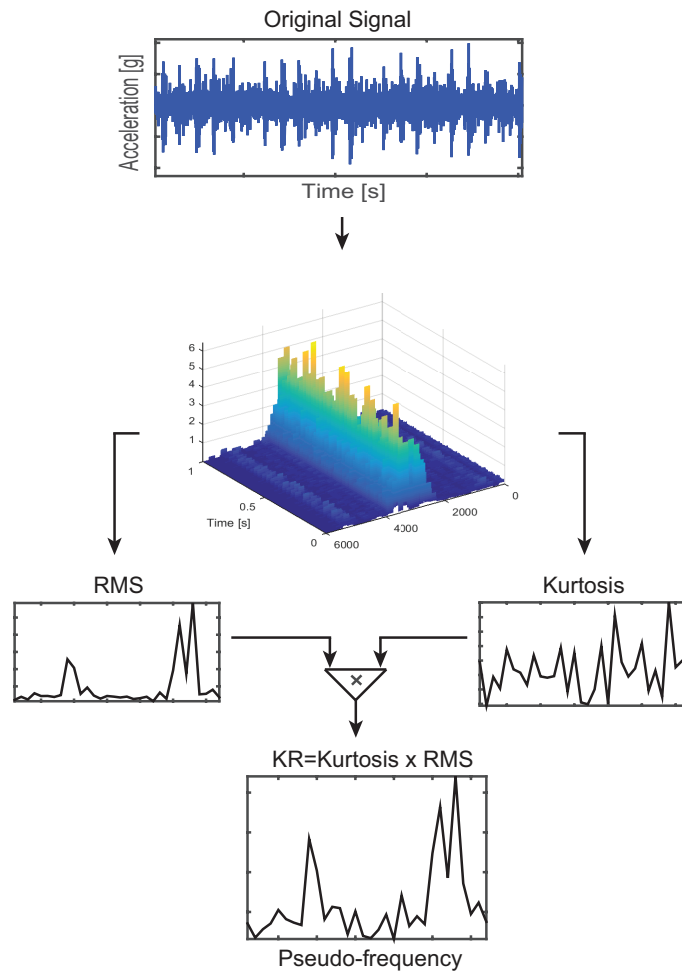


Figure 3.6: Generation of the KR employing wavelet coefficients

cases the generated envelope has a continuous component, which appears as a peak at 0 Hz in the frequency spectrum, to overcome this problem, the signal is adjusted to zero.

6. FFT

The FT is applied to know the frequency spectrum of the enveloped signal and to distinguish, if the presented peaks match with some of the values of the eqn. (2.2).

7. Differentiate the faults

The frequency spectrum has peaks if a fault is present. The values are evaluated to know if they correspond to the $BPFO$, $BPFI$ or BSF . If there is not peak, there is not fault.

The peaks in the frequency spectrum are accompanied by harmonics and sidebands, the $BPFO$ has a peak in the fault frequency as well as harmonics that become small as

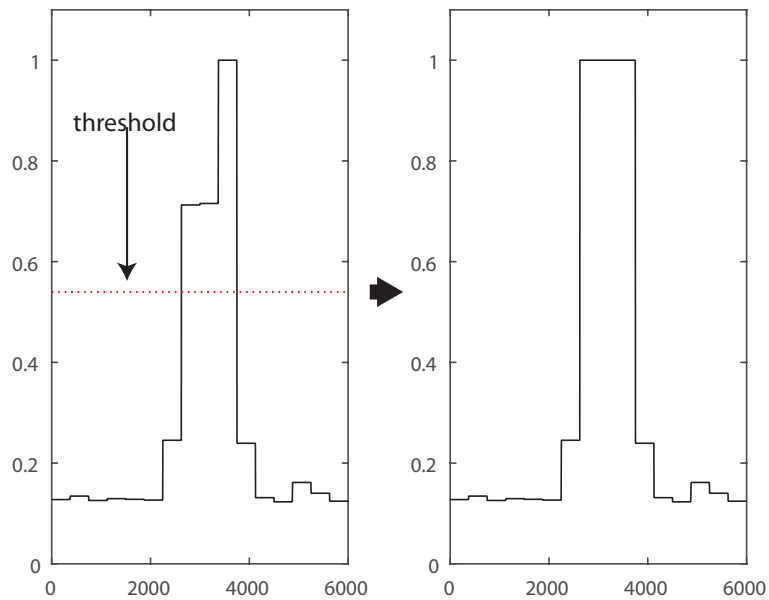


Figure 3.7: Threshold application for *KR* indicator

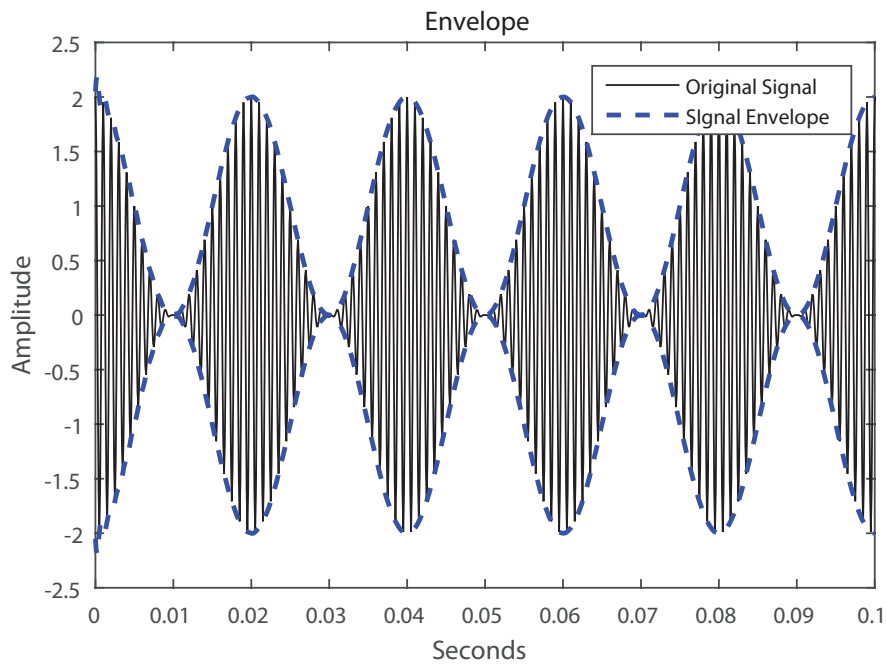


Figure 3.8: Hilbert envelope applied to a signal with 50 Hz and 1,000 Hz

the frequency increases. If the signal has an *IR* fault, there will be peaks in the *BPFI* frequency and its respective harmonics, besides both of them have sidebands spaced the shaft speed that in certain cases have higher amplitude than the fault frequency.

Something similar happens with the *BSF* with the difference that the sidebands are spaced *FTF* frequency, Fig. 3.9.

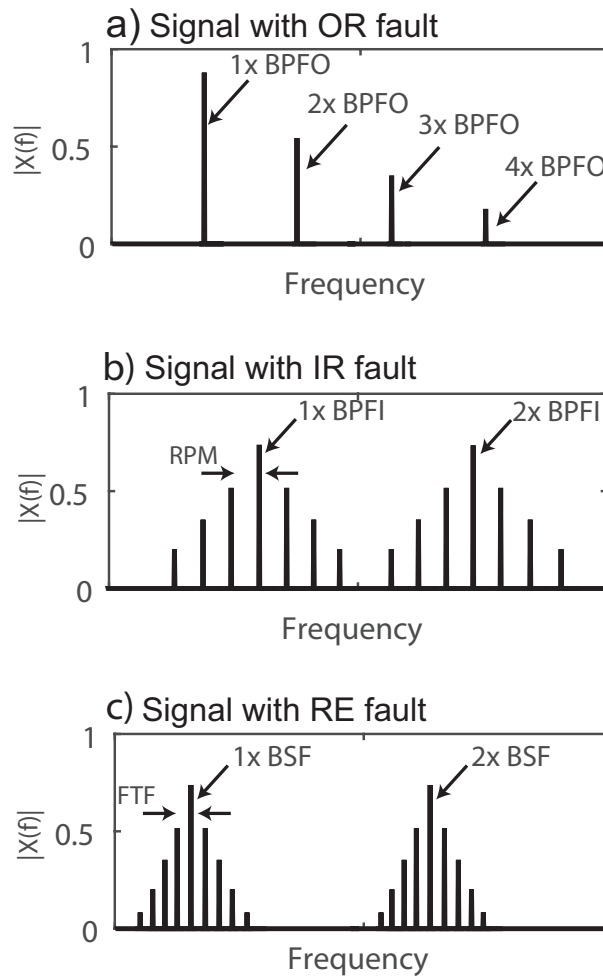


Figure 3.9: Bearing faults behavior in the frequency spectrum

Chapter 4

Experimental System

4.1 Case studies

It has been considered 2 datasets provided by the *Case Western Research University (CWRU)* and the center of *Intelligent Maintenance Systems (IMS)*. Additionally, a set of data was generated through a set of experiment tests using a GROB 550 machining center.

The use of data from *CWRU* will provide an understanding of the robustness of the proposed method, since some of the signals have noise that makes difficult the fault detection with the traditional methods. The data from the *IMS* will help to identify, if the algorithm detects faults at early stages (incipient faults).

4.1.1 CWRU Bearing Data Center

The data with bearing defects was provided from the website of the *CWRU*, in the tests are included data from normal and faulty bearings. the data was recorded at different loads: 0-3 Hp and the rotation speed was kept constant (1,797 - 1,720 RPM). Fig 4.1 shows the components of the test rig which include: a 2 Hp motor, dynamometer, accelerometers located on the drive end, fan end and base (some experiments), encoder and two types of bearings (drive end bearing: 6205-2RS JEM SKF, fan end bearing: 6203-2RS JEM SKF).

The bearings were seeded with defects using *Electro-Discharge Machining (EDM)*. The diameter of the fault goes from 0.007 to 0.040 inches located on the *IR*, *OR* and/or *RE*.

The values showed in Table 4.1 allows to detect the bearing fault frequencies by multiplying them by the rotational speed in Hertz. The values were proportionated by the *CWRU*.

The data was collected at 12,000 and 48,000 samples/second for drive end bearing experiments. All fan end bearing data was collected at 12,000 samples/second.

Each file contains fan and drive end vibration data as well as motor rotational speed. For all files, the following item in the variable name indicates: *DE* - Drive End accelerometer data, *FE* -

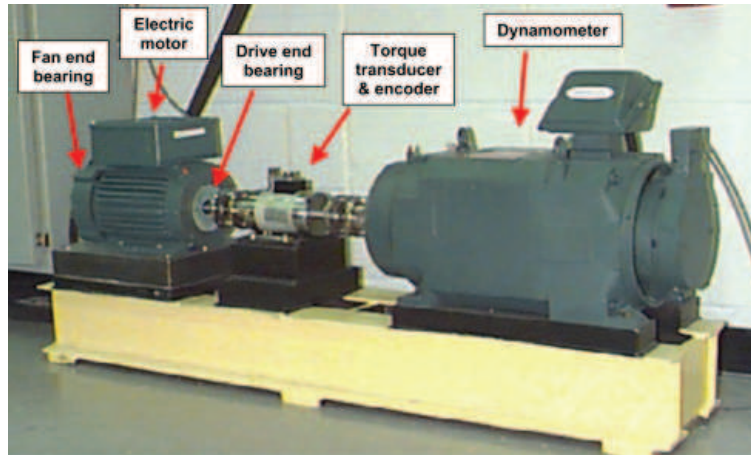


Figure 4.1: CWRU Bearing test rig.

Table 4.1: CWRU Bearing Defect frequencies (multiple of running speed in Hz)

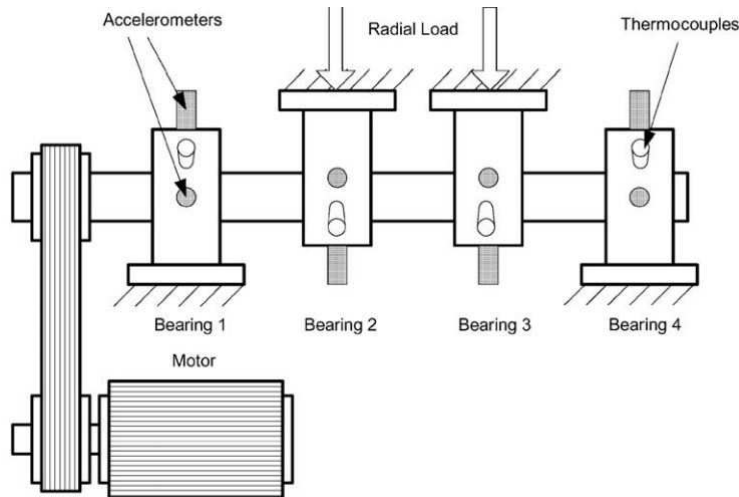
<i>Bearing</i>	<i>Inner Ring</i>	<i>Outer Ring</i>	<i>Cage Train</i>	<i>Rolling Element</i>
6205-2RS	5.4152	3.5848	0.39828	4.7135
6203-2RS	4.9469	3.0530	0.3817	3.9874

Fan End accelerometer data, *BA* - Base Accelerometer data, Time - Time series data and the RPM during testing [CWRU, 1999].

4.1.2 *IMS* Bearing Data

This data was obtained from the *IMS* with support from Rexnord Corporation Milwaukee, WI. There are three tests in the data, but only two were chosen for the analysis because the third one presents the same failure conditions as the second. In all of them, the rotational speed was kept constant at 2,000 RPM by an AC motor coupled to the shaft via rub belts and a 6,000 lbs radial load was applied on the shaft. As seen in Fig. 4.2, the test rig consists of: AC motor, PCB 353B33 High Sensitivity Quartz ICP accelerometers, Rexnord ZA-2115 double row bearings, NI DAQ Card 6062E, [CWRU, 1999].

Each data set describes a test-to-failure experiment, it consists of individual files that are 1-second vibration signal snapshots recorded at specific intervals. Each file consists of 20,480 points with the sampling rate set at 20 kHz. The *Table B.1 (Appendix B)* shows the data structure for each experiment and the cause of damage in the corresponding bearing. The defect frequencies are presented in the Table 4.2. The selection of the stages and the rest of information of the data set is located in the *Appendix B*.

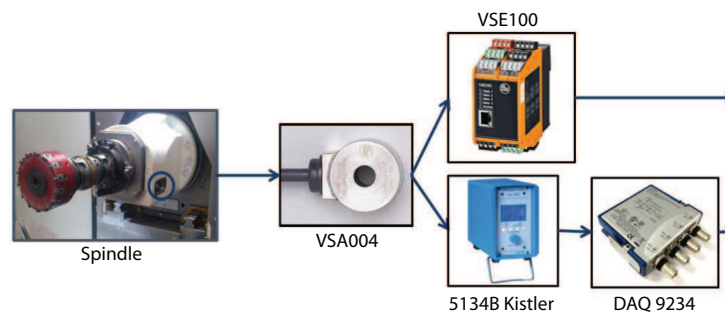
Figure 4.2: *IMS* bearing test rig.Table 4.2: *IMS* Bearing defect frequencies (multiple of running speed in Hz)

<i>Inner Ring</i>	<i>Outer Ring</i>	<i>Cage Train</i>	<i>Rolling Element</i>
8.8078088	7.1921912	0.55048805	3.88353658

4.1.3 GROB 550 recorded data

The *GROB 550* machining center has its own data acquisition system which includes the *VSA004* accelerometer located in the housing of the spindle and a diagnostic electronic *VSE100* with *FFT*, and the Envelope Fast Fourier Transform analysis integrated.

The time domain signal was recorded with an additional equipment. The coupled system has the *VSA004* accelerometer connected to a *5134B Kistler* amplifier and a *DAQ 9234* as seen in Fig. 4.1. The bearing information for this spindle is showed in Table 4.3.

Figure 4.3: *GROB 550* acquisition system

The data was recorded at different speeds ranging from 1,000 to 12,000 RPM and several levels of *UB* tool. For the analysis, signals with *UB* equal to 1.1, 10.5 and 26.1 were chosen, each one

Table 4.3: *GROB 550* Bearing defect frequencies (multiple of running speed in Hz)

<i>Inner Ring</i>	<i>Outer Ring</i>	<i>Cage Train</i>
12.95	10.55	8.83

of this signals has a duration of 2 seconds recorded at 12,000 RPM; the frequency sample was $f_s = 51200$

Chapter 5

Results

5.1 Introduction

The methodology was validated by using several case studies were analyzed for detecting *UB*, *MA*, *ML*, *IR*, *OR* and *RE* faults. It was established that there are no signals with all the spindle faults, that is why, for the case of *UB*, *MA* and *ML*, the signals obtained from the *GROB 550* machining center were taken. For the other cases (bearing faults), both *IMS* and *CWRU* data signals were used.

Firstly, the original signals are presented to emphasize the difficulty of detecting faults in the time domain, then the results of the method are presented and some discussions are included. Finally, a comparison with other methods is included to know the advantages or disadvantages of the method.

5.2 Method Results

5.2.1 Shaft faults: GROB 550 data set

The signals collected from the machining center were recorded with several levels of *UB* and diverse speeds. To test the proposed method, three signals were selected each one with a different level of *UB*: 1.1, 10.5 and 26.1 and the shaft speed was kept constant: 12,000 RPM.

When the method is evaluated for the shaft defects, it returns a reconstructed signal with nodes beyond 500 Hz, as result, the signal is modified, Fig. 5.1.

5.2.2 Bearing Faults case 1: IMS dataset

For the *IMS* database 9 signals were studied considering each type of bearing fault (*IR*, *OR* and *RE*) at three categorized levels depending on the stage of the fault: early, when the *Kurtosis* level

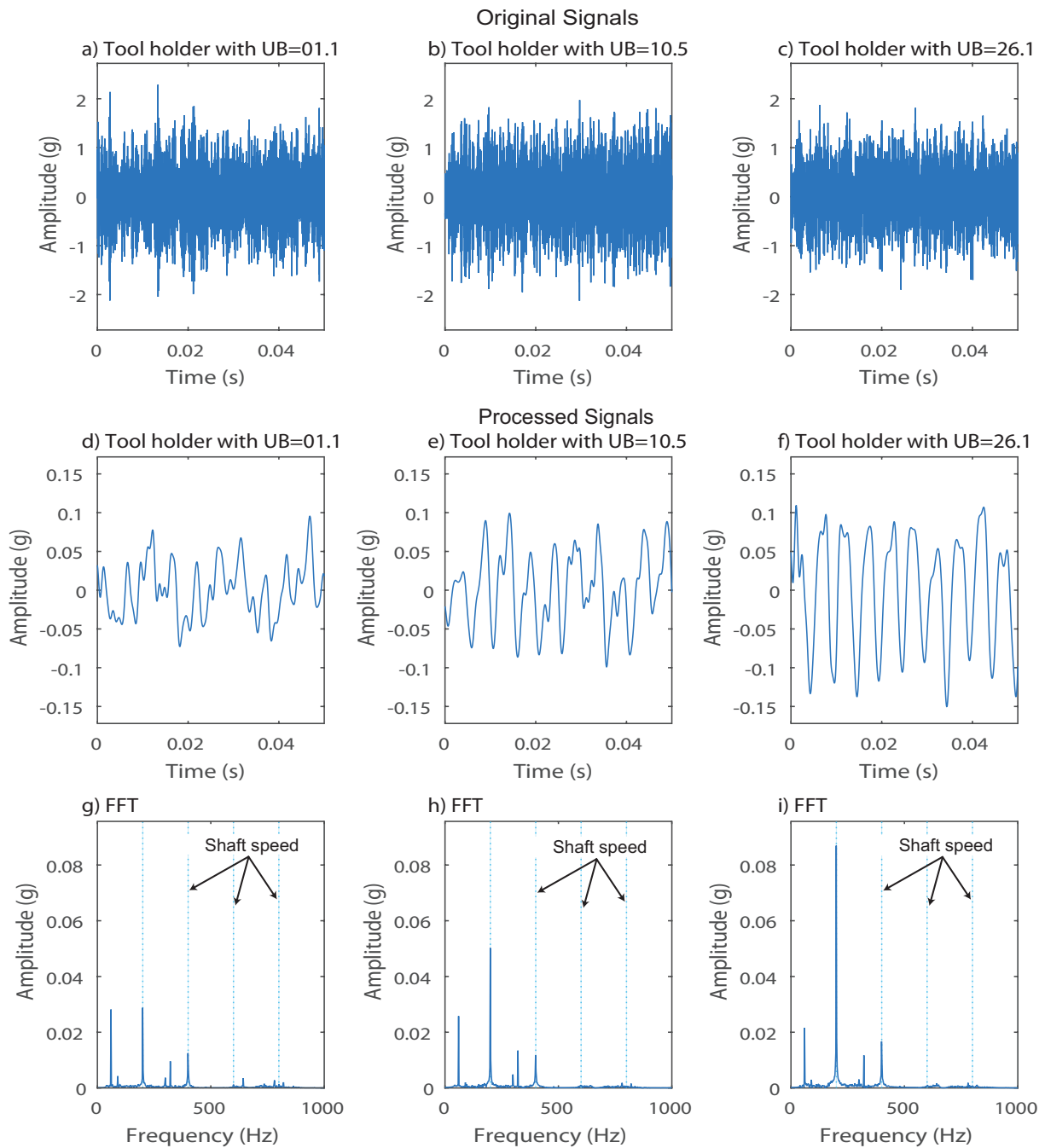


Figure 5.1: *GROB* signals after the application of the proposed methodology

begins to rise; medium, an intermediate point between the first appearance of the fault and the end of the tests and critical, when the bearing stopped working, *Fig B.5*, (*Appendix B*).

For bearing faults, the method returns the *FFT* of a reconstructed signal. From this graph the diagnosis can be performed in a visual way by knowing the frequency behavior of the different faults. The Figure 5.2 presents the results for the *IMS* signals, the sidebands and shaft speed harmonics are still present; the light blue lines are the expected frequency fault and its harmonics.

The shaft speed harmonics and the faults sidebands are hidden to make it easier to observe the faults, Fig. 5.3. The reader can analyze in detail the 9 signals by going to the *Appendix D*, where the results for each signal are presented with and without harmonics and sidebands.

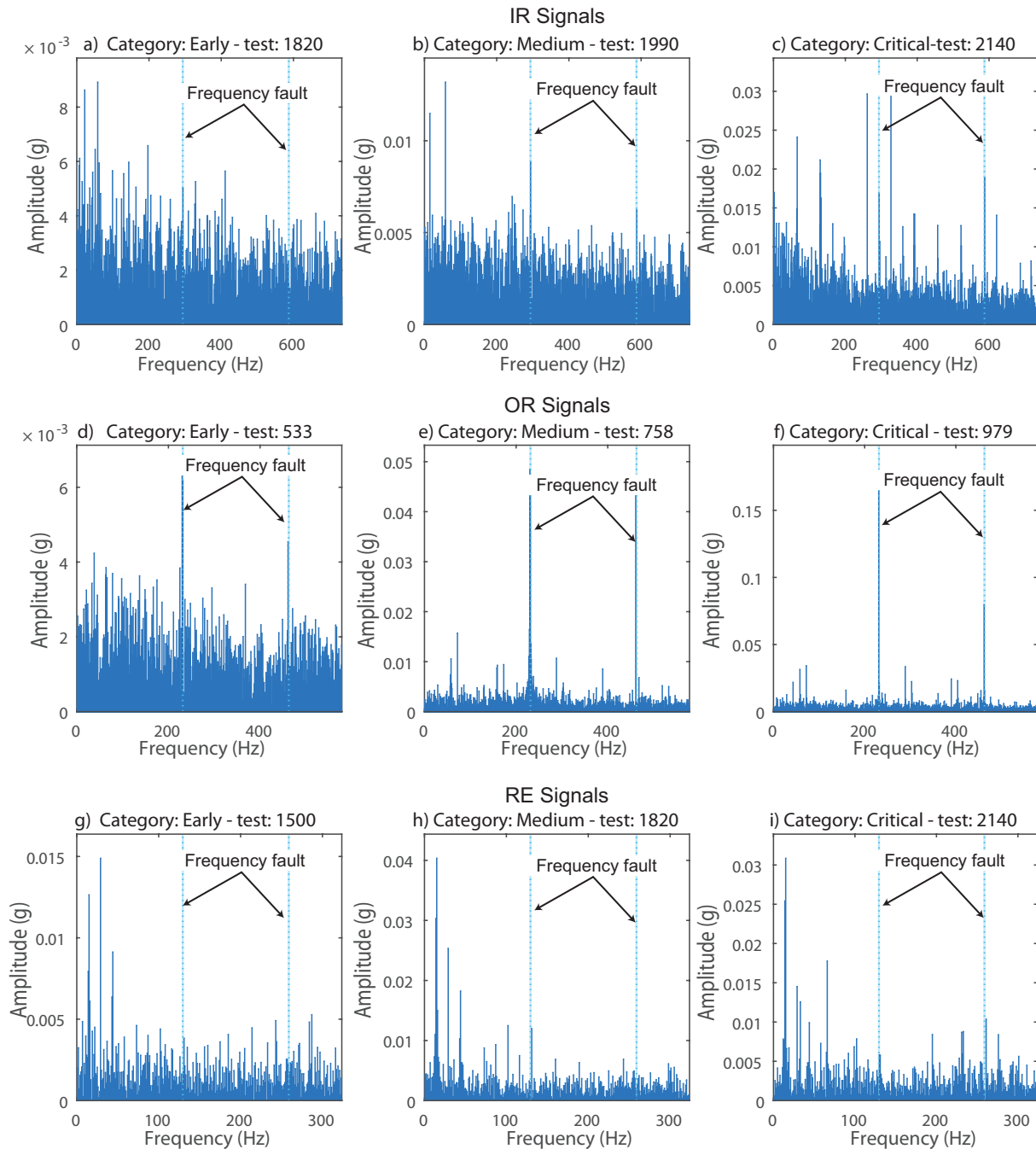


Figure 5.2: *IMS* signals after the application of the proposed methodology showing sidebands and shaft speed harmonics

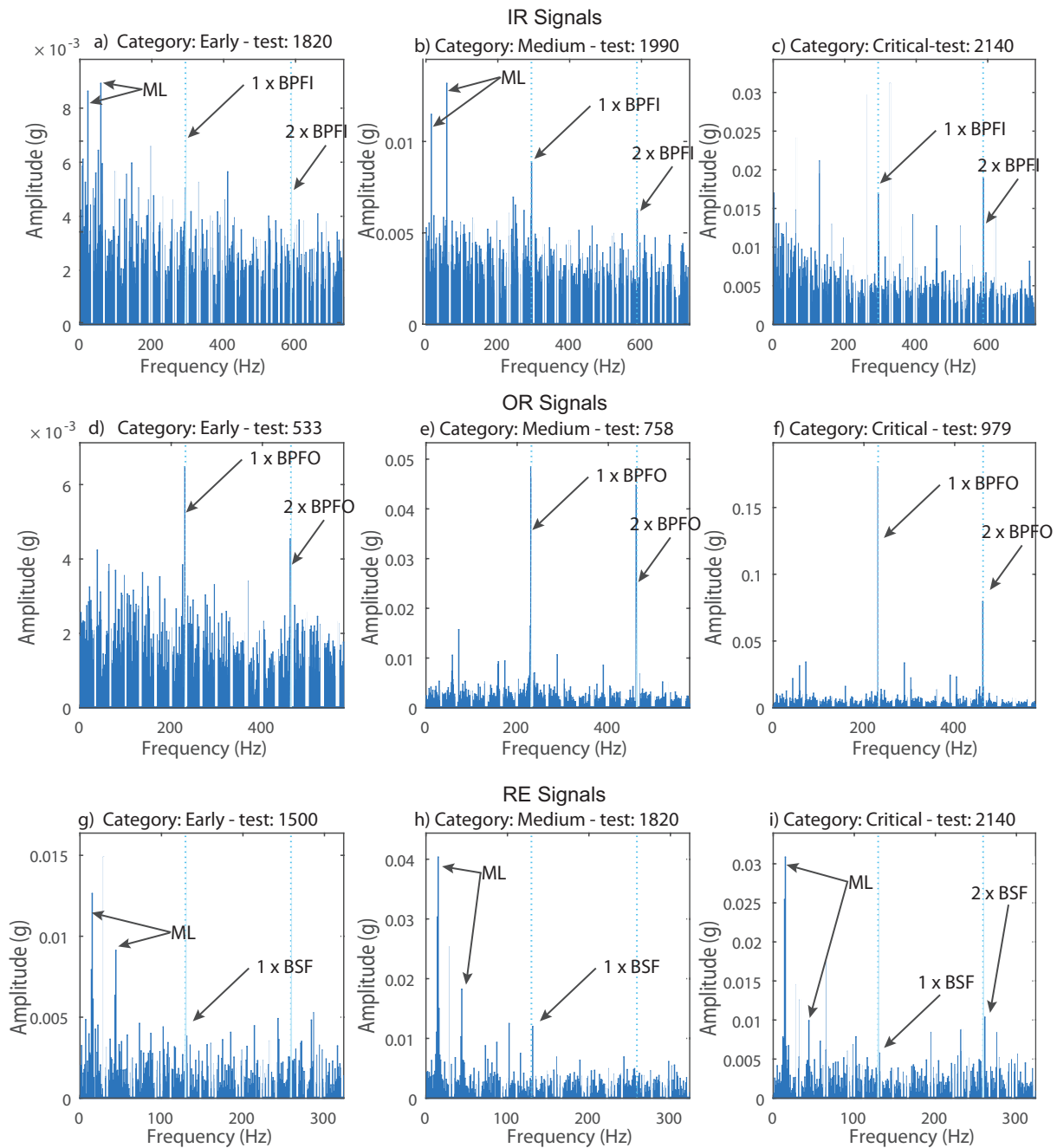


Figure 5.3: *IMS* signals after the application of the proposed methodology

5.2.3 Bearing Faults case 2: *CWRU* database

From the *CWRU* database 3 signals were selected for each type of fault, there were contemplated 3 categories: *N*, *P*, *Y*, which states the difficulty of fault detection according to [Smith and Randall, 2015]: the signals belonging to the *Y* group are the signals with an easy detection, in *P* are the signals with are partially diagnosed and the *N* signals are not diagnosable using traditional

methods.

Figure 5.4 shows the results of the applied method to the 9 signals with the shaft speed harmonics and sidebands removal.

In *Appendix D* can be found the results for each signal with and without harmonics and sidebands.

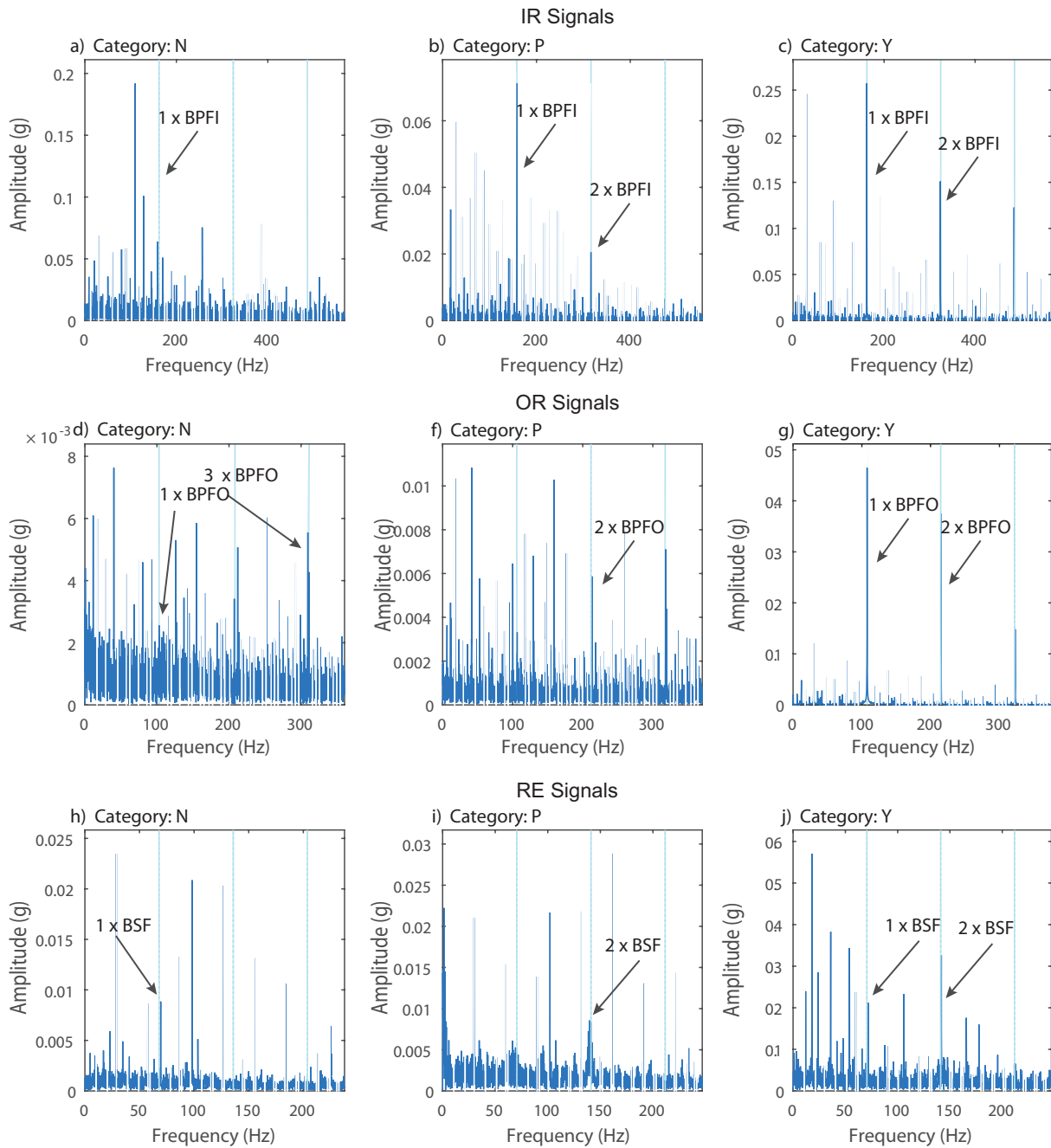


Figure 5.4: CWRU signals after the application of the proposed methodology

5.3 Discussions

5.3.1 Shaft faults: GROB 550 data set

In the Fig. 5.1(a,b,c) can not be distinguished the *UB* and at first sight because the signals have similar amplitudes. The method reconstruct a signal where the amplitude increases proportionally with the *UB* level and the difference is observed in more detail in the *FFT* of the reconstructed signals. The peak at the shaft speed (200 Hz) increases as the level of *UB* grows, this demonstrate the *UB* detection.

The second shaft speed harmonic is small relative to the first harmonic in all the cases, this establish there is no *MA*. *ML* is not present either because there are not peaks at the half of the shaft speed. There are peaks at 60 Hz, but it is assumed that they are electric noise, possibly coming from the motor.

The results indicate the method acts as filter because it reconstructed the nodes beyond the firsts shaft harmonics, Fig. 5.1(g,h,i) show peaks only in peaks within that range the peaks above are reduced to values close to zero.

5.3.2 Bearing Faults (case 1: *IMS* database)

The results after the signal processing are observed in the Fig.5.2. After the reconstruction stage, the new signal has a change on its offset and some peaks are attenuated. In the *IMS* signals the first statement is the most notorious, particularly for the *IR* and *RE* signals. In the Fig. 5.5 is shown a signal with offset removal using the proposed method. The results are as follows:

- ***OR* Signals**

The frequency graph generated by the proposed method in a signal with *OR* fault Fig. 5.3d, indicates the method detected the fault at early stages. There is a fault in the *OR* because some peaks match the frequency fault *BPFO* not only in the carry frequency, but also in its harmonics. However, the method does not remove all the white noise because it is similar to the noise found at the signal baseline in the test 1, Fig 5.3 (*Appendix B*), there is a lot of randomness of the data in the range below 0.003 and the unknown peak at 500 Hz it is still presented. For the consecutive tests where the crack gets bigger, the method does not have any inconvenience in detecting the fault because the peaks in the *BPFO* increase, Fig. 5.3 (e,f), the amplitude of the *BPFO* went up from 0.0062 to 0.18, almost 30 times the original value. Additionally, the peak at 500 Hz is completely attenuated and the noise remains low.

- ***IR* Signals**

At an early stage fault Fig. 5.3a, there is a peak that matches with the expected frequency fault *BPFI*; However, the peak is opaqued by the background noise and others peaks at low frequencies, their values are mostly *ML*, the others peaks are the peak in 7 Hz and 197 Hz,

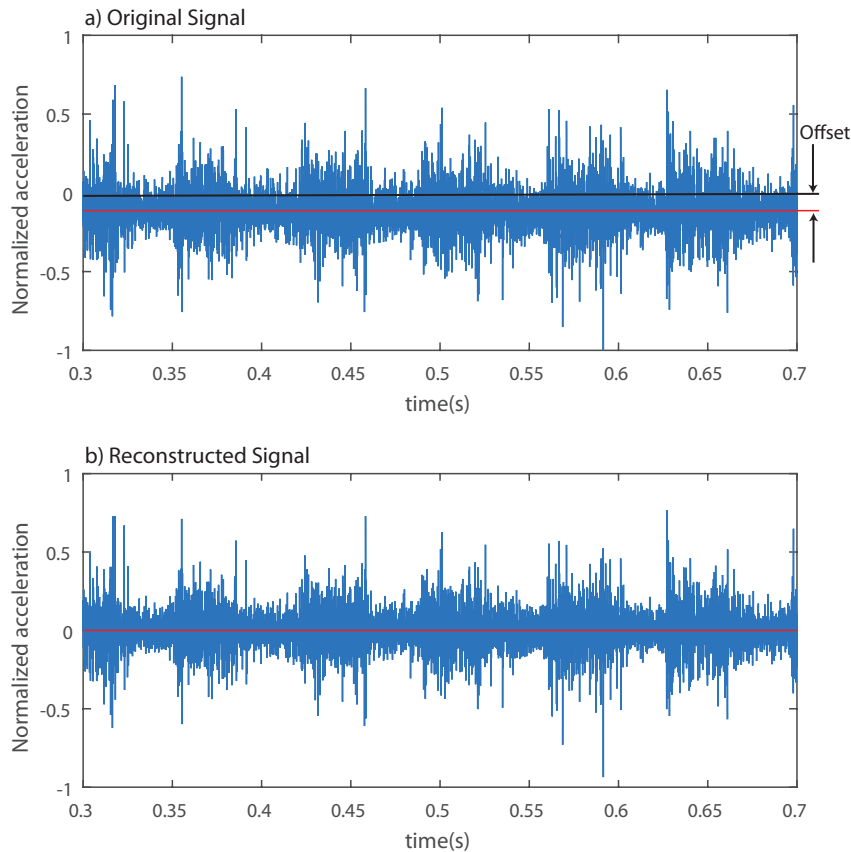


Figure 5.5: *RE* signal with offset removal

they do not belong to the frequency and their origin are unknown. In the next test, Fig. 5.3b, where the category is medium and the fault is bigger, some peaks stand out among others: the first two correspond to *ML*, the peaks at 290 and 590 Hz are the frequency fault and its first harmonic. When the faults become critical and the bearing is ready to fail Fig. 5.3c, an increase in amplitude of the frequency fault *BPFI* is presented, the *ML* is not longer displayed and the second harmonic also increases, this evidences the clear detection of the fault. Therefore, the method is capable of detect faults from the medium category onward although it is not efficient in removing the shaft frequency fault nor the entire background noise.

- ***RE* Signals**

Figure 5.3g, shows the method proposed to a signal with an early stage *RE* fault, the white noise was not completely removed because it present the same behavior as the noise in the *RE* baseline. Furthermore, there are peaks in the *ML*, this leads to an opacity of the *BSF* peak at 131 Hz and the second harmonic is not presented either, for those reasons it is considered the method do not distinguish *RE* faults at early stages.

The *ML* and the *BSF* peaks increase when the fault grows Fig.5.3h, although the second

harmonic of the *BSF* is not observable, the peak at 131 Hz confirms the presence of *RE* fault; the peak at 102 Hz is a sideband of the $BSF = 131Hz$ and has higher amplitude than the carry frequency because this frequency matches with a harmonic of the *ML* which increases its amplitude.

At the end of the bearing useful life, the failure in the *RE* is more evidenced by the presence of peaks in the fault frequency and its harmonics Fig.5.3i. However, their amplitude varies with a not proportional relation because instead of increasing the first fault peak as the later harmonics do, it decreases. The same happens with the peaks in the low frequencies belonging to *ML* and the shaft speed. The incident is not a fact of a single partition. Tests above and below 1,800 and 2,140 had similar behaviors. The fact could be due to a poor location of the applied force, its movement could cause a decrease of the load towards the bearing and therefore the reduction of its vibration.

The results demonstrate the method can be used to detect nearing early stage faults for the case of the *OR* and intermediate stages for the case of *IR* and *RE* with a 1 second recording.

The method does not remove the *ML* neither shaft speed peaks, those values interfere with the detection because they opaque the frequency fault.

5.3.3 Bearing Faults (case 2: *CWRU* database)

- ***OR* Signals**

When the fault signal belongs to the not diagnosable group, the fault is detectable by evaluating harmonics of the fault frequency, in this case Fig. 5.4d, the 3th peak confirms the presence of the fault. There are several peaks that have greater amplitude than any fault harmonic, this makes difficult their detection. A similar behavior occurs with the group *P* where the frequency peak is not the highest. However, the frequency peak and its harmonics are clearly visible. The signals in the category *Y* are easy to diagnose, there is not present any white noise.

- ***IR* Signals**

The results obtained for *IR* signals indicate: the *BPFI* peak does not match with the first harmonic despite the proximity to this value, as result it is establish the method do not detect de fault for this case Fig. 5.4a. In the other signals, the method can diagnose clearly the fault, the fault peaks match not only in the $1 \times BPFI$ but also in the second harmonic ($2 \times BPFI$).

- ***RE* Signals**

The *RE* signals are diagnosable by examining the first or second *BSF* harmonic, in the Fig. 5.4 (h,j), the fault is detectable for the first harmonic and for the category *P* Fig. 5.4i, the fault is detectable in the second harmonic.

For the *CWRU* database signals, the method can be used for detecting faults in signals with noise because it detects the peaks in its corresponding frequency fault ; however, in some cases the method does not reduce all the noise, this is caused because the high frequencies are not only excited by the frequency faults, but also by other faults in the elements coupled to the bearing.

5.4 Comparison

5.4.1 Shaft faults: GROB 550 data set

The method is compared with the *FFT* of the original signal. Figure 5.6a shows the filter effect occurring with the reconstructed signal, the frequencies above the selected nodes are totally removed. It can be observed more precisely in the Fig. 5.6 (c,d). The same graphs indicates the method keeps the same amplitude in all the peaks in the range of 0-500 Hz, this establishes the method does not improve or worsen these peaks and only acts as a low-pass filter.

5.4.2 Bearing Faults case 1: IMS Dataset

The method will be compared with: *FFT* and the enveloped-*FFT* by checking the amplitude at the frequency fault, Fig 5.7; all of them were compared by normalizing the time domain signals. The comparison is made in the range of 0 - 1,200 Hz, where it can be seen clearly the frequency fault and some of its harmonics.

At first glance the proposed method and the enveloped-*FFT* have a similar behavior; however, in all cases, the peak in the fault frequency is higher with the proposed method than with the other methods (enveloped-*FFT*, *FFT*), the amplification value varies depending on the type and stage of the fault. Figure 5.7 shows a signal with *OR* fault applied the three studied method, in the *FFT* the fault is present; but, its value is low. In the enveloped-*FFT* the fault and its harmonics are clearly detectable the same way proposed method does with the advantage that this method magnifies all the important frequencies. In the graphs can also be notice the peak at 0 Hz which appears in the enveloped-*FFT*, and it disappears when it is compared with the proposed method. This is of great advantage because the maximum value is not longer the peak at 0 Hz but the peak at the frequency fault.

In most cases, the method eliminates the peaks of 500 and 1,000 Hz. These frequencies do not belong to any of the contemplated faults and possibly are electric noise. These components are present in the *FFT* and in some of the enveloped-*FFT*, their appearance makes it difficult to distinguish the fault because of its high amplitude opaque the rest of the frequencies. Figure 5.8 shows a case where the unknown peaks considered as noise were not eliminated neither by the enveloped-*FFT* nor *FFT* only by the proposed method.

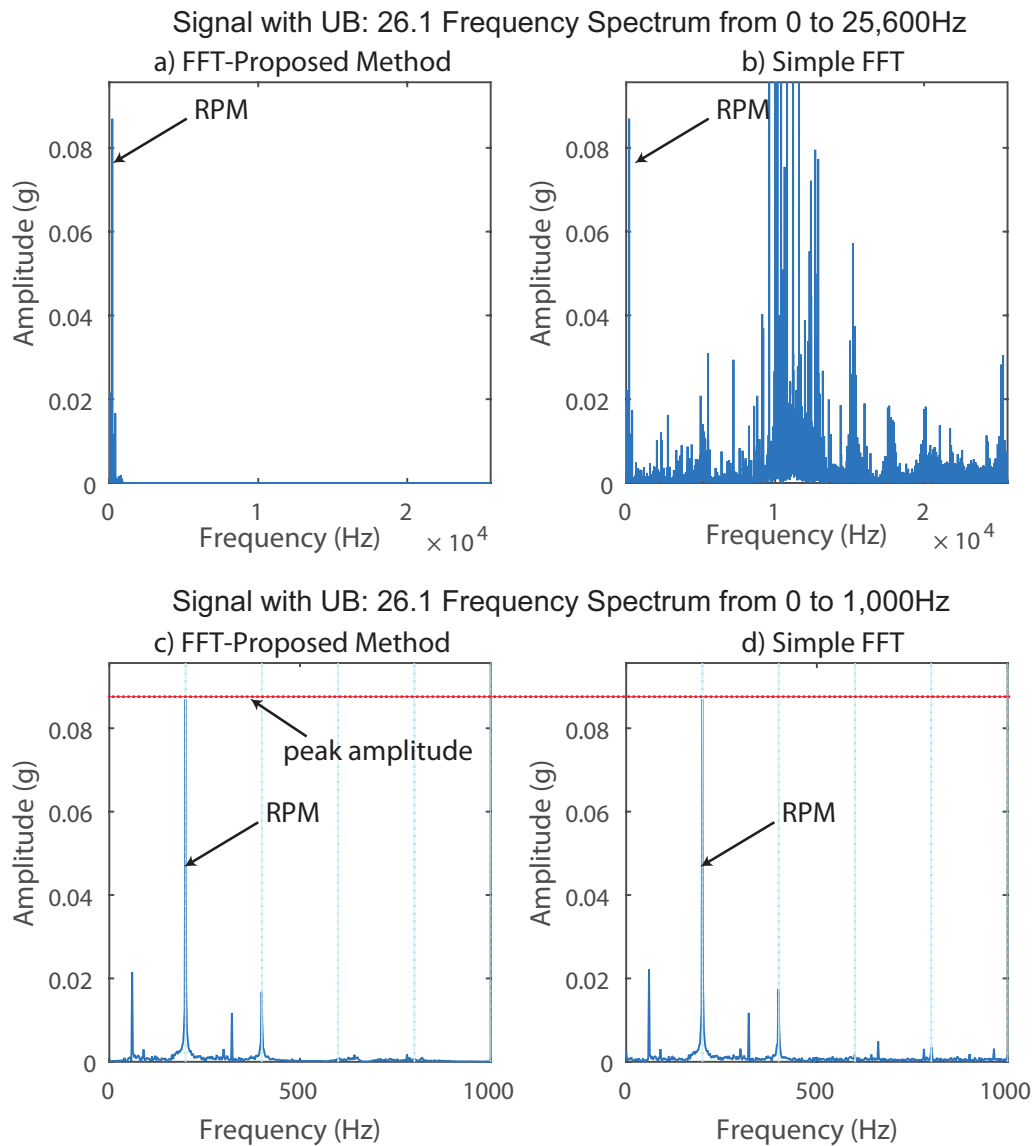
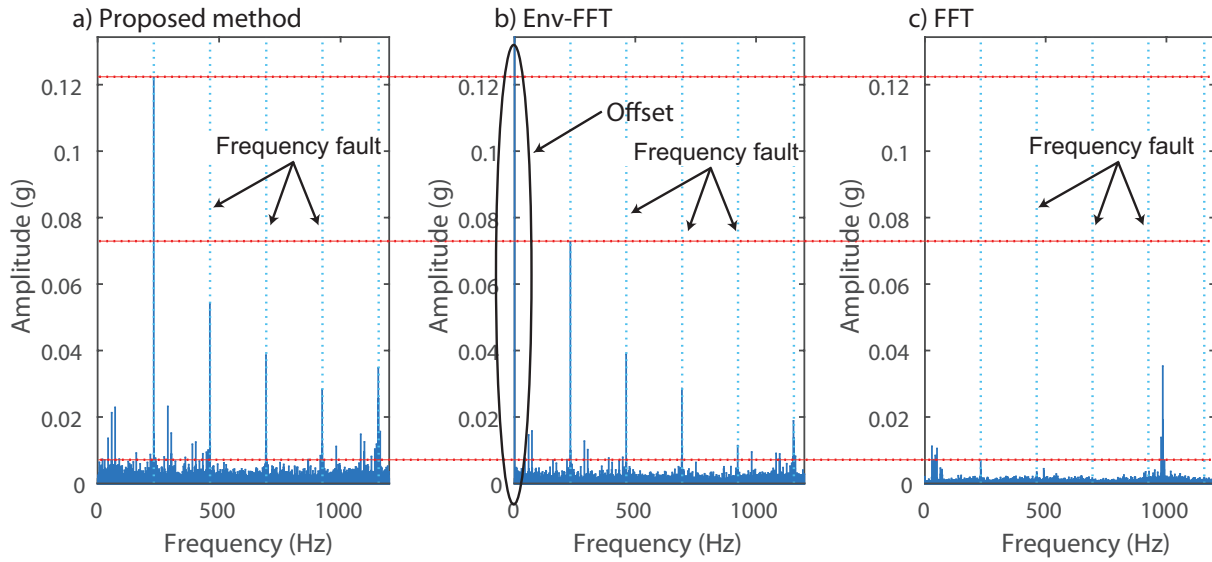
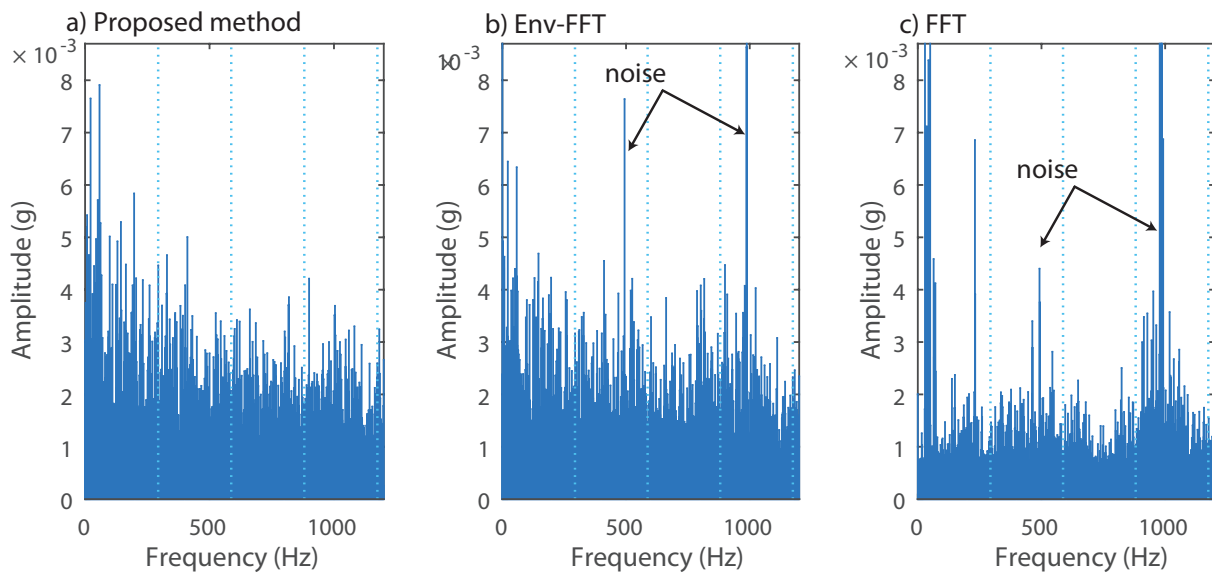


Figure 5.6: Signal with UB=26.1

In all the cases the *FFT* had the worst performance when are analyzed the first frequency fault harmonics, the peaks are only distinguished for cases of *OR* fault and even so, their value is low. In the cases where are presented *IR* and *RE* faults, the *FFT* do not detect them and can only be observed the peaks at 500 and 1,000 Hz.

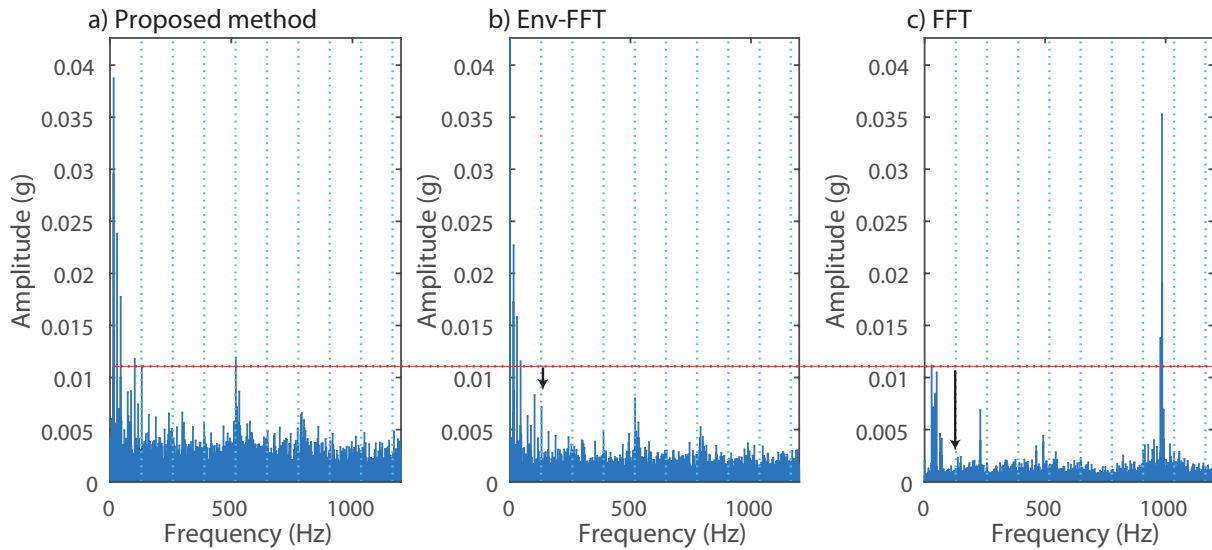
The enveloped-*FFT* has proven to be a good method for bearing fault detection; its behavior is similar to the proposed method nonetheless it does not remove entirely the peaks at 500 and 1,000 Hz and the value of the frequency fault is less than the one obtained by the proposed methodology, Fig. 5.9.

Despite being proven the proposed method is the best among the other studied, it can not detect *IR* and *RE* at early stage faults, the white noise and the non-important frequencies such as: *ML*

Figure 5.7: *OR* fault signal (*IMS* database)Figure 5.8: *IR* fault signal (*IMS* database)

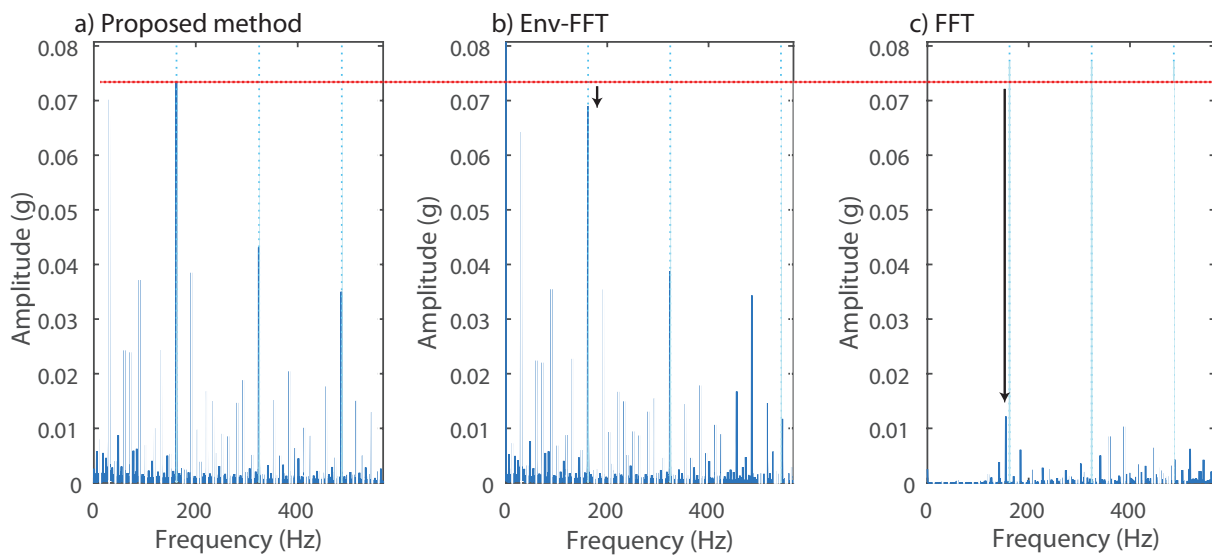
and shaft rotation are not completely eliminated.

The *IMS* data set was used in [Li *et al.*, 2017], the authors applied the tunable *QFWT* to a signal with *OR* fault to identify early stage faults. The authors were able to detect the *OR* fault at the 643th test. The proposed method and the enveloped-*FFT* are capable of detect the fault in the test 533 which means they detect faults earlier than the *QFWT*.

Figure 5.9: *IR* fault signal (*IMS* database)

5.4.3 Bearing Faults case 2: *CWRU* Database

The comparison indicates again, the *FFT* does not diagnose the fault in all the signal only when the fault belongs to the easy diagnosable group. The proposed method and the enveloped-*FFT* present a similar behavior over the frequency range with difference in the amplitudes. When the method is performed with the *CWRU*, it amplifies the peaks shown in the enveloped-*FFT* in all the analyzed signals, as example the Fig. 5.10 presents the behavior described. The observed gain depends on the signal and the noise level.

Figure 5.10: *OR* fault signal (*CWRU* database)

In the same way as in the *IMS* database, the method removes the offset and eliminates the 0 Hz

peak, this allows the detection of the maximum peaks. Figure 5.11 shows the offset removal in the frequency spectrum and its equivalent in the enveloped-*FFT*.

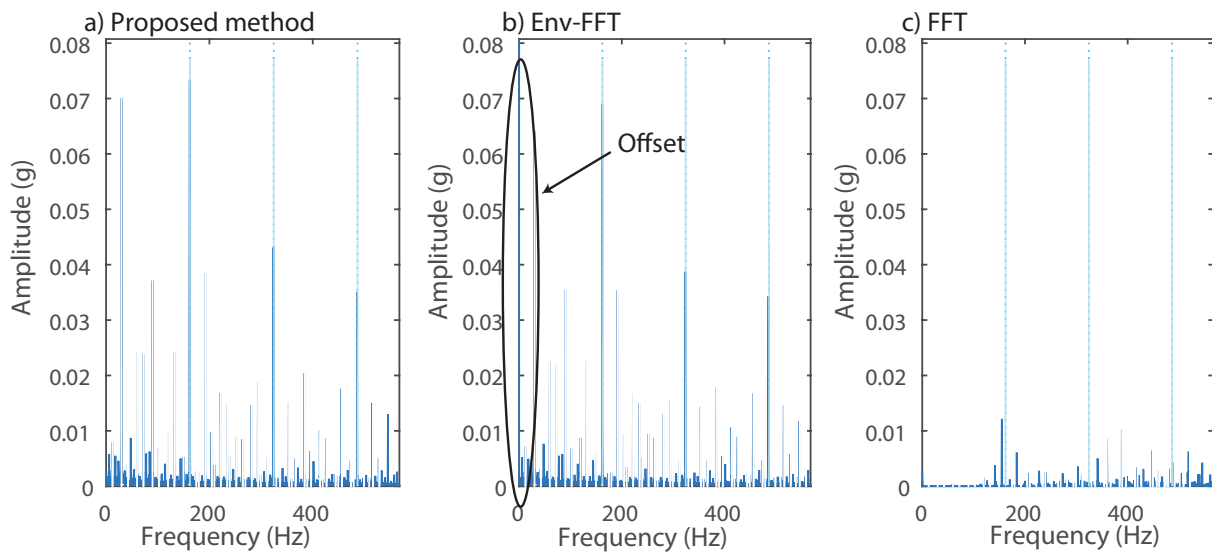


Figure 5.11: *IR* fault signal (*CWRU* database)

An additional analysis was performed adding *Gaussian* noise to the signal, aiming to have noise throughout the frequency range and not only in the resonance range of the studied components. It was added noise with a *Signal to Noise Ratio (SNR)* of 1.

In the Fig. 5.13a is shown an *OR* signal with added noise in the time domain, It can be seen the fault can not be distinguished because the noise taints the original signal. When the method is applied, the reconstructed signal has a clearly noise reduction, Fig.5.12.

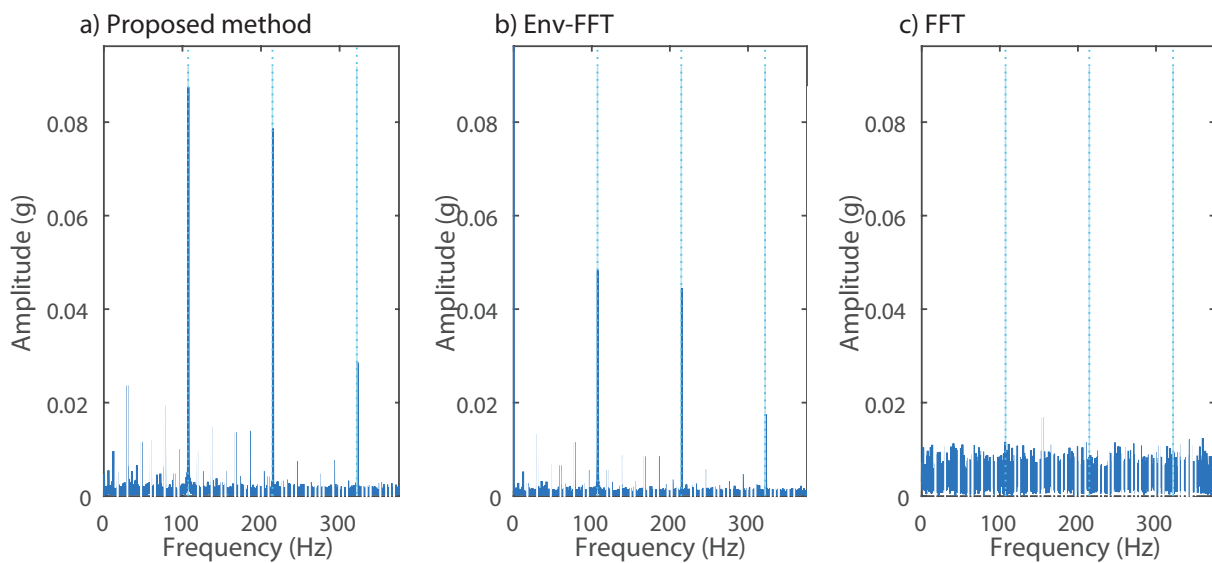


Figure 5.12: *OR* fault signal with *SNR* (*CWRU* database)

The effectiveness of the proposed method is observed in more detail: the method keep the same results shown in the Fig. 5.10a and Fig. 5.12a; however, when the noise is added, the amplitude of the frequency fault is reduced, Fig. 5.12b, because the method reduces the magnitude of these noise frequencies.

The method modifies the signal, it reconstructed the signal with a ponderation in the frequencies to the presented case, when the signal has noise Fig. 5.13a, the fault is difficult to detect but the method returns a new signal with some improvements, because the frequency peaks are more visible Fig. 5.13b. The frequency domain also brings great information to the results, as seen in the Fig. 5.13d, the range from 2,500 - 4,500 Hz remains the same and the rest of the frequency range gets modified: the frequencies beyond 500 Hz reach zero and, from 500 - 200 Hz and 4,500-6,000 Hz the noise is reduced.

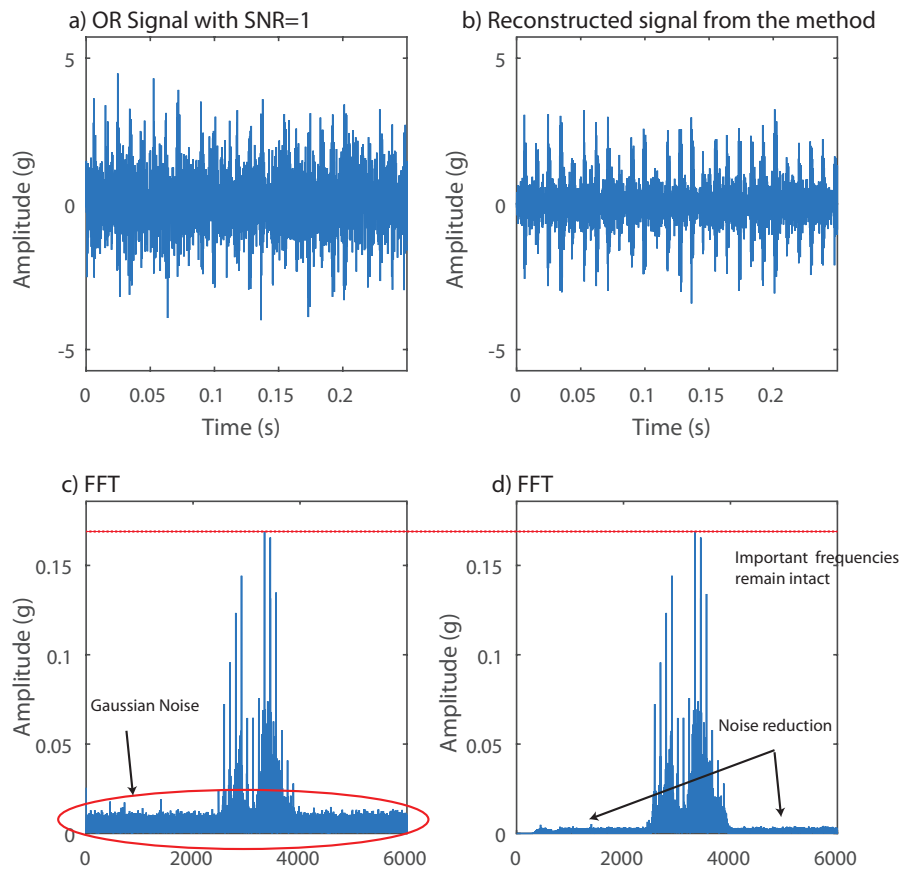


Figure 5.13: OR fault and $SNR=1$ (CWRU database)

Chapter 6

Conclusions

6.1 Summary

Vibration-based condition monitoring has proved to be an efficient way to detect faults in machining centers, the vibration signature changes in a way related to a fault and it is avoided the component disassemble. In this work, a methodology for spindle faults detection has been proposed, the method evaluates the vibration signal with the *WT*, *Hilbert* envelope and the *FT* to diagnose: *UB*, *MA*, *ML*, *IR*, *OR* and *RE* faults. The proposed methodology provides better results compared to common methods for fault detection because, it gives more weight to high energy frequencies.

The results indicate the fault can be detected accurately even at early stages (when the element starts to crack) which allows to perform proper maintenance before the fault can affect the other components and damage them. Additionally, the method is able to deal with noise at low frequencies by removing it or reducing its amplitude. Therefore, the presented method may be used to identify the health status of the spindle in noisy industrial environments. When the signal present other types of faults at high frequencies the method can not eliminated them because the reconstructed signals also have this parasitic signals.

Figure 6.1 shows the comparison between the frequency fault frequency resulting from the proposed methodology and the obtained by the Enveloped-*FFT*. The results indicate an going from 6-69 %. For the *CWRU* case, the average increase percentage is 16%, and for the *IMS* database is 33%.

CWRU signals with added *Gaussian* noise showed, had an higher increase, the value reached up to 57 percent.

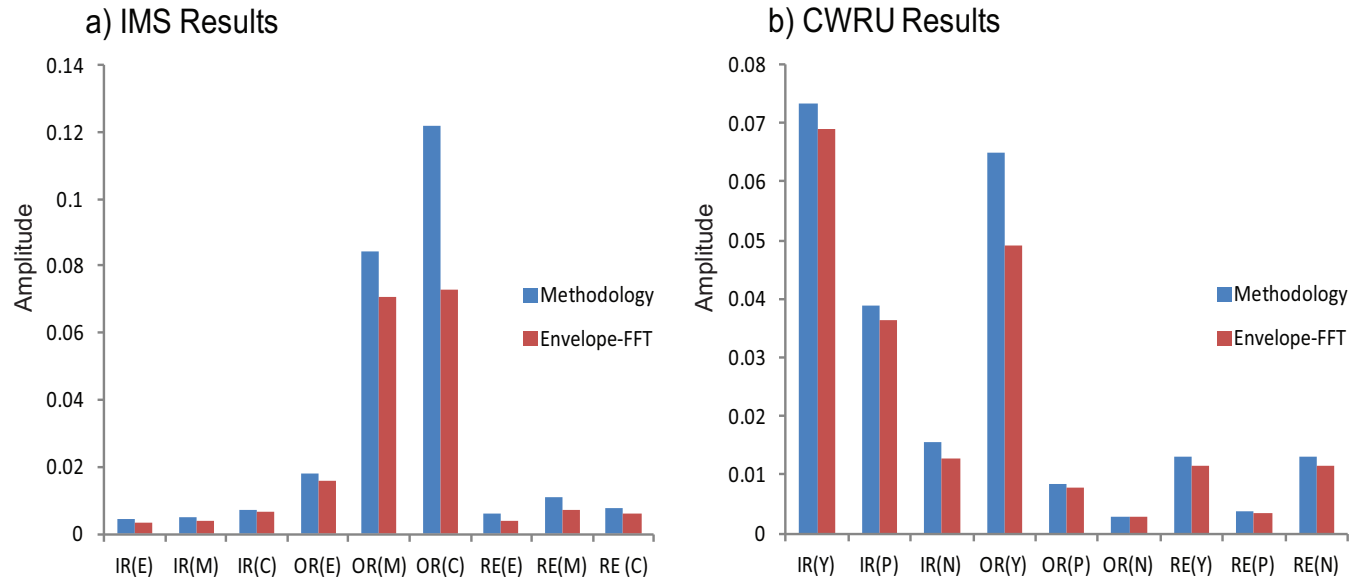


Figure 6.1: Comparison of the characteristic fault frequency amplitude between the proposed Methodology and the enveloped-*FFT*

6.2 Contributions

The main contribution of this thesis resides in the method proposed, the selection of the best parameters, it offers a robust analysis for spindle faults detection.

There are three complementary studies to clarifying which are the best parameters among those presented in the literature: in this thesis was analyzed which statistical indicator detects the frequencies where the bearing fault is located, the *KR* had the better results even when the signal has *Gaussian* noise and low frequency peaks; moreover, the optimal threshold for the reconstruction and the best type of *WT* were also evaluated. The combination of the three parameters allows the method to detect the frequency range excited by the bearing fault vibration and reduce the weight of the frequencies outside this range.

6.3 Publications

Two publications were presented during the research.

- "Diagnóstico de Fallas en Husillos de Mecanizado de Alta Velocidad usando Onduletas - Estado del Arte". Presented in the XXIII Annual International Congress of SOMIM (20-22 september 2017, Cuernavaca, Morelos, México)

- "Monitoreo de Husillos usando la Transformada de Onduletas". Presented in the National Congress of Automatic Control 2017 (04-06 october 2017, Monterrey, Nuevo León, México)

6.4 Future Work

The present thesis has made a contribution towards the development of a methodology for online spindle fault detection. In reference to the obtained results, some interesting points have been identified:

- As a starting point, the method can be used in conjunction with a classifier, it will automatically detect the type of fault and can be used for an online system. Moreover, A hybrid method could be developed by using the proposed methodology as signal preprocessing for new techniques such as: *HHT* and *WVD*.
- The obtained results can be evaluated to detect a pattern of the amplitude of the *FFT* and related them with the fault size. The cut frequency for the shaft reconstruction must be studied in deep, it has to be adaptive to content at least two speed harmonics.
- As a further extension of this work, the method can be applied to a bearing fault in *HSM* database. Additionally, other faults can be investigated as cage and rotor faults. The method is not limited to signals obtained by accelerometers, acoustic emissions can be used as input to the method.
- Finally, the performed wavelet analysis in this thesis would be easily expanded by attaching the wavelet denoising and try to eliminate the remaining noise in the reconstructed nodes. It would be compelling to design a wavelet with similar behavior to the vibration signal generated by a fault.

Bibliography

- [Chancey *et al.*, 2002] V.C. Chancey, G.T Flowers, and C.L. Howard. A Harmonic Wavelets Approach for Extracting Transient Patterns From Measured Rotor Vibration Data. *J of Eng for Gas Turbines and Power*, 125(1):81–89, 2002.
- [Chandel and Patel, 2013] A.K. Chandel and R.K. Patel. Bearing Fault Classification based on Wavelet Transform and Artificial Neural Network. *IETE J of Research*, 59(3):219–225, 2013.
- [Chen *et al.*, 2013] D. Chen, J. Fan, and F. Zhang. Extraction the Unbalance Features of Spindle System using Wavelet Transform and Power Spectral Density. *Measurement*, 46(3):1279–1290, 2013.
- [Cui *et al.*, 2016] H. Cui, Y. Qiao, Y. Yin, and M. Hong. An Investigation of Rolling Bearing Early Diagnosis based on High-Frequency Characteristics and Self-Adaptive Wavelet De-noising. *Neurocomputing*, 216:649–656, 2016.
- [CWRU, 1999] CWRU. Case Western Reserve University Bearing Data Center Seeded Fault Test Data. <http://csegroups.case.edu/bearingdatacenter/pages/apparatus-procedures>, Accessed 01-12-2016, 1999.
- [He *et al.*, 2009] W. He, Z.N. Jiang, and K. Feng. Bearing Fault Detection based on Optimal Wavelet Filter and Sparse Code Shrinkage. *Measurement*, 42(7):1092–1102, 2009.
- [Kankar *et al.*, 2011] P.K. Kankar, S.C. Sharma, and S.P. Harsha. Rolling Element Bearing Fault Diagnosis using Wavelet Transform. *Neurocomputing*, 74(10):1638 – 1645, 2011.
- [Kedadouche *et al.*, 2016a] M. Kedadouche, Z. Liu, and V.H. Vu. A New Approach based on OMA-Empirical Wavelet Transforms for Bearing Fault Diagnosis. *Measurement*, 90:292–308, 2016.
- [Kedadouche *et al.*, 2016b] M. Kedadouche, M. Thomas, and A. Tahan. A Comparative Study Between Empirical Wavelet Transforms and Empirical Mode Decomposition Methods: Application to Bearing Defect Diagnosis. *Mechanical Systems and Signal Processing*, 81:88 – 107, 2016.

- [Khanam *et al.*, 2014] S. Khanam, N. Tandon, and J.K. Dutt. Fault Size Estimation in the Outer Race of Ball Bearing using Discrete Wavelet Transform of the Vibration Signal. *Procedia Technology*, 14:12–19, 2014.
- [Lauro *et al.*, 2014] C.H. Lauro, L.C. Brand ao, D. Baldo, R.A. Reis, and J.P. Davim. Monitoring and Processing Signal Applied in Machining Processes - A Review. *Measurement*, 58:73–86, 2014.
- [Law *et al.*, 2012] L.S. Law, J.H. Kim, W.Y.H Liew, and S.K. Lee. An Approach based on Wavelet Packet Decomposition and Hilbert-Huang Transform (WPD-HHT) for Spindle Bearings Condition Monitoring. *Mechanical Systems and Signal Processing*, 33:197–211, 2012.
- [Lei, 2016] L. Yaguo Lei. *Intelligent Fault Diagnosis and Remaining Useful Life Prediction of Rotating Machinery*. Elsevier. Joe Hayton, 2016.
- [Li *et al.*, 2017] Y. Li, X. Liang, M. Xu, and W. Huang. Early Fault Feature Extraction of Rolling Bearing based on ICD and Tunable Q-factor Wavelet Transform. *Mechanical Systems and Signal Processing*, 86, Part A:204 – 223, 2017.
- [Liu, 2012] J. Liu. Shannon Wavelet Spectrum Analysis on Truncated Vibration Signals for Machine Incipient Fault Detection. *Measurement Science and Technology*, 23(5):055604, 2012.
- [Mais, 2002] J. Mais. *Spectrum Analysis: the Key Features of Analyzing Spectra*, 2002.
- [Mori *et al.*, 1996] K. Mori, N. Kasashima, T. Yoshioka, and Y. Ueno. Prediction of Spalling on a Ball Bearing by Applying the Discrete Wavelet Transform to Vibration Signals. *Wear*, 195(1-2):162–168, 1996.
- [Nikolaou and Antoniadis, 2002] N.G. Nikolaou and I.A. Antoniadis. Rolling Element Bearing Fault Diagnosis using Wavelet Packets. *NDT & E Int*, 35(3):197 – 205, 2002.
- [Pandya *et al.*, 2012] D.H. Pandya, S. Upadhyay, and S.P. Harsha. ANN Based Fault Diagnosis of Rolling Element Bearing using Time-Frequency Domain Feature. *Int J of Eng Science and Technology*, 4(6):2878–2886, 2012.
- [Paya *et al.*, 1997] B.A. Paya, I.I. Esat, and M.N.M. Badi. Artificial Neural Network based Fault Diagnostics for Rotating Machinery using Wavelet Transforms as a Preprocessor. *Mechanical Systems and Signal Processing*, 11(5):751 – 765, 1997.
- [Peng *et al.*, 2007] Z.K. Peng, F.L. Chu, and P.W. Tse. Singularity Analysis of the Vibration Signals by Means of Wavelet Modulus Maximal Method. *Mechanical Systems and Signal Processing*, 21(2):780–794, 2007.

- [Prabhakar *et al.*, 2002] S. Prabhakar, A.R. Mohanty, and A.S. Sekhar. Application of Discrete Wavelet Transform for Detection of Ball Bearing Race Faults. *Tribology Int*, 35(12):793 – 800, 2002.
- [Purushotham *et al.*, 2005] V. Purushotham, S. Narayanan, and S.A.N. Prasad. Multi-Fault Diagnosis of Rolling Bearing Elements using Wavelet Analysis and Hidden Markov Model based Fault Recognition. *NDT & E Int*, 38(8):654 – 664, 2005.
- [Rafiee *et al.*, 2010] J. Rafiee, M.A. Rafiee, and P.W. Tse. Application of Mother Wavelet Functions for Automatic Gear and Bearing Fault Diagnosis. *Expert Systems with Applications*, 37(6):4568 – 4579, 2010.
- [Randall, 2011] R.B. Randall. *Vibration-based Condition Monitoring: Industrial, Aerospace and Automotive Applications*. EBL-Schweitzer. John Wiley & Sons, 2011.
- [Rathbone, 1939] T.C. Rathbone. Vibration Tolerance. *Power Plant Engineering*, 43(1939):721–724, 1939.
- [Scheffer and Girdhar, 2004] Cornelius Scheffer and Paresh Girdhar. *Practical machinery vibration analysis and predictive maintenance*. Elsevier, 2004.
- [Shi *et al.*, 2004] D.F. Shi, W.J. Wang, and L.S. Qu. Defect Detection for Bearings using Envelope Spectra of Wavelet Transform. *J of Vibration and Acoustics*, 126(4):567–573, 2004.
- [Smith and Randall, 2015] Wade A Smith and Robert B Randall. Rolling element bearing diagnostics using the case western reserve university data: A benchmark study. *Mechanical Systems and Signal Processing*, 64:100–131, 2015.
- [Tse and Leung, 2010] P.W. Tse and C.T. Leung. *Advanced System For Automatically Detecting Faults Occurring in Bearings*. Nova Science Publishers, 2010.
- [Tse *et al.*, 2001] P.W. Tse, Y.H. Peng, and R. Yam. Wavelet Analysis and Envelope Detection for Rolling Element Bearing Fault Diagnosis Their Effectiveness and Flexibilities. *J of Vibration and Acoustics, Trans of the ASME*, 123:303–10, 2001.
- [Tse *et al.*, 2004] P.W. Tse, W.X. Yang, and H.Y. Tam. Machine Fault Diagnosis through an Effective Exact Wavelet Analysis. *J of Sound and Vibration*, 277(4):1005–1024, 2004.
- [Wang *et al.*, 2011] S. Wang, W. Huang, and Z.K. Zhu. Transient Modeling and Parameter Identification Based on Wavelet and Correlation Filtering for Rotating Machine Fault Diagnosis. *Mechanical Systems and Signal Processing*, 25(4):1299 – 1320, 2011.

- [Yan and Gao, 2005] R. Yan and R.X. Gao. An Efficient Approach to Machine Health Diagnosis based on Harmonic Wavelet Packet Transform. *Robotics and Computer-Integrated Manufacturing*, 21(4-5):291–301, 2005.
- [Yan and Gao, 2011] R. Yan and R.X. Gao. Wavelet Domain Principal Feature Analysis for Spindle Health Diagnosis. *Structural Health Monitoring*, 10(6):631–642, 2011.
- [Yan *et al.*, 2014] R. Yan, R.X. Gao, and X. Chen. Wavelets for Fault Diagnosis of Rotary Machines: A Review with Applications. *Signal Processing*, 96:1–15, 2014.
- [YanPing *et al.*, 2006] Z. YanPing, H. Shuhong, H. Jinghong, S. Tao, and L. Wei. Continuous Wavelet Grey Moment Approach for Vibration Analysis of Rotating Machinery. *Mechanical Systems and Signal Processing*, 20(5):1202–1220, 2006.
- [Zhang and Gao, 2004] L. Zhang and R.X. Gao. Customized Wavelet for Bearing Defect Detection. *J of Dynamic Systems, Measurement, and Control*, 126:740–745, 2004.
- [Zhang *et al.*, 2005] L. Zhang, R.X. Gao, and K.B Lee. Wavelet-based Enveloping for Spindle Health Diagnosis. In *Instrumentation and Measurement Technology Conf, 2005. Proc of the IEEE*, volume 2, pages 1203–1208, 2005.
- [Zhang *et al.*, 2006] L. Zhang, R.X. Gao, and K.B. Lee. Spindle Health Diagnosis based on Analytic Wavelet Enveloping. *IEEE Trans on Instrumentation and Measurement*, 55(5):1850–1858, Oct 2006.
- [Zhu *et al.*, 2009] Z.K. Zhu, R. Yan, L. Luo, Z.H. Feng, and F.R Kong. Detection of Signal Transients based on Wavelet and Statistics for Machine Fault Diagnosis. *Mechanical Systems and Signal Processing*, 23(4):1076–1097, 2009.

Appendix A

Acronyms Definition

Table A.1: Acronyms Definitions

<i>Acronyms</i>	<i>Definition</i>	<i>Acronyms</i>	<i>Definition</i>
ANN	Artificial Neural Network	AWT	Analytic Wavelet Transform
BPFI	Ball-Passing Frequency Inner-Race	BPFO	Ball-Passing Frequency Outer-Race
BPFR	Ball-Passing Frequency Roller	BS	Bent Shaft
BSF	Ball Spin Frequency	C	Cage
CO	Combined Defects	CWT	Continuous Wavelet Transform
DWT	Discrete Wavelet Transform	EEMD	Ensemble Empirical Mode Decomposition
EMA	Exponential Moving Average	ESER	Energy to Shanon Entropy Ratio
EWA	Exact Wavelet Analysis	EWT	Empirical Wavelet Transform
FDC	Fisher Discriminant Criterion	FEM	Finite Element Model
FFT	Fast Fourier Transform	FTF	Fundamental Train Frequency
HHT	Hilbert Huang Transform	HMM	Hidden Markov Models
HSM	High Speed Machining	HW	Harmonic Wavelet
ICD	Intrinsic Characteristic-scale Decomposition	IFFT	Inverse Fast Fourier Transform
IMF	Intrinsic Mode Function	IR	Inner Race
ITD	Intrinsic Time Decomposition	K-S	Kolmogorov-Smirnev
MA	MisAlignment	MEC	Maximum Energy Criterion
MFCC	Mel Frequency Complex Ceptrum	ML	Mechanical Looseness
MLP	Multiplayer Perception	MSEC	Minimum Shannon Entropy Criterion
OMA	Operational Modal Analysis	OR	Outer Race
PFA	Principal Feature Analysis	PSD	Power Spectral Density

Table A.1: Acronyms Definitions (Continued)

<i>Acronyms</i>	<i>Definition</i>	<i>Acronyms</i>	<i>Definition</i>
QFWT	Q Factor Wavelet Transform	RBF	Radial Basis Functions
RE	Rolling Element	SCS	Sparse Code Shrinkage
SGWT	Second Generation Wavelet Transform	SSA	Statistical Signal Analysis
STFT	Short Time Fourier Transform	SVM	Support Vector Machine
UB	UnBalance	WGM	Wavelet Grey Moment
WGMV	Wavelet Grey Moment Vector	WPT	Wavelet Packet Transform
WT	Wavelet Transform	WTMM	Wavelet Transform Modulus Maxima
WVD	Wigner-Ville Distribution	f_s	Sampling Frequency
SNR	Signal to Noise Ratio	KR	Kurtosis \times RMS
IMS	Intelligent Maintenance System	CWRU	Case Western Reserve University
RI	Rub Impact System	OW	Oil Whipping

Appendix B

IMS Data selection

IMS dataset is studied to differentiate in which test begins to appear the faults and the acquisition channel with more information about them.

Table B.1: IMS bearing bata structure

Set number	1
<i>Recording Duration:</i>	October 22, 2003 12:06:24 to November 25, 2003 23:39:56
<i>No. of Files:</i>	2,156
<i>No. of Channels:</i>	8
<i>Channel Arrangement:</i>	Bearing 1 Ch 1&2; Bearing 2 Ch 3&4; Bearing 3 Ch 5&6; Bearing 4 Ch 7&8.
<i>File Recording Interval:</i>	Every 10 min(except the first 43 files were taken every 5 min)
<i>Description:</i>	At the end of the test-to-failure experiment, inner race defect occurred in bearing 3 and roller element defect in bearing 4.
Set number	2
<i>Recording Duration:</i>	February 12, 2004 10:32:39 to February 19, 2004 06:22:39
<i>No. of Files:</i>	984
<i>No. of Channels:</i>	4
<i>Channel Arrangement:</i>	Bearing 1 Ch 1; Bearing 2 Ch 2; Bearing 3 Ch3; Bearing 4 Ch 4.
<i>File Recording Interval:</i>	Every 10 min
<i>Description:</i>	At the end of the test-to-failure experiment, outer race failure occurred in bearing 1.

B.1 Identification and categorization of the bearing faults

According to [Li *et al.*, 2017], the *Kurtosis* index is employed to reflect the degradation process over its whole life, when it is present an abruptly increase in the index the bearing has a defect. The results are presented in the Fig B.1 - B.3 where can be seen that the early stage faults are present approximately since the test 1800, 700 and 1,400 for the *IR*, *OR* and *RE* respectively, (for this thesis will be select tests close to these points).

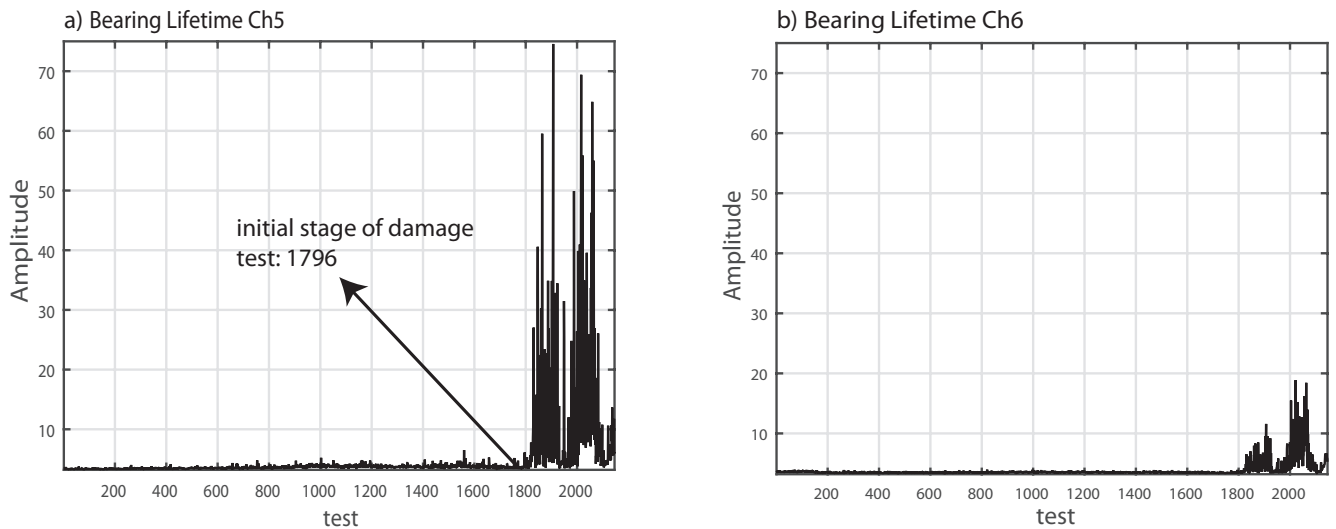


Figure B.1: *Kurtosis* values for the bearing with *IR* at the end of its useful life. a) Channel 5, b) Channel 6

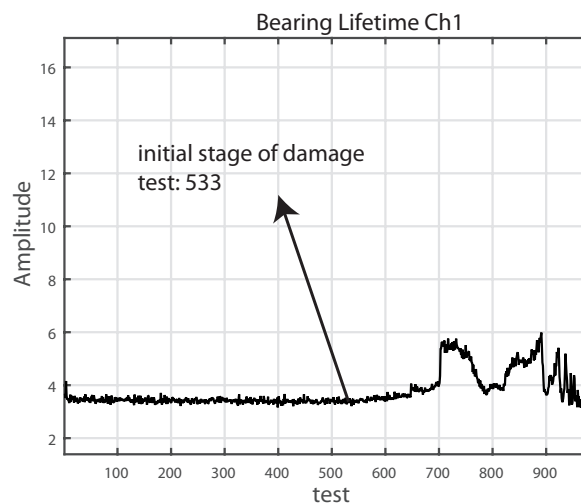


Figure B.2: *Kurtosis* values for the bearing with *OR* fault at the end of its useful life

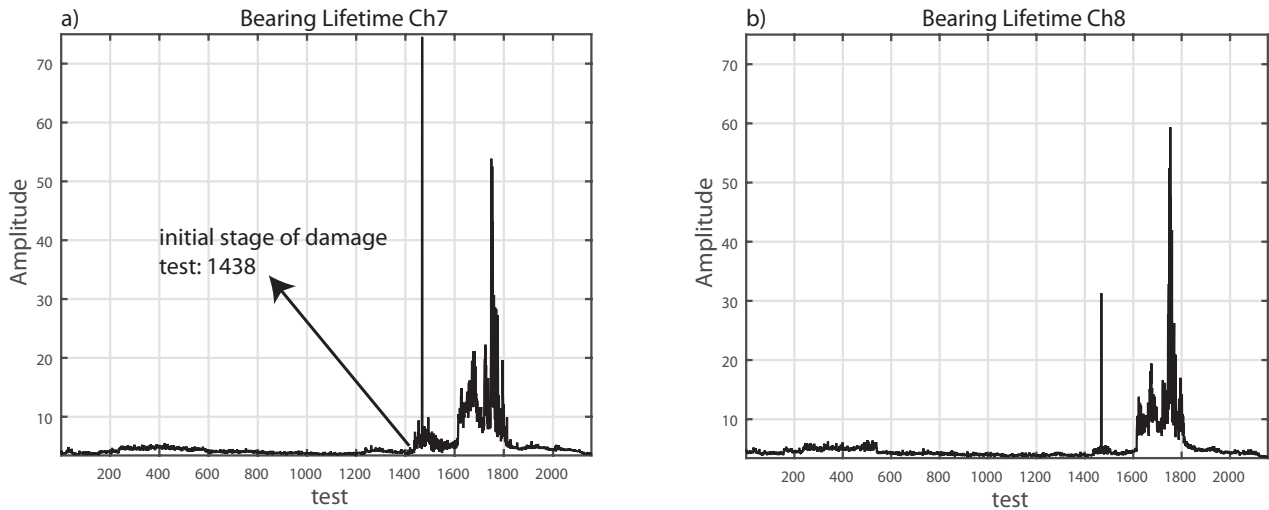


Figure B.3: *Kurtosis* values for the bearing with *RE* fault at the end of its useful life. a) Channel 7, b) Channel 8

By examining the *Kurtosis*, a signal in which the value of *Kurtosis* starts to rise will be selected as an early stage fault, the critical fault signal is selected as the last signal before the test stoppage; and the medium fault signal is an intermediate signal between the early and the critical signal. The selected tests are summarized in the Table B.2. For the selection were considered the signals that were recorded with a shaft speed of 2,000 RPM; although the information collected from the *IMS* states that all the recordings were performed at the same speed, it was observed that many of the speeds in certain recordings oscillated between 1,800-2,000 RPM.

Table B.2: Number of the selected tests

<i>Fault</i>	<i>Test for early stage fault</i>	<i>Test for medium stage fault</i>	<i>Test for critical stage fault</i>
<i>IR</i>	1,820	1,990	2,140
<i>OR</i>	533	758	979
<i>RE</i>	1,500	1,820	2,100

B.2 Initial considerations

The signals from the *IMS* dataset have a lot of white noise and unknown peaks that are possibly caused by other types of faults. These peaks are best evidenced in the stages where the fault is critical. To corroborate that the mentioned peaks and the noise do not belong to the fault or any of its harmonics, signals before the appearance of the fault were analyzed, when the bearings were in

the best conditions Fig, B.4.

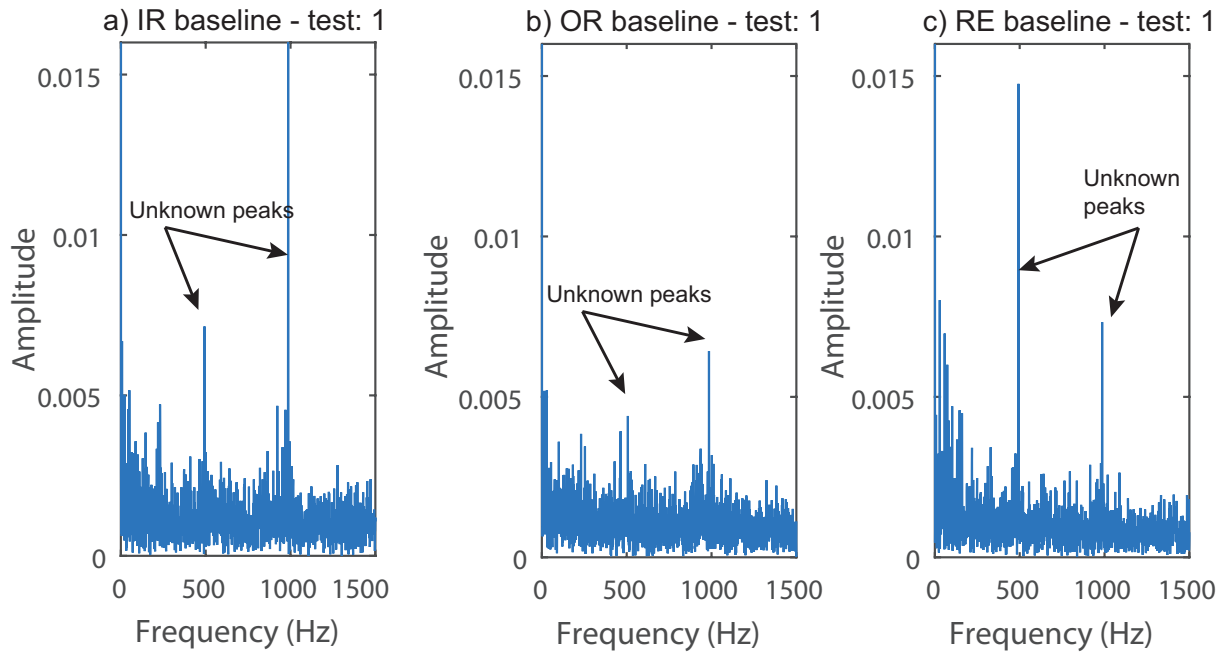


Figure B.4: Frequency spectrum of the signal envelope of a signal at the beginning of the tests

The unknowns peaks are present in the three baselines, they are not in function of any of the frequencies of failure or of the speed, they are two peaks in the frequencies of 500 and 1,000 Hz, that can be due to an electrical noise. For the moment as it does not belong to any harmonic of the fault frequencies will be considered as noise. Furthermore, in all the signals there is white noise (random peaks at different frequencies).

There are several remarkable points that can be observed in the behavior of the original *IMS* signals. As the category of the fault increases, the vibration peaks also increase, this statement is observed more clearly in the signals with *OR* faults. In addition, the 9 signals are immersed in a noise especially the signals of the *IR* and *RE* faults, in which the peaks are not distanced the fault frequency, and finally all the signals have an offset that affects the signal processing (if it is not removed).

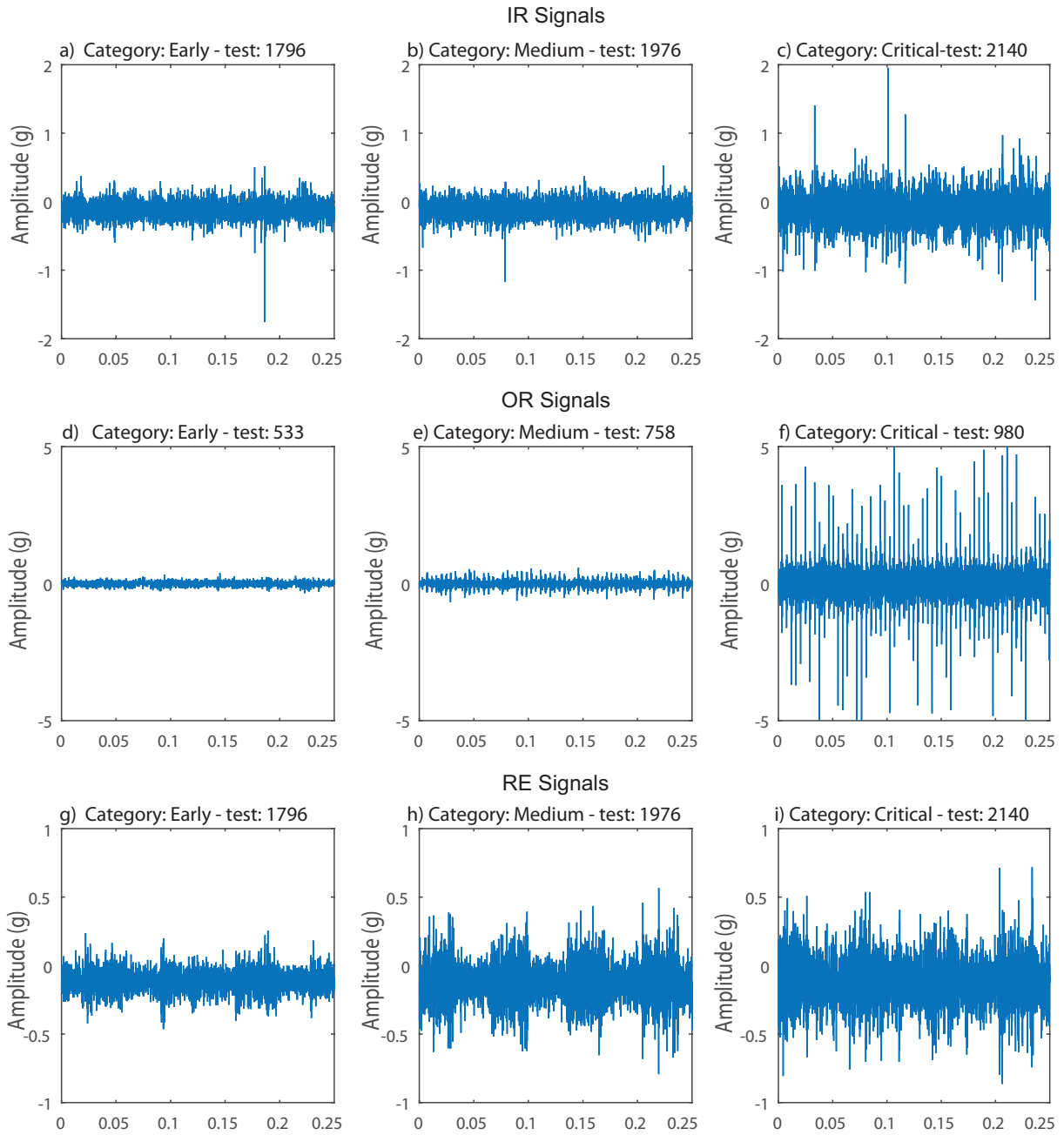


Figure B.5: Considered signals from *IMS* database

Appendix C

Parameters Selection

The parameters for the proposed methodology were analyzed, they include the ideal wavelet, the statistical method and the threshold for the reconstruction. The *MW* was selected taking into consideration computing time and frequency resolution, for the case of the statistical indicator, the most used were compare to know which one correctly detects the desired frequencies and its robustness in the presence of noise. Finally, different thresholds were based on a relation between the energy and nodes to magnify the important nodes.

C.1 Wavelet Transform

There are different types of the *WT* such as: *CWT*, *DWT*, *WPT*, *EWA*, *AWT* and *SGWT* [Yan *et al.*, 2014], in the reviewed articles it can be observed that each transform has its advantages; but, it is not yet known which predominates among the others for the detection of this type of faults. Same applies to *MW*, the use of them goes from fix wavelets such as *Symlets* or *Morlets* until adaptives wavelets [Kedadouche *et al.*, 2016a], [Cui *et al.*, 2016]. Among the diverse transforms *CWT*, *DWT* and *WPT* were selected to find out which one has better performance for the problem. They were based in computing time and time-frequency resolution.

As the condition monitoring demands real-time results, the computing time is important for the choice of the kind of transformation, for that reason, the transform with the lowest computing time it is considered as the most adept for the method where the computing time is the time it takes for the signal to be decomposed. As the bearing fault excites high frequencies and the *UB* low frequencies, it is said the transform that contains a good frequency accuracy in all range is best suited for the problem. It should be noted that the resolution in frequency of a *WT* is not equal to the one generated by the *FFT*, where the latter causes its resolution to go from 1 Hz to $f_s/2$ with a 1 Hz interval. The *WT* has an interval that depends on the *MW*, so in most cases it is greater than 1 Hz and it may contain a whole frequency range, which can be very large and important information

will be lost.

C.1.1 Computing time

The time is calculated by measuring the duration it takes the signal to be decomposed to a same level, to perform it was used the tic-toc function in *MATLAB* which only evaluates the time of the selected code. The runtime results are presented in the Table C.1, where it is showed that the *DWT* is fastest among the others followed by the *WPT* considering *CWT* as reference which consumes many computational resources and makes it the less useful for our purpose.

Table C.1: Decomposition time of each *WT*

<i>Wavelet Transform</i>	<i>% Time respect to CWT</i>
<i>DWT</i>	31.12%
<i>WPT</i>	52.3%
<i>CWT</i>	100 %

C.1.2 Frequency Resolution

To evaluate the time-frequency resolution of each transform, it was a selected a bearing signal with *OR* fault from the *CWRU* dataset where the frequency sampling is 12,000 Hz. It was analyzed with the wavelet *db44* and decomposed until the 32 scale for the case of the *CWT* and level 5 for the *DWT* and the *WPT*, Fig C.4. Taking into consideration the frequency sampling and the Nyquist theorem, the maximum frequency that can be reconstructed is $f_s/2$ for all the transforms including the *FT*. The frequency resolution for each *WT* states as follows:

The *CWT* decomposes the signal according to the scales; for the case of the *db44*, its scale-pseudo frequency behavior is presented in the Fig. C.1 where the frequency range varies with scale. At lower scales the delta frequency is high and in higher scales the delta frequency is low, this means the resolution is low at high frequencies, but good at low frequencies. It was previously mentioned, it is important a good resolution in high frequencies for the case of bearing faults.

At the level n , the *DWT* returns $n + 1$ coefficients, for the studied case, when the level is $n = 5$ the number of coefficients reach up to 6, each one of them acts as a filter, where the first range starts at $F_c = f_s/(2 \times 2^n)$ and the subsequent ones contain a greater frequency, Fig C.2.

The frequency resolution rises as the level increases, but only at low frequencies, in the case of bearings faults where the high frequencies are important [Tse and Leung, 2010], the information is lost, if it is desired to analyze the range from 1.5 to 6 KHz the values will be uncertain, Fig C.4.

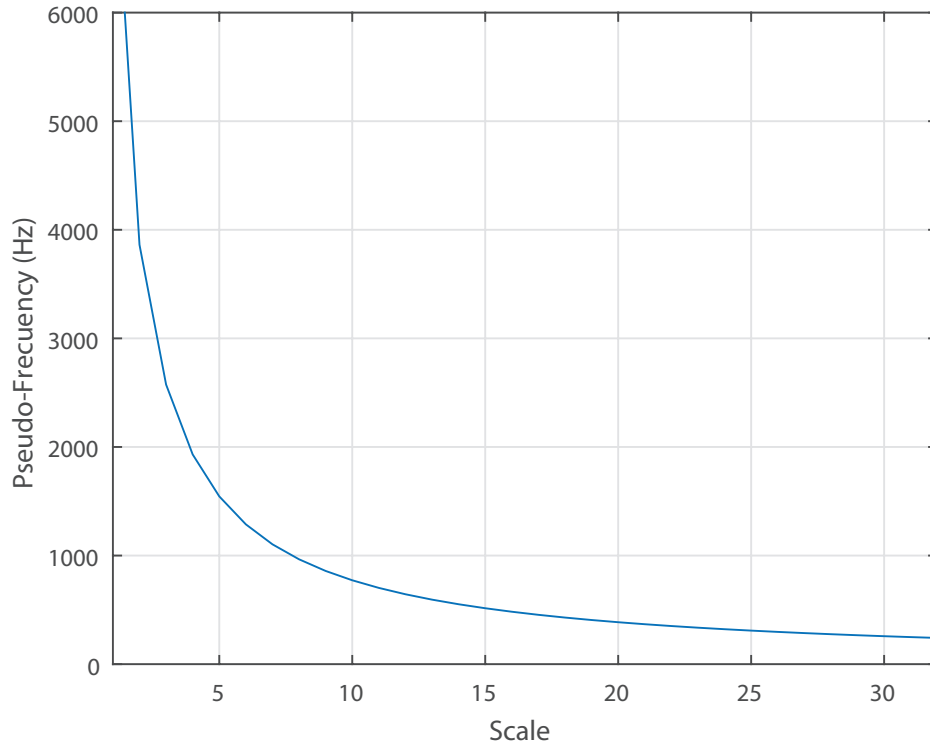


Figure C.1: Scale-Frequency relation of the *MW db44*

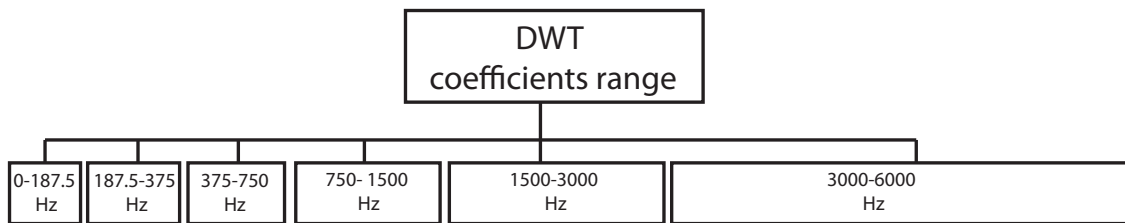


Figure C.2: Frequency range for each *DWT* coefficient of a signal sampled at 12,000 Hz

With $n = 5$, the *WPT* has the same frequency resolution of 187.5 Hz, not only in low frequencies; but, also in high frequencies, Fig C.3. The decomposition occurs in both detail and approximation coefficients which gives 32 frequency divisions in the scalogram, Fig. C.4.

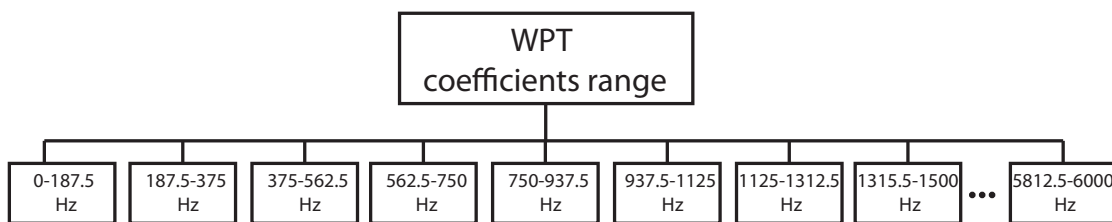
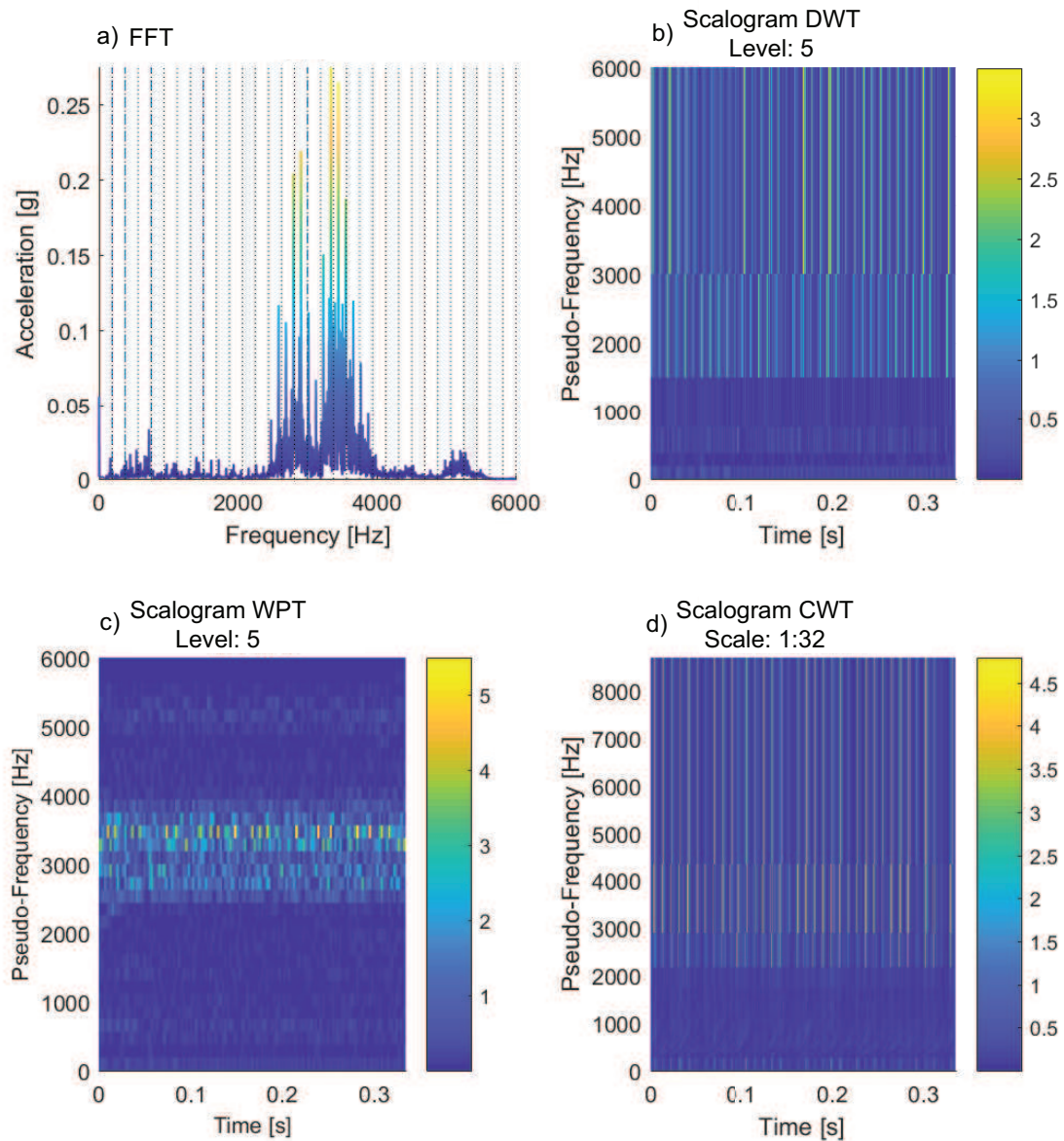


Figure C.3: Frequency range for each *WPT* coefficient of a signal sampled at 12,000 Hz

Figure C.4: *OR* fault decomposition

The *CWT* delays more than the others and does not have good resolution at high frequencies, the *DWT* is faster than the others, but it has a poor resolution in high frequencies; and the *WPT* has a balance between computing time and frequency resolution, by using it, the method is capable of detect faults at low and high frequencies. For this reason, *WPT* was the chosen transform for the methodology.

C.2 Statistical method

Several methods were reviewed to distinguish which coefficients belong to a fault and which are noise. There are several methods to select and detect faults in the bearings, the statistical methods presented are based on a change in the signal caused by the shock of the fault on the track, where the distribution is modified.

To evaluate the performance of the proposed method, it is necessary to know that frequency ranges correspond to the failures of a bearing. The most common methods for detecting faults applied to the coefficients from the *WT* were studied: *RMS*, *Kurtosis Spectral*, *Skewness* and *KR*. Additionally, it was considered to analyze the crest factor and the standard deviation to have a more global view about its behavior to a signal with faults in the bearing.

- **Kurtosis** and **Spectral Kurtosis** are mathematical tools used for fault detection, the *Kurtosis* does not need a trend over time which makes it a reliable for bearing health indicator:

$$Kurtosis = \frac{1}{n} \sum_{i=1}^n \left(\frac{x_i - \mu}{\sigma} \right)^4 \quad (C.1)$$

where μ represents the average, σ the standard deviation and n the number of sample. When the *Kurtosis* is applied in each frequency band is called *Spectral Kurtosis*. It was based in the *STFT* and it is used in the *WPT* to determine which frequency bands contain a signal of maximum impulsivity.

- **Root Mean Square (RMS)** is one of the most common vibration indicators, it characterizes the intensity of a signal:

$$RMS = \sqrt{\frac{1}{n} \sum_{i=1}^n x_i^2} \quad (C.2)$$

where n is the number of samples.

- **Skewness** is a measure of the asymmetry of the probability distribution of a signal about its mean. The value can be positive, negative or undefined:

$$Skewness = \frac{1}{n} \sum_{i=1}^n \left(\frac{x_i - \mu}{\sigma} \right)^3 \quad (C.3)$$

If the computed value of *Skewness* is negative the curve is shifted to the left and if that value is positive the curve is shifted for the right. If it is null, the curve is perfectly symmetric.

- **Standard deviation** (σ) quantifies the amount of variation or dispersion of a set of data values:

$$\sigma = \sqrt{\frac{1}{n} \sum_{i=1}^n (x_i - \mu)^2} \quad (C.4)$$

- **Peak Value** is the maximum value in a signal, usually when the peak value is large, it means there is a fault and as its amplitude increases, the fault becomes larger. It can be said that if the signal is immersed in noise, this value can be affected and generate errors in the detection

$$Peak\ value = \max(x) \quad (C.5)$$

- **Crest factor** is defined as the ratio of *Peak Value* and *RMS*. As a localized fault develops, the resulting short burst increases the peak level, but it has little influence on the *RMS* value.

$$Crest\ factor = \frac{Peak\ value}{RMS} \quad (C.6)$$

A negative aspect that presents the crest factor, in the same way as *Kurtosis* lies in the fact that it is very sensitive to noise.

- **KR=(Kurtosis × RMS)** is an indicator proposed by [Tse and Leung, 2010], as the fault increases the *kurtosis* is amplified:

$$KR = Kurtosis \times RMS \quad (C.7)$$

Kurtosis is a measure of impulsiveness in the context of fault detection for rotating components; however, with the presence of noise, this value get modified and may lead to incorrect diagnosis, in consequence, it is used together with *RMS* which detect the energy of the coefficients and therefore the maximum values of this multiplication indicates the frequency range where the fault is located .

- **Energy coefficient** is the amplitude of a value, in the case of wanting to know the energy of a set, each value is summed:

$$Energy = \sum_{i=1}^n x_i^2 \quad (C.8)$$

To know which indicator works for the method, all of them were studied in cases with a clear defect and were compared with the *FT* to know the bands where the fault of the bearing resounds. The high frequencies are those that have information of the fault since it excites the resonances of the bearing. As the decomposition works like a filter bank, the indicator will show which frequency ranges are the most important for the posterior reconstruction of the signal. The used signal for this test corresponds to an easily detectable external fault with low noise [Smith and Randall, 2015].

Firstly, the frequency spectrum is computed by the *FT* to verify that the high frequencies are the ones with the highest energy and have it as an indicator where this energy is presented Fig. C.5.

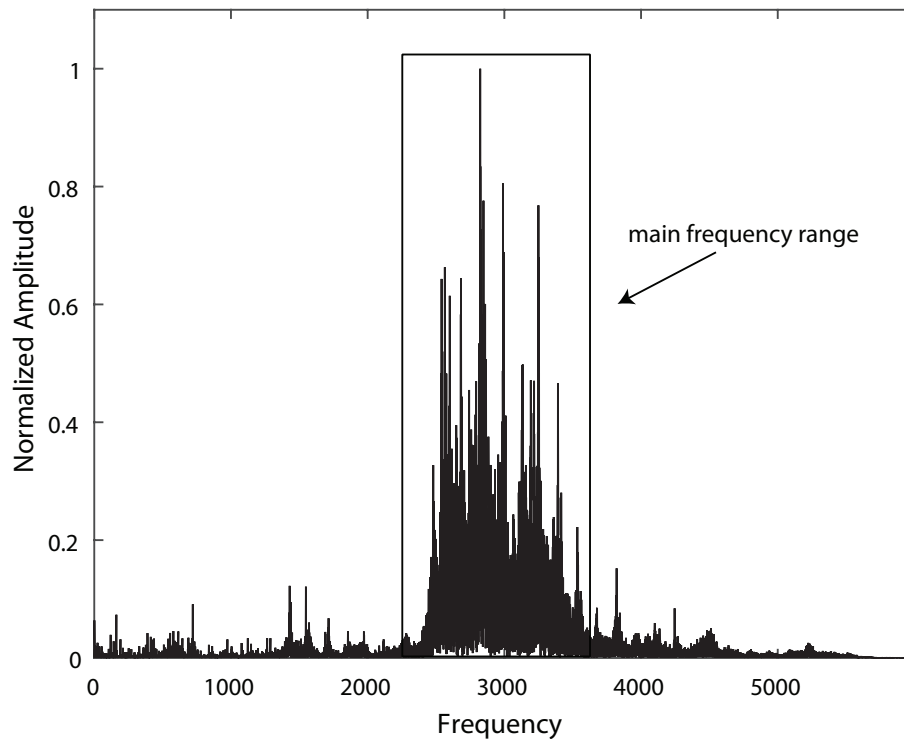
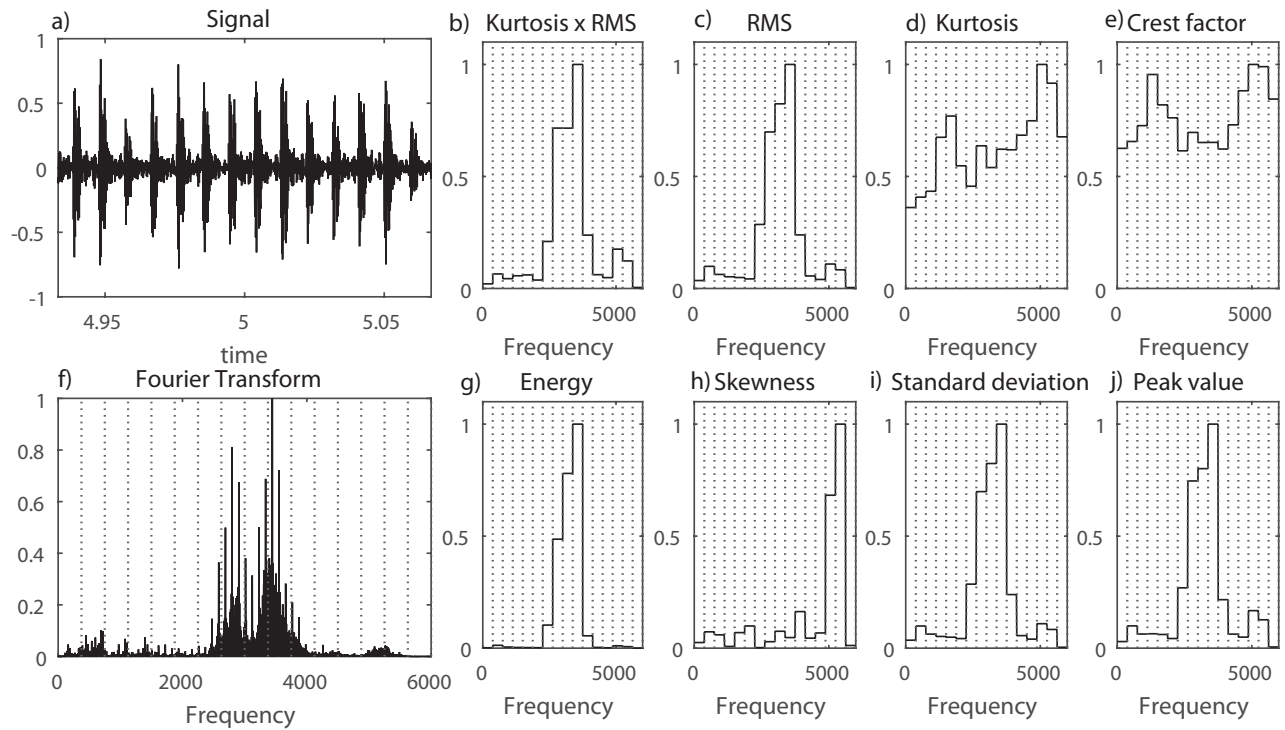
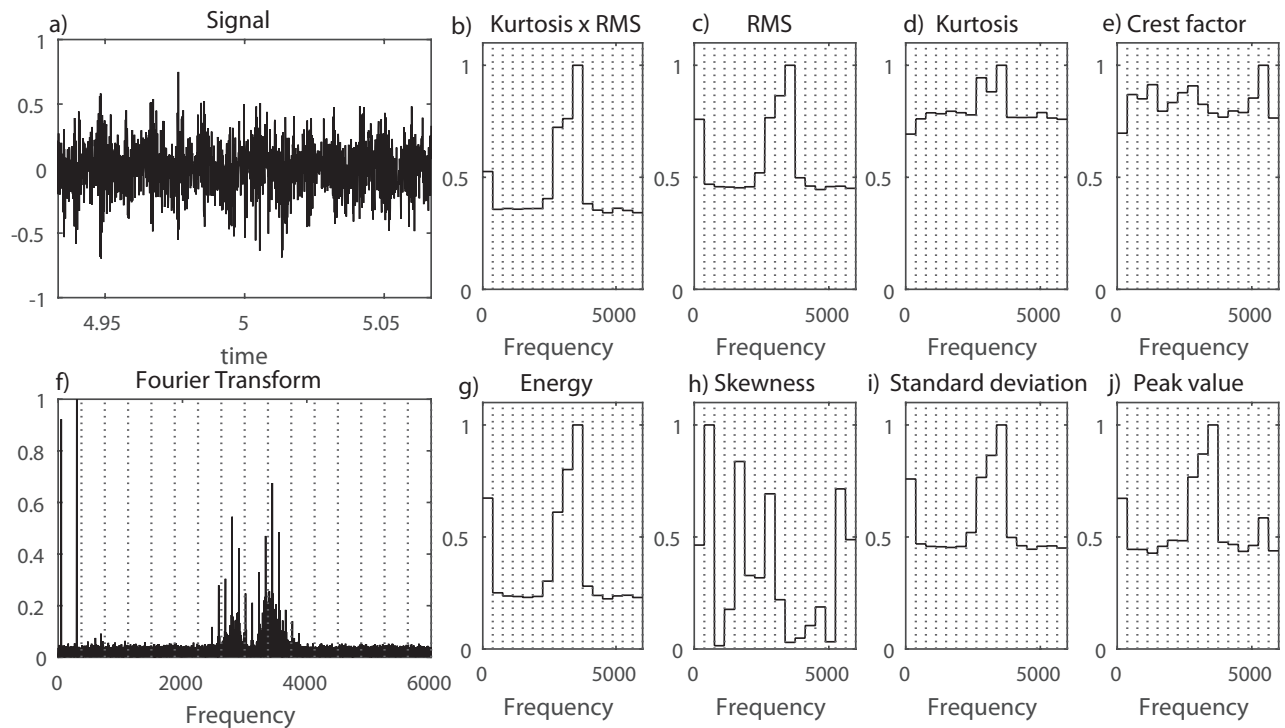


Figure C.5: Frequency spectrum for a noise-free signal with an outer race fault

A decomposition was performed using *WPT* with a *MW dmey* at a level 4. The result throws coefficients with a length in frequency of 16, each one of these new frequencies group contemplates the information of a whole range, for the studied case as the original signal has a frequency sampling of 12,000 Hz each one of the coefficients covers 375 Hz.

The 16 ranges were analysed using the statistical methods previously mentioned. The results were normalized to detect easily which indicator exalts the main frequency range and at the same time discriminates to the frequencies with little information about the fault, Fig. C.6. An additional test is performed to determine the robustness of the indicators. *Gaussian* noise is added to the signal and sine waves with high amplitudes at low frequencies Fig. C.7.

Reviewing the results provided by the statistical indicators, it is determined that *Skewness* is the method less indicated to detect the faults, since in both tests it does not choose the range of the fault. The *Crest Factor* behaves similarly to *Kurtosis* in the original signal but when there is noise, *Kurtosis* outperforms because it has high values in the frequency range of the bearing fault. The *RMS* value, *KR*, *Peak Value*, *Standard deviation* and *Energy* have a similar behavior when the signal has no noise and all of them detect the range fault. In contrast, when there is noise, especially at low frequencies (specifically sinusoidal signals), *KR* behaves better because it

Figure C.6: Statistical parameter applied to an *OR* fault signalFigure C.7: Statistical parameter applied to an *OR* fault signal with a $SNR = 1$ and two sinusoidal signals of 300 Hz and 50 Hz

decreases the peak that does not belong to a bearing fault, this effect can be observed in the first frequency range. Additionally, it must be remarked the noise modifies the results making it more difficult to know the expected ranges.

It is concluded that using *RMS* value, *KR*, *Peak Value*, *Standard deviation* and *Energy* as indicator is plausible when the signal does not have any type of noise. If there is noise and the signal is present to another type of fault, *KR* is the best indicator.

As the tests were only for evaluated for *OR* faults, it was performed an additional analysis amplifying the noise at low frequencies and adding 4 new indicators: *Kurtosis* \times *Energy*, *Shannon Entropy*, *Kurtosis* \times *RMS* \times *Shannon* and *Kurtosis* \times *Peak Value*.

To evaluated them was selected the following criterion: which indicator shows a high value at the important frequency range (the 7th to 10th node for the *CWRU* database) and at the same time has a low value in the rest frequency range, the relation stays as follows:

$$Relation = \frac{\text{mean value of the important nodes}}{\text{mean value of the rest of nodes}} \quad (C.9)$$

The calculation was made for each of the methods presented, the results are shown in the Fig.C.8 and more visually in the Fig. C.9-C.13.

By reviewing the results, specifically the bar chart, it can be seen the new added parameters have good relation for detecting the main frequency range. However, the best parameter depends on the fault and the noise conditions. When the signal is not tainted by any type of fault, those which behave better are: *Kurtosis* \times *Energy*, *Skewness* and *Kurtosis* \times *Shannon* \times *Energy*. Nonetheless, the rest of indicator except for the kurtosis and Shannon Entropy give acceptable results, Fig. C.9-C.11. The suitable among the two depend on the type of the fault: for this studied case, when the fault belongs to an *OR* or *RE* fault, the most effective is the proposed indicator *Kurtosis* \times *Energy*. For the signal with *IR* fault, the one that best suits is the combination *Kurtosis* \times *Shannon* \times *Energy*.

The noisy signals have a different behaviour, there is not any indicator that surpass the others and the results depend of the type of fault. In the signal with *OR* fault, the simplest have the same result as the *KR* and the indicators that predominated when there was no noise are opaque. For the rest of the cases (*IR* and *RE*), the results are different which indicates there is not a single indicator that works in the best way for all cases. But the results shows the presented methods have the best results. This means the use of this new indicators may be useful for future work, and the best combination among them could generate an indicator that works in all cases with or without noise. As there was not a one indicator that surpass the others in all the cases for future analysis it was use the *KR* as the optimum indicator because of the results gathered before and the results present in the *State of the Art* using this indicator.

Additionally it was observed the *Shannon Entropy* had similar results as the *Kurtosis*, in future research may be considered the possibility to replace the *Kurtosis* for *Shannon Entropy*, because

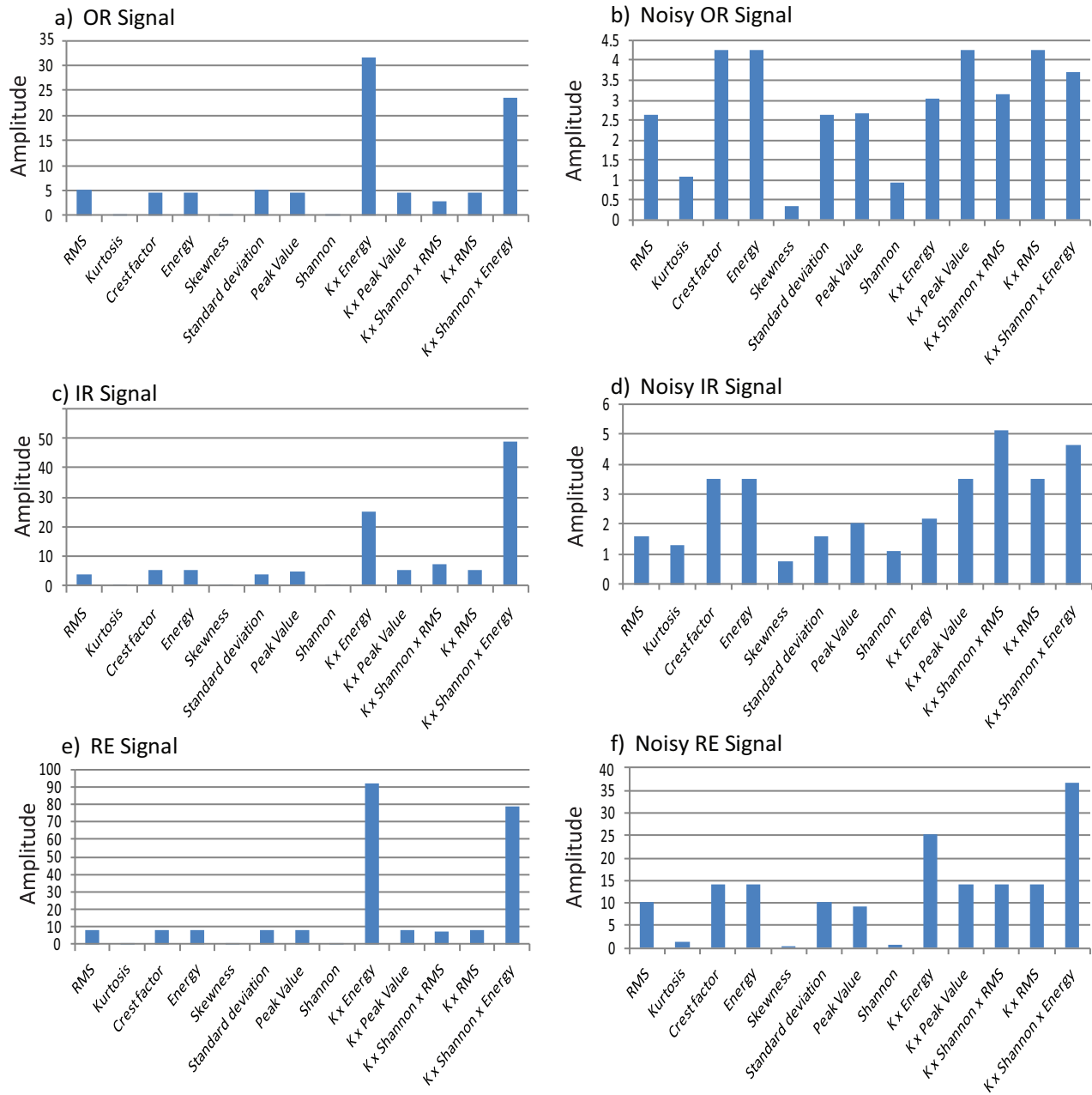


Figure C.8: Comparison of the different indicators

its computing time is faster Fig. C.15.

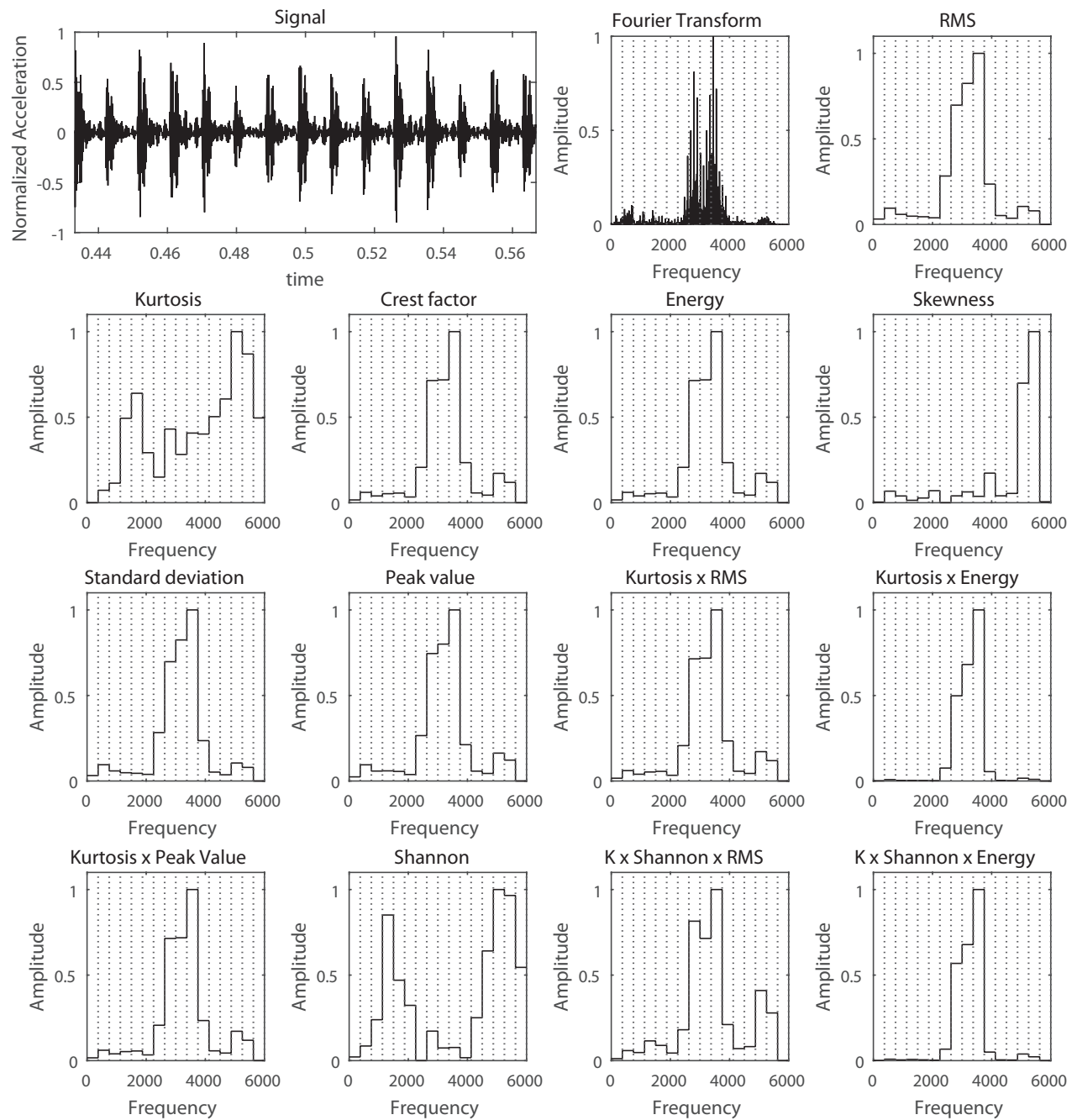


Figure C.9: Parameters applied to an OR fault signal

C.3 Threshold

To calculate the best threshold, there are different parameters such as: standard deviation (σ), quartiles and average (μ), Fig. C.16 :

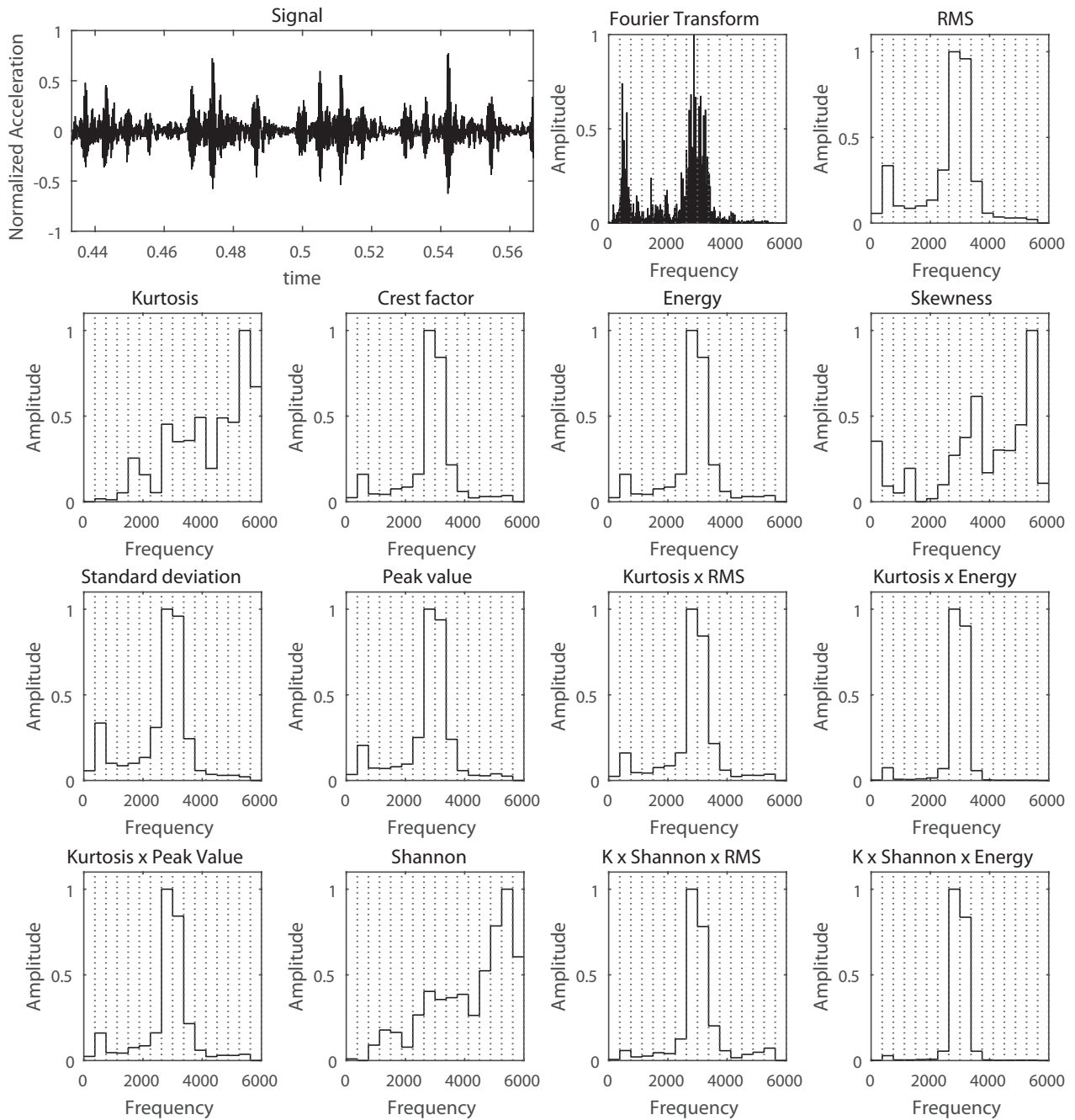


Figure C.10: Parameters applied to an IR fault signal

1. max /maximum node
2. $\mu + 2\sigma$
3. $\mu + \sigma$
4. $\mu + 0.5\sigma$
5. μ
6. $\mu - 0.5\sigma$
7. $\mu - \sigma$
8. $\mu - 2\sigma$
9. min/ all nodes
10. $Q_1 = \frac{1}{4}$ quantile
11. $Q_2 = \frac{1}{2}$ quantile / median
12. $Q_3 = \frac{3}{4}$ quantile

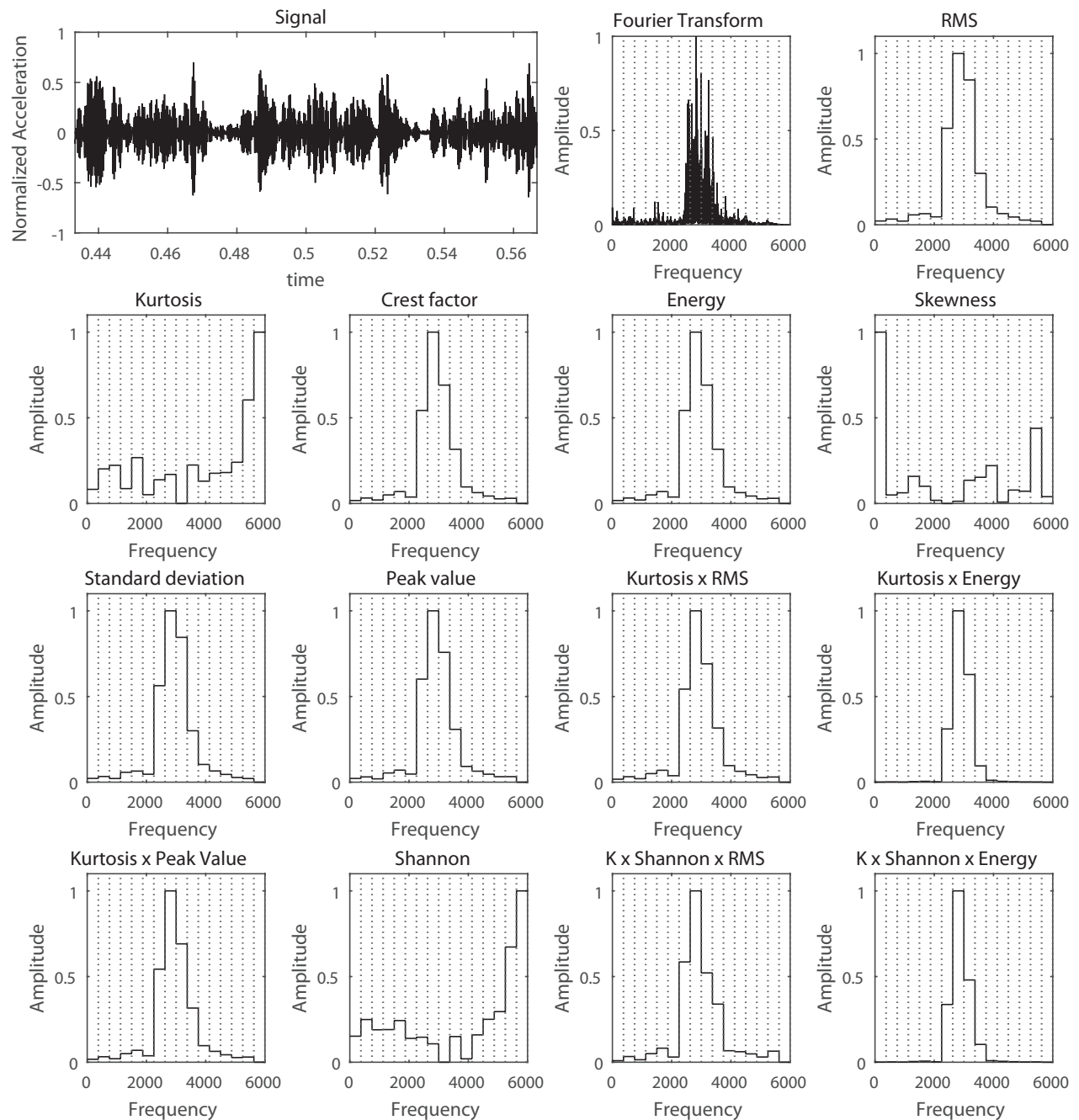


Figure C.11: Parameters applied to an RE fault signal

The thresholds were analysed taking into consideration the number of nodes above the correspond threshold and the contained energy of each of these nodes. The two parameters were compare in a two dimension graph Fig. C.17. At this point it must be chosen the threshold which is closest to maximum energy using the least percentage of nodes. This is obtained by the *Pythagoras Theorem* with a modification taking into consideration the energy must be close to 1, eqn (C.10) The result of this equation would be named (x).

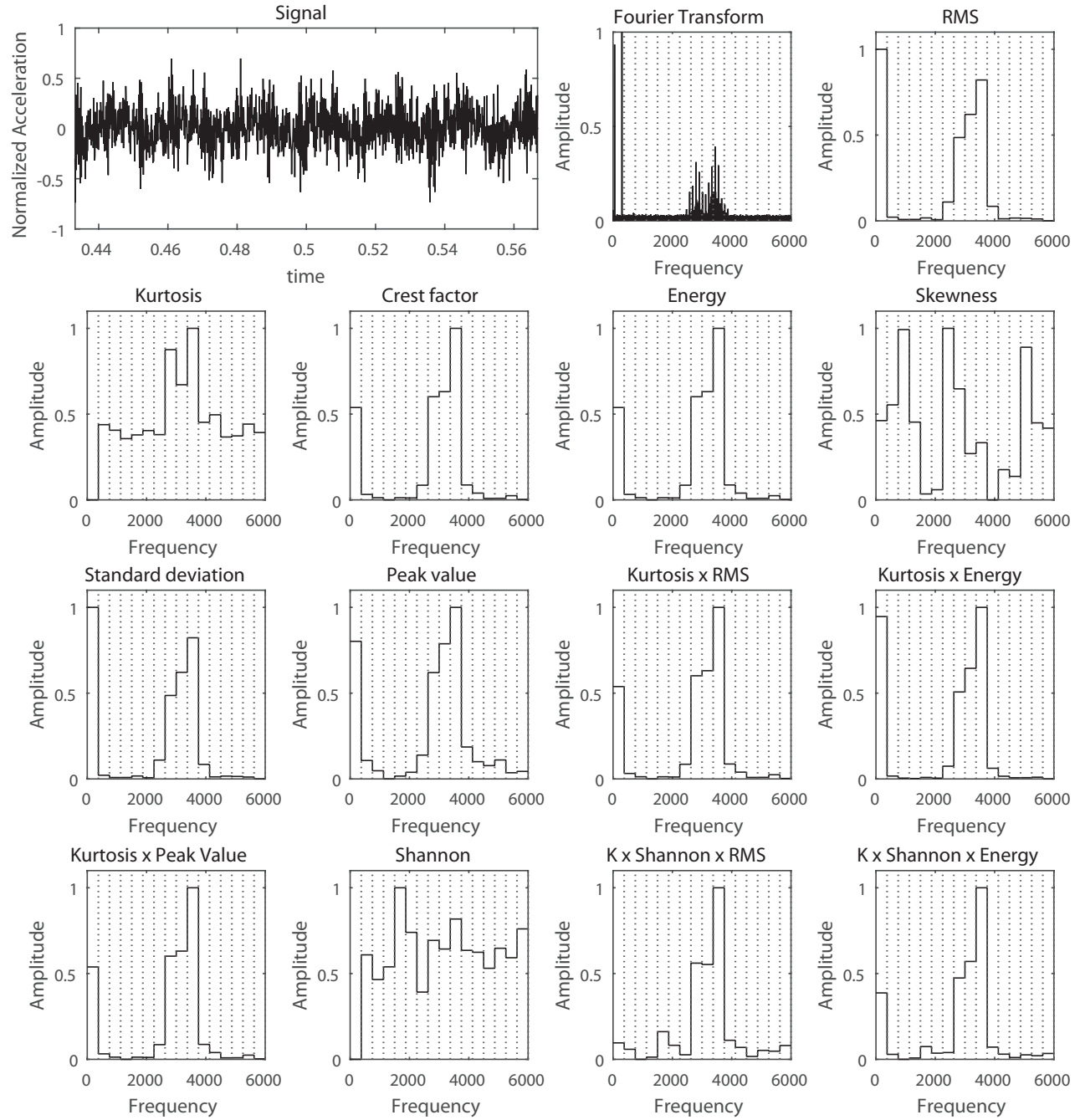


Figure C.12: Statistical parameter applied to an *OR* fault signal with a $SNR = 1$ and two sinusoidal signals of 300 Hz and 50 Hz

$$x = \sqrt{n^2 + (1 - e)^2} \quad (C.10)$$

where n represents the nodes above the threshold and e the sum of the energy of the nodes. The results are shown in the Table C.2.

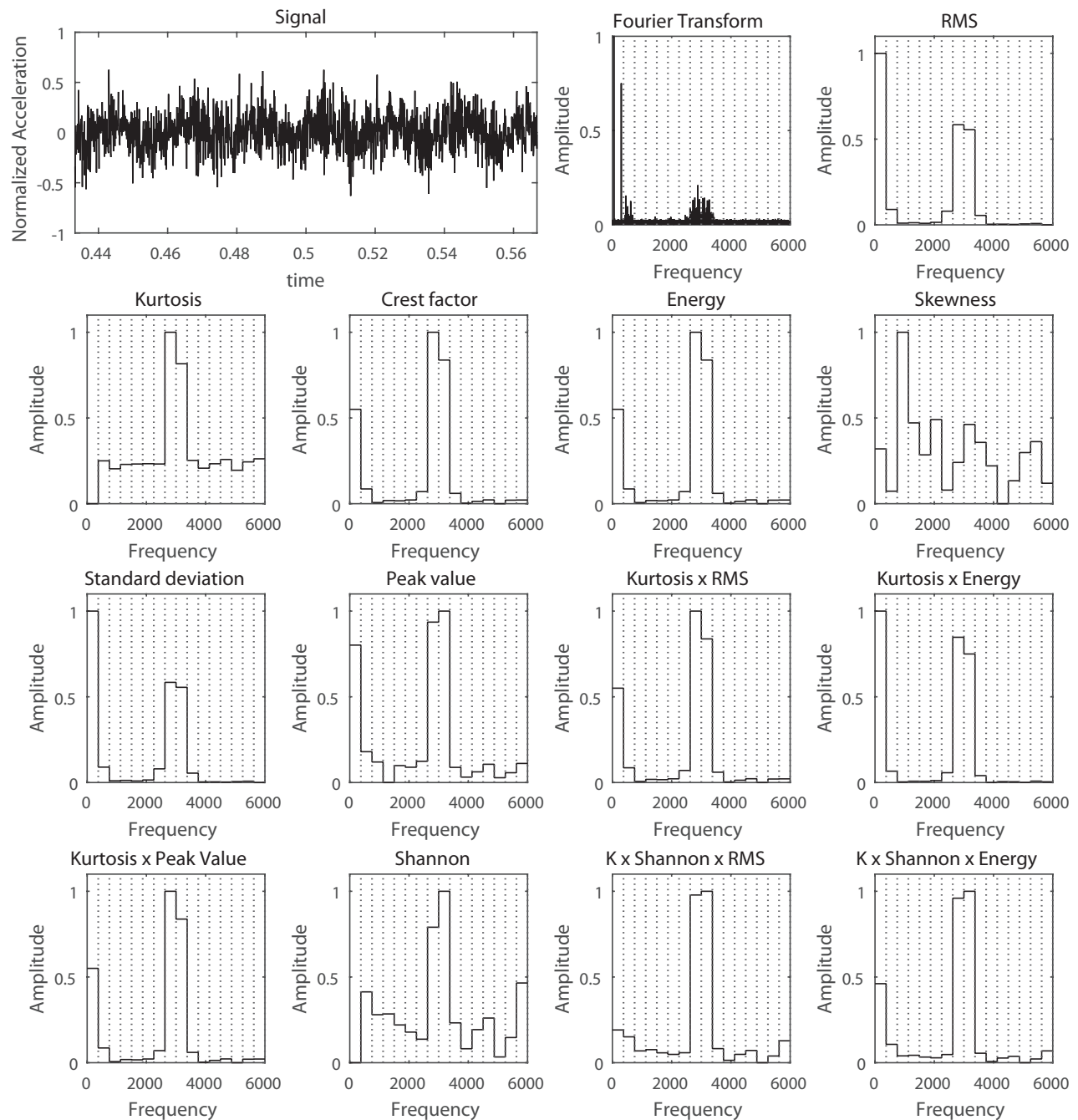


Figure C.13: Statistical parameter applied to an *IR* fault signal with a $SNR = 1$ and two sinusoidal signals of 300 Hz and 50 Hz

When x reaches lowest values, it indicates the threshold has more energy in the smaller number of nodes and thereby is considered as the optimum.

The criterion of energy-nodes indicates for all the presented cases, by using the average (μ) as a threshold generates the best results: it distinguishes the vital nodes from the trivial ones, as a matter of fact the relation generated when it is used the (μ) in the *CWRU* database (easiest data to

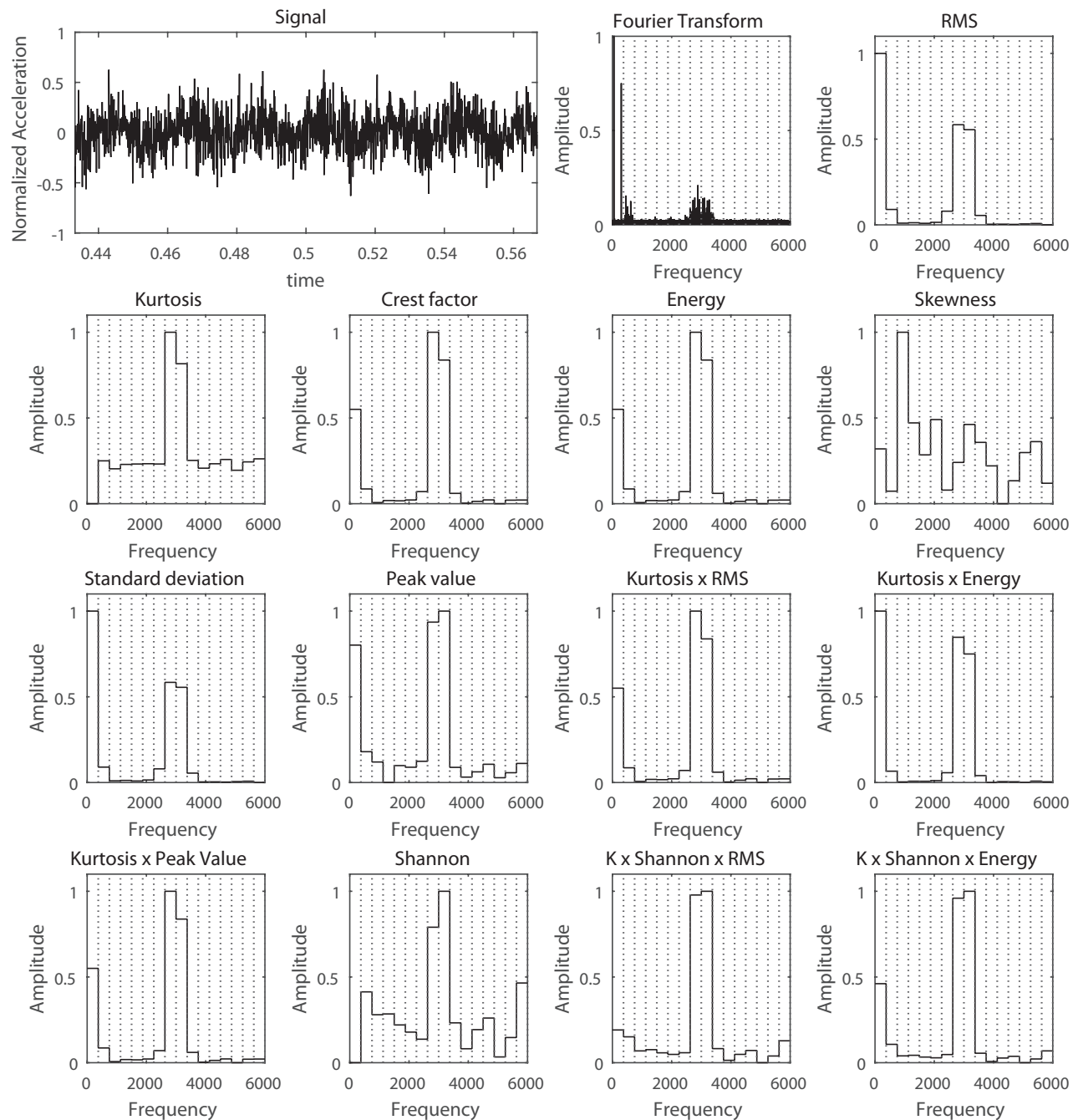


Figure C.14: Statistical parameter applied to an *IR* fault signal with a $SNR = 1$ and two sinusoidal signals of 300 Hz and 50 Hz

distinguish) follows the rule 80 20, where the 80% of the signal information is contained in the 20% of nodes, Table C.3:

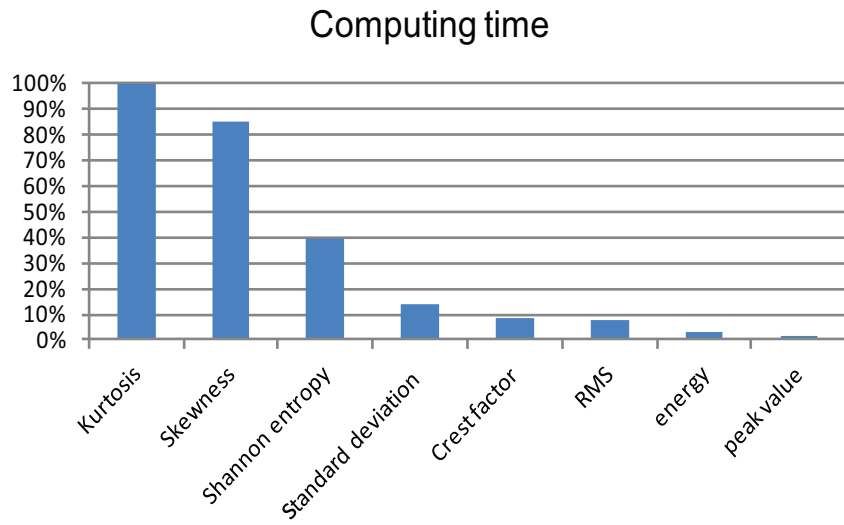


Figure C.15: Execution time of the different indicators

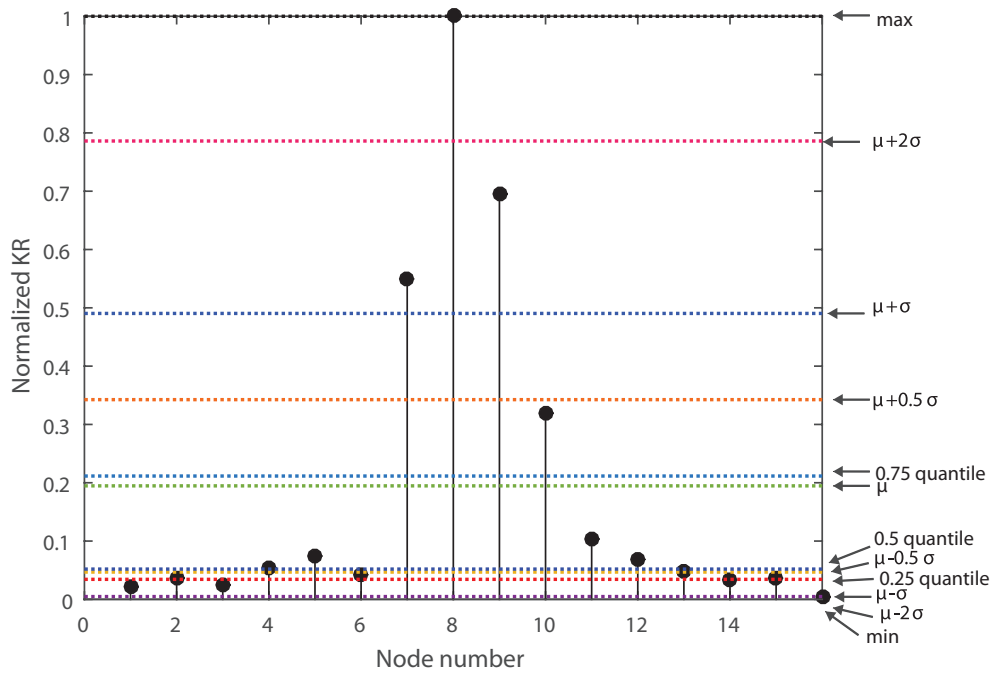


Figure C.16: Different thresholds applied to *OR* signal decomposition at 6th level

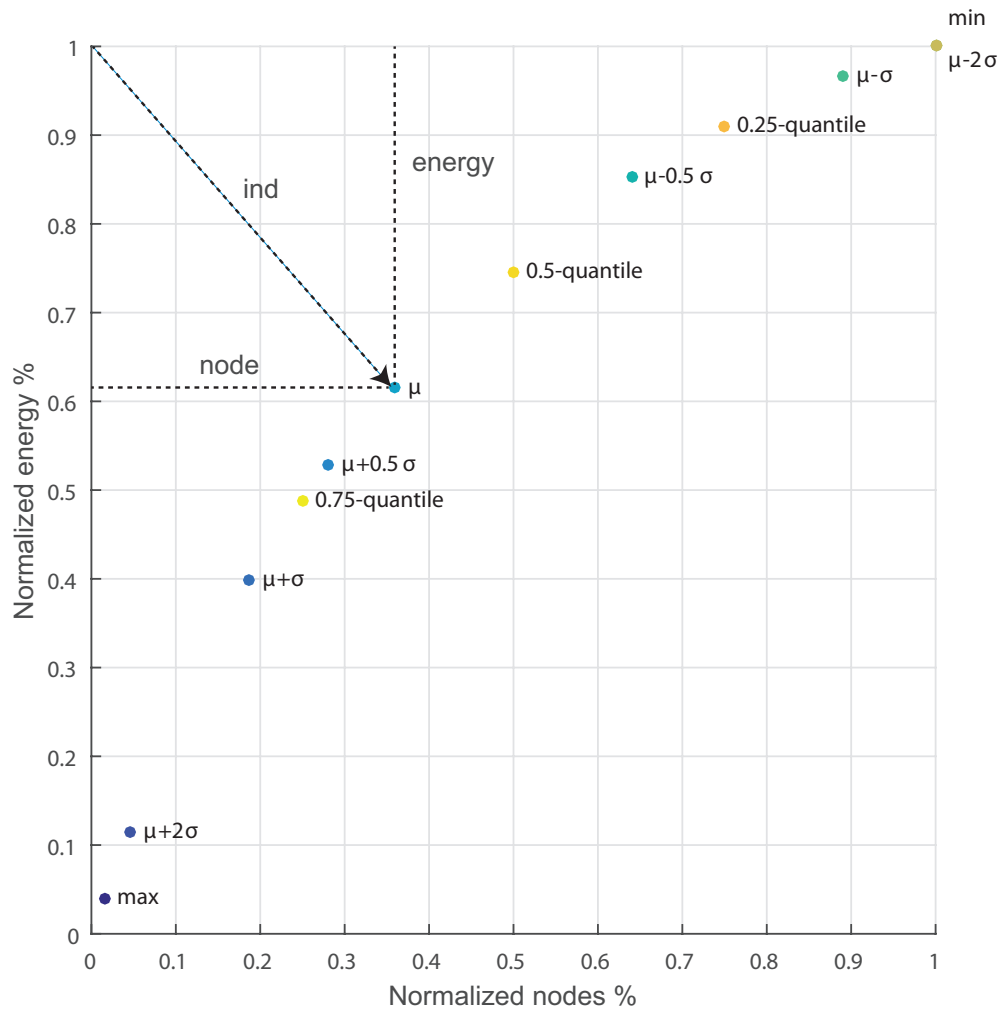


Figure C.17: Relation energy-node with different thresholds

Table C.2: Index (x) results for several thresholds and different signals

	<i>OR-IMS</i>	<i>IR-IMS</i>	<i>RE-IMS</i>	<i>OR-CWRU</i>	<i>IR-CWRU</i>	<i>RE-CWRU</i>
<i>max</i>	0.960	0.964	0.969	0.910	0.894	0.895
$\mu + 2\sigma$	0.886	0.878	0.890	0.766	0.518	0.441
$\mu + \sigma$	0.630	0.830	0.752	0.379	0.389	0.317
$\mu + 0.5\sigma$	0.548	0.712	0.672	0.345	0.363	0.295
μ	0.526	0.609	0.619	0.339	0.330	0.286
$\mu - 0.5\sigma$	0.657	0.693	0.707	0.523	0.703	0.688
$\mu - \sigma$	0.891	0.862	0.877	1.000	1.000	1.000
$\mu - 2\sigma$	1.000	1.000	1.000	1.000	1.000	1.000
<i>min</i>	1.000	1.000	1.000	1.000	1.000	1.000
0.25-quantile	0.755	0.765	0.766	0.750	0.750	0.750
0.5-quantile / median	0.561	0.618	0.625	0.509	0.507	0.504
0.75-quantile	0.570	0.675	0.683	0.338	0.333	0.303
BEST	μ	μ	μ	$Q_3 = \frac{3}{4}$	μ	μ

Table C.3: *Pareto* principle check for the *CWRU* database with the threshold average.

<i>Signal</i>	<i>Nodes %</i>	<i>Energy %</i>
OR- <i>CWRU</i> fault	0.265	0.788
IR- <i>CWRU</i> fault	0.218	0.751
RE- <i>CWRU</i> fault	0.1875	0.783

Appendix D

Additional Results

The purpose of this section is to show the results of all the analyzed signals, they are presented in two ways: in the first image the processed signal is shown with all the harmonics of the fault, the harmonics of the frequency of rotation and the fault sidebands, in the second image the signal will be presented with all these hidden values so it is easiest to appreciate only the analyzed fault.

In the Fig D.1 is observe a signal with RE fault, it was added lines in the expected shaft speed harmonics and sidebands of the fault. The light blue line correspond to the frequency fault, the green lines coincide with the shaft speed harmonics, the yellow lines fit with the sidebands and the sidebands of the RE spaced the cage frequency FTF are located under the red lines. As can be seen these values can affect the diagnose and therefore they are hidden, Fig D.2, only remains visible the frequency fault and its harmonics.

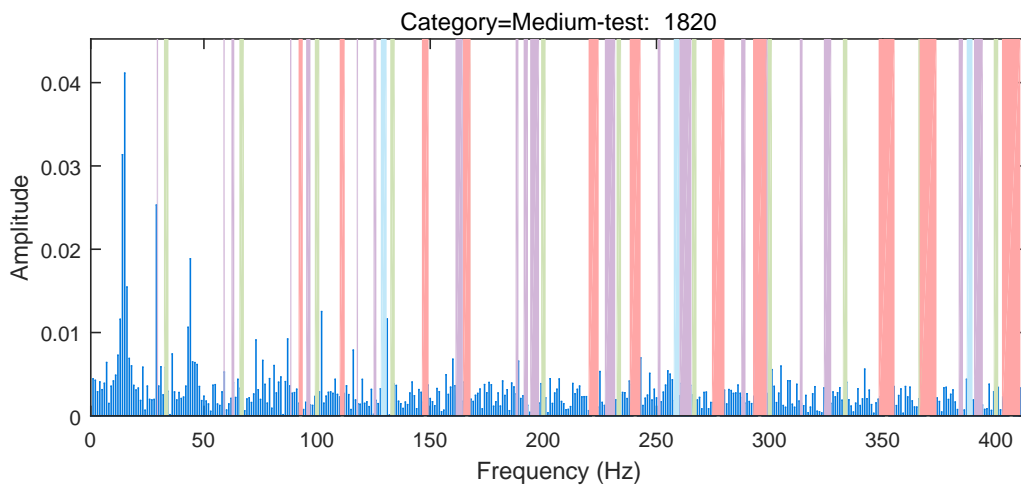


Figure D.1: Harmonics and sidebands location in an *IMS* signal with *RE* fault

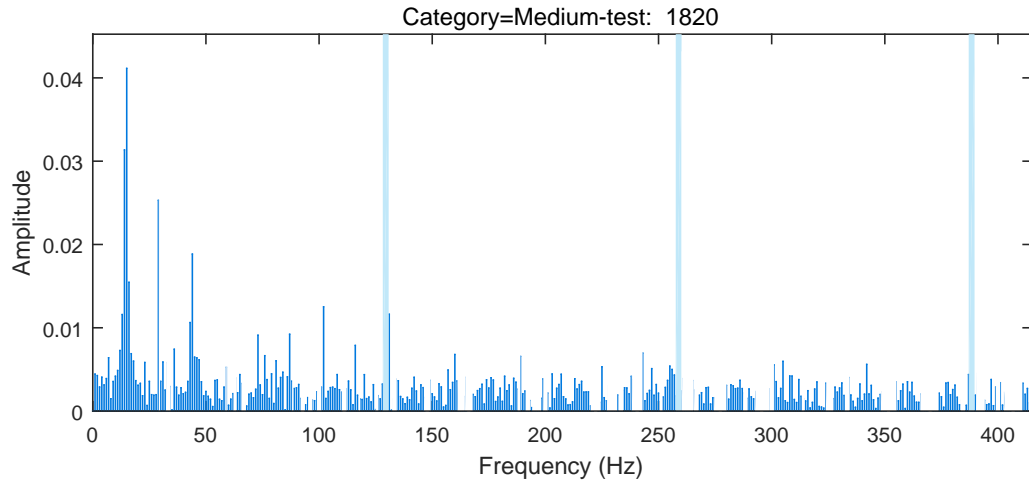
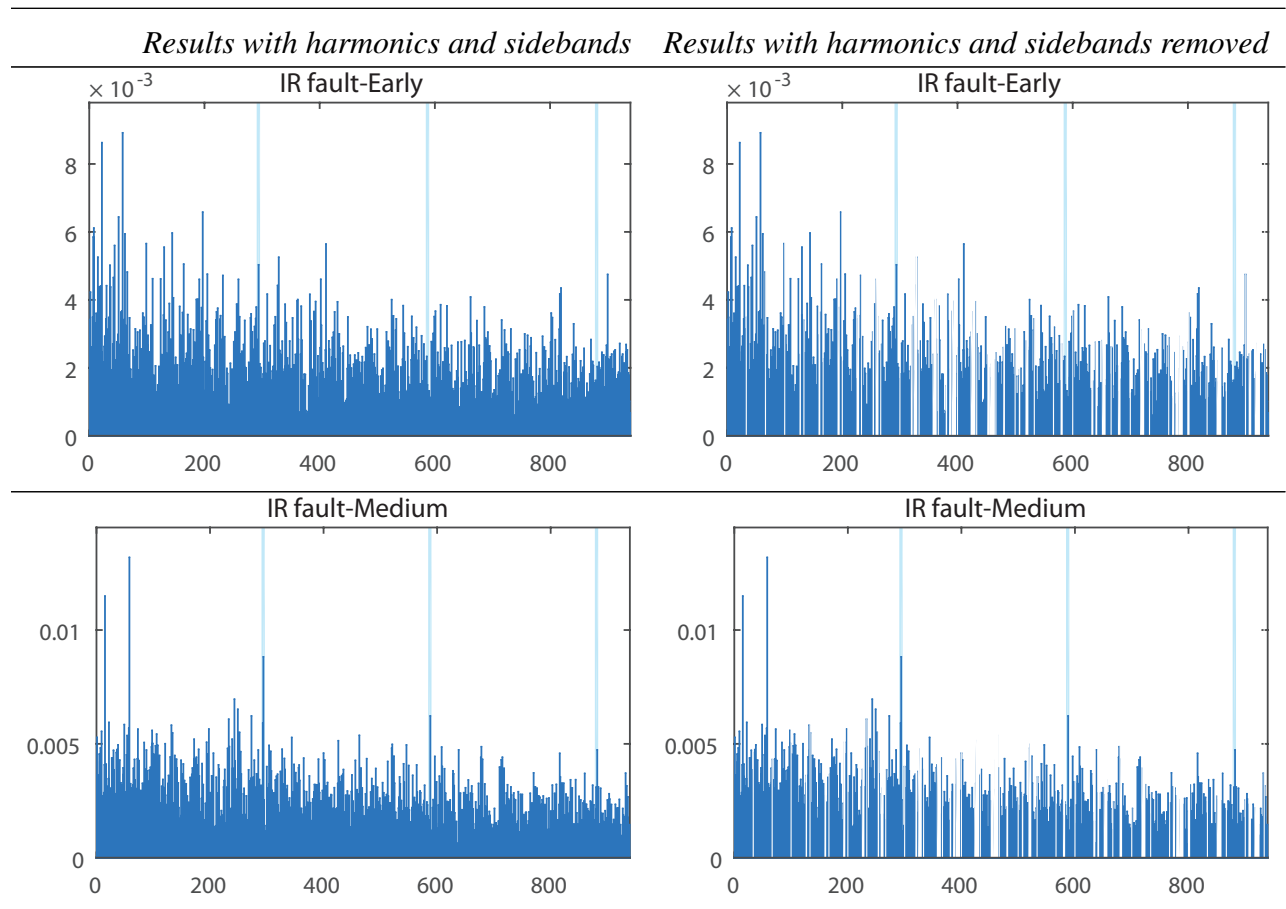
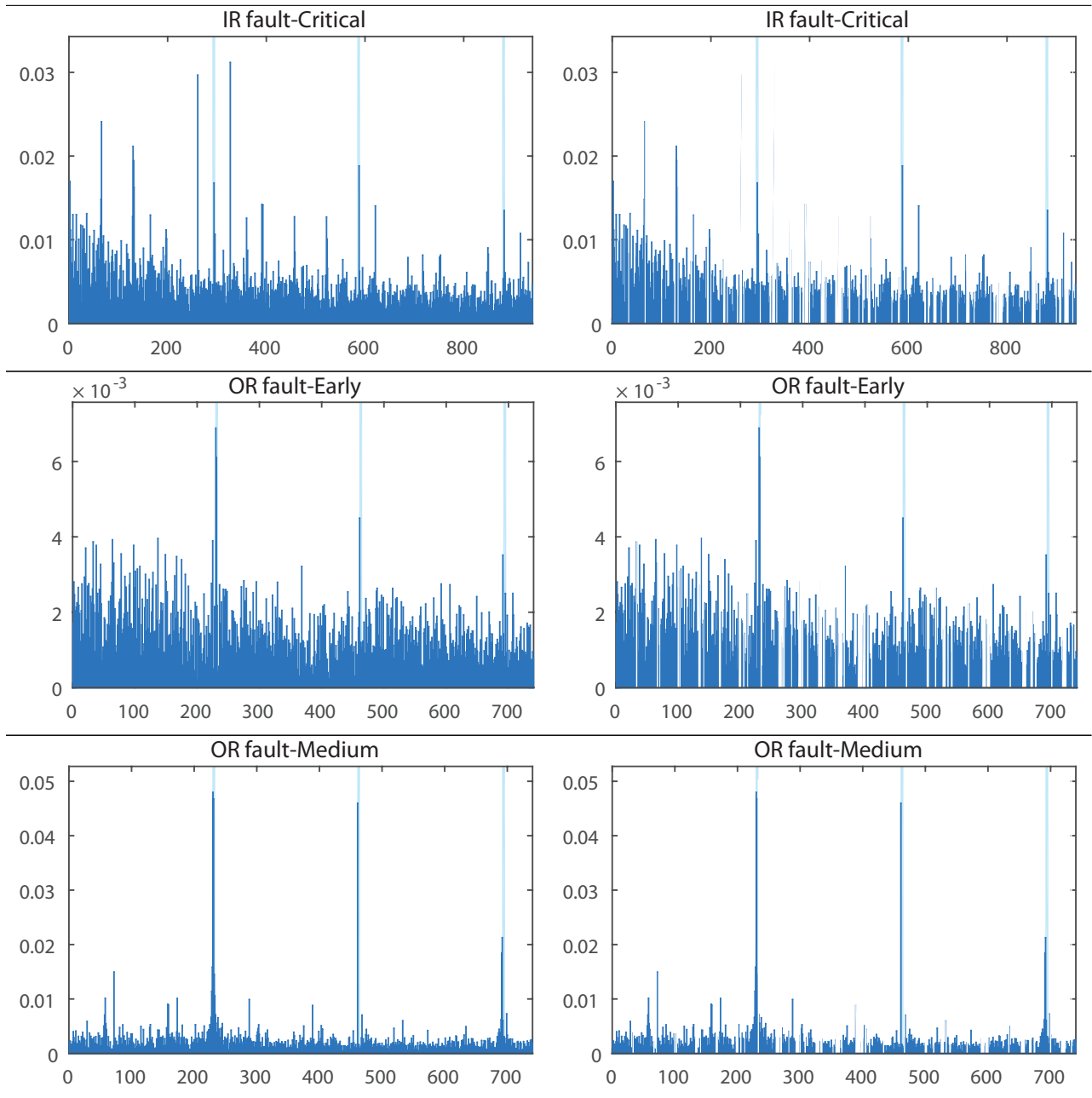
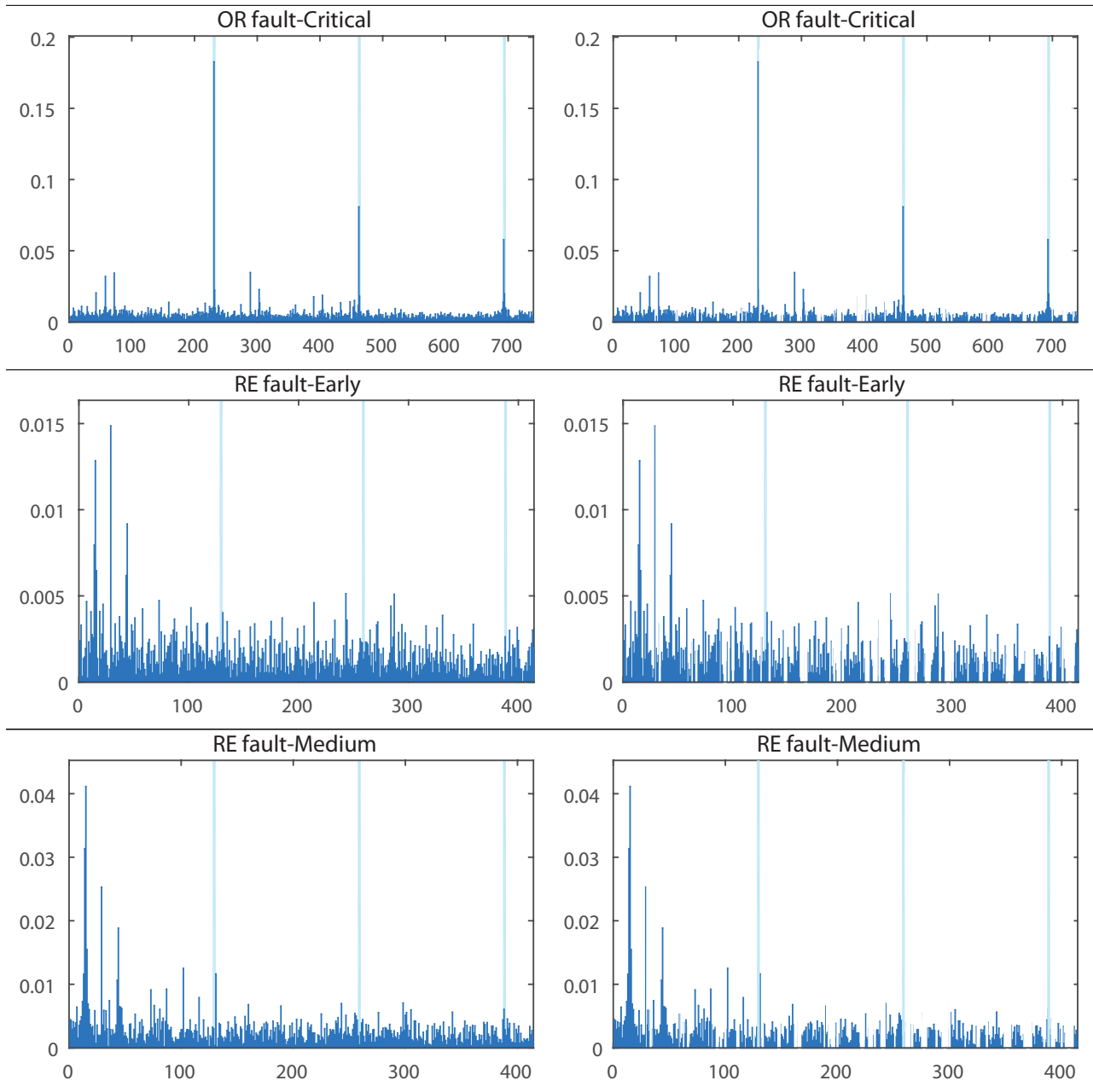


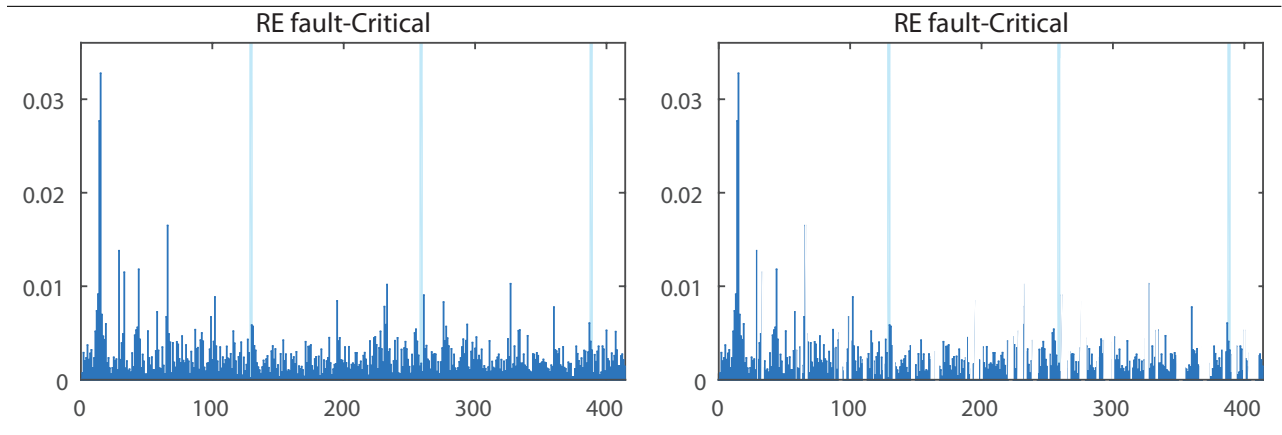
Figure D.2: Harmonics and sidebands hidden in an *IMS* signal with *RE* fault

D.1 *IMS* Data

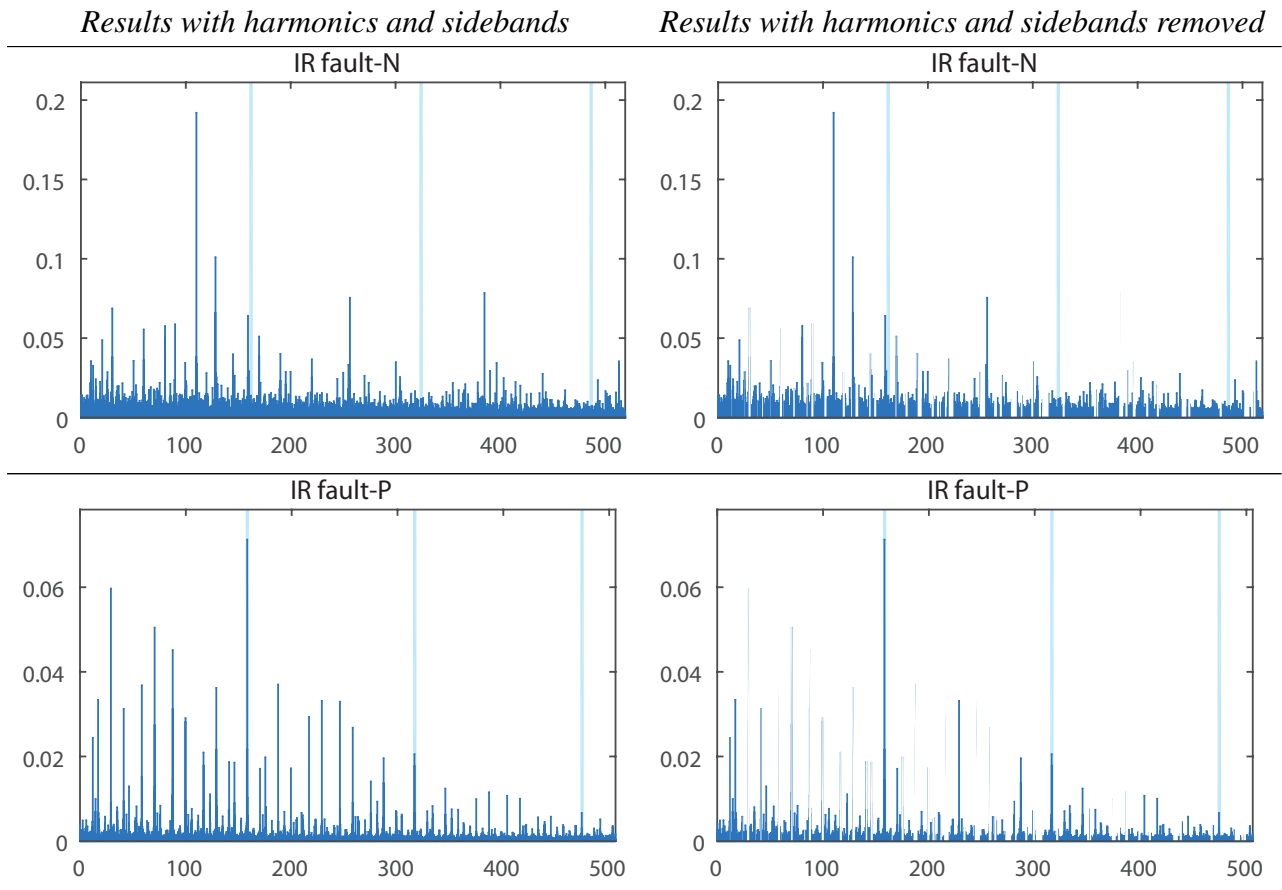


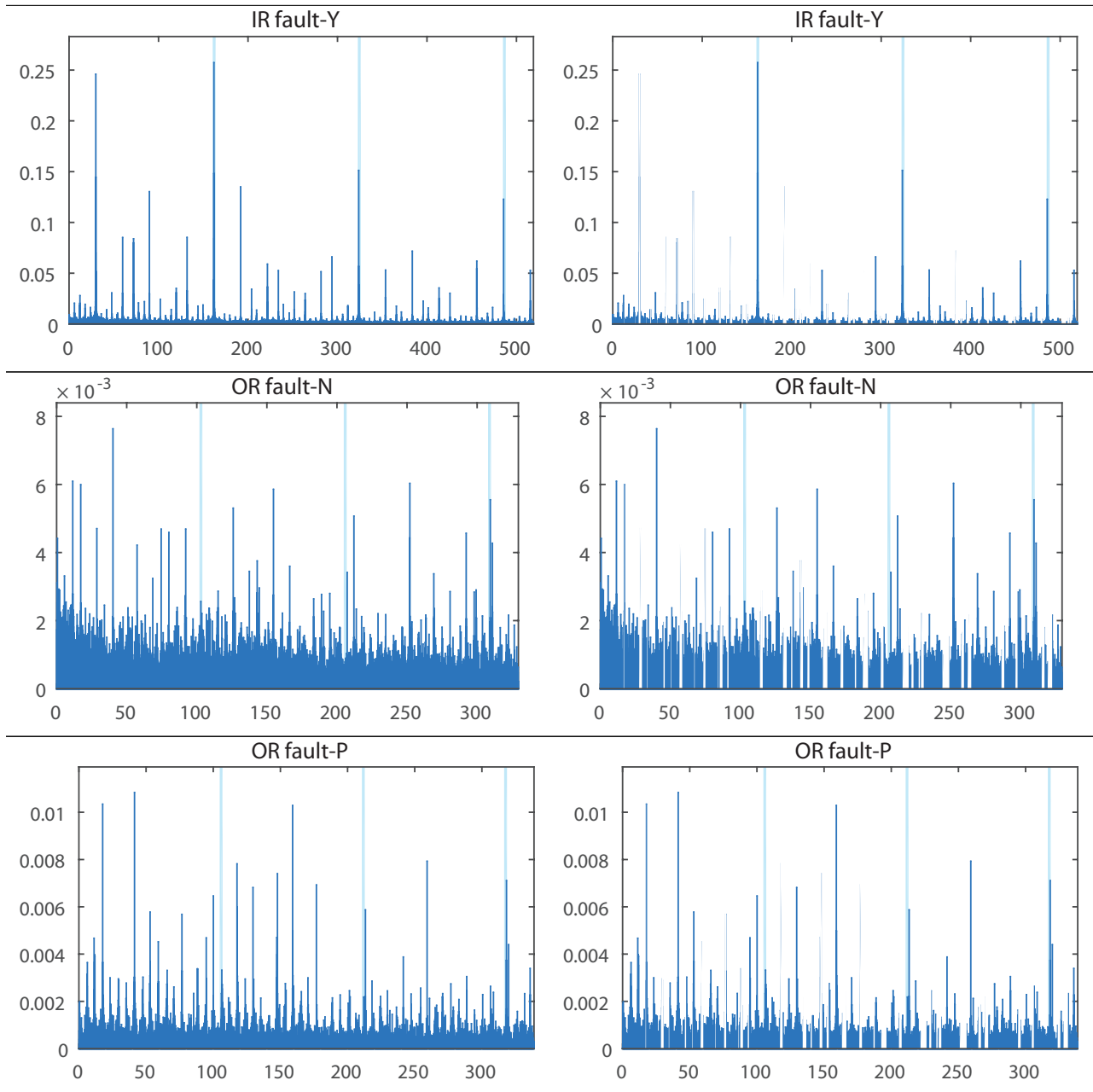


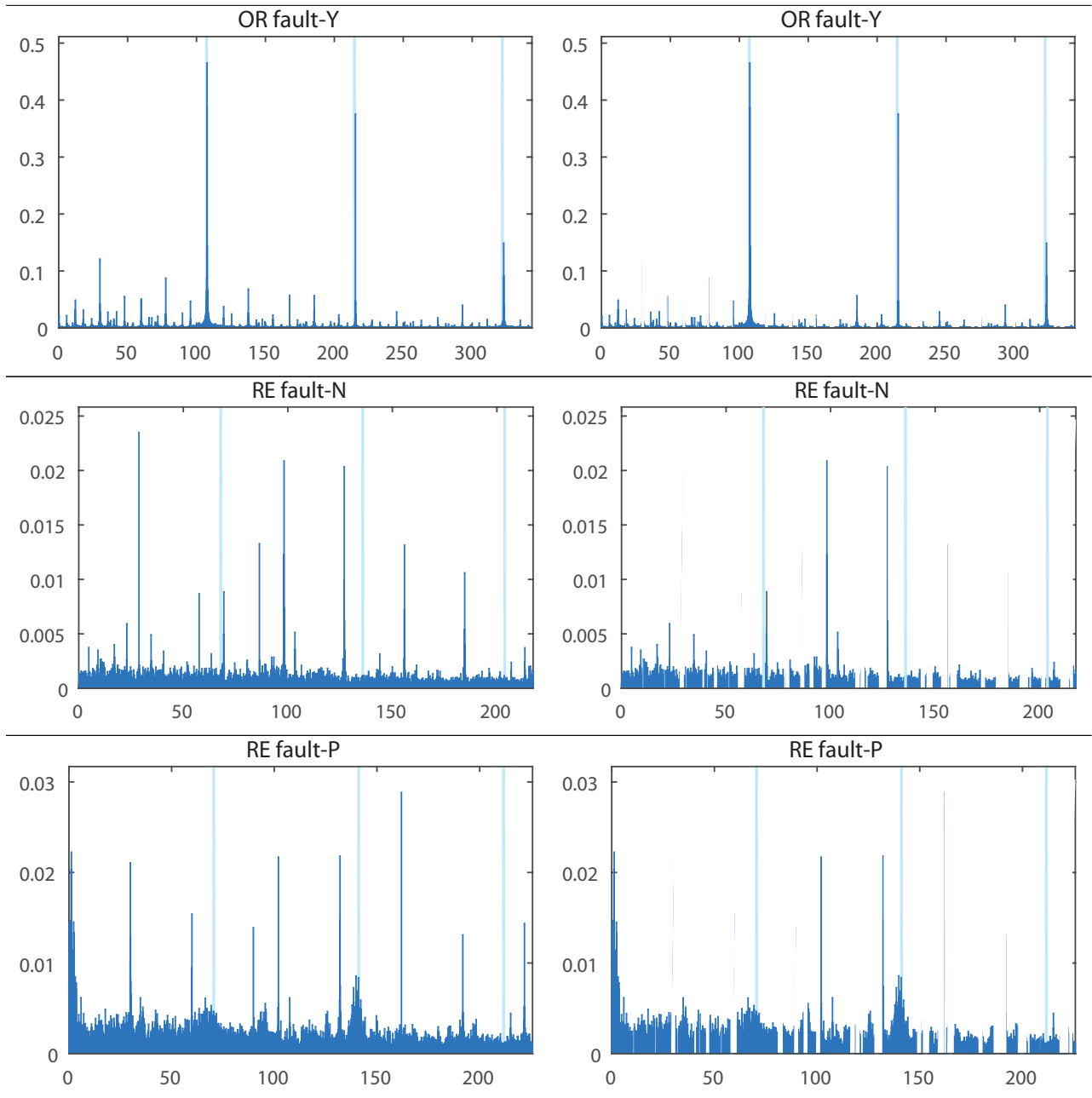


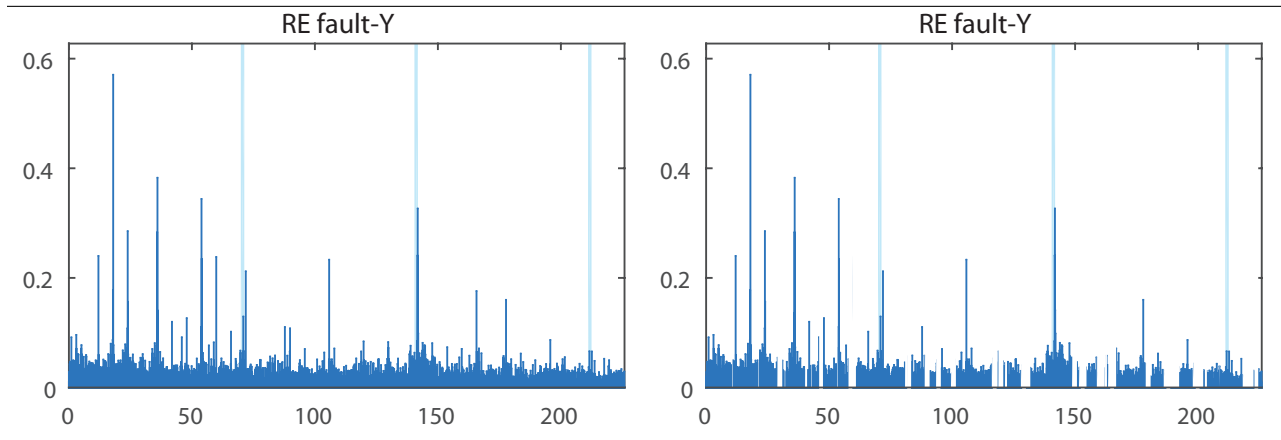


D.2 CWRU Data









Appendix E

Published papers

Tema A1b. Automatización y Control Mecánico y A2b. Manufactura

“Diagnóstico de Fallas en Husillos de Mecanizado de Alta Velocidad usando Onduletas – Estado del Arte”

Cristina Villagómez Garzón, George Batallas Moncayo, Diana Hernández-Alcántara, Antonio Jr Vallejo Guevara, David Ibarra-Zarate and Ruben Morales-Menendez
Tecnológico de Monterrey, Escuela de Ingeniería y Ciencias
Monterrey Nuevo León, México
Email: {A00819778, A01361945, dianahalc, avallejo, david.ibarra, rmm} @itesm.mx

RESUMEN

La detección y diagnóstico de fallas es una estrategia muy eficiente para dar mantenimiento y servicio en muchas industrias. Particularmente, en sistemas de mecanizado de alta de velocidad, la calidad de las piezas depende en buena parte del desempeño del husillo, donde los rodamientos representan los componentes mecánicos más vulnerables, estadísticamente el 30% de los paros de operación se debe a una falla en los rodamientos. Un sistema de detección y diagnóstico de fallas en rodamientos es una herramienta de competitividad industrial, no solo por evitar productos fuera de especificación, sino por evitar daños extremos. Se presenta una revisión bibliográfica de la investigación del uso de la Transformada de Onduletas para el análisis de vibraciones mecánicas que permitan la detección y diagnóstico confiables de fallas en rodamientos de husillos.

Palabras Clave: Detección, Diagnóstico, Fallas, Rodamientos, Husillos, Mecanizado.

ABSTRACT

Detection and fault diagnosis is a very efficient strategy for maintenance and service in many industries. Particularly in high speed machining systems, the quality of the parts is highly dependent on the performance of the spindle where the bearings represent the most vulnerable mechanical components; statistically, the 30% of breakdowns are due to bearing failures. A detection and fault diagnosis system in bearings is a tool of industrial competitiveness not only to avoid products out of specification; but to avoid extreme damages. A full review of the research about the use of Wavelet Transform for the analysis of mechanical vibrations that allow a reliable fault detection and diagnosis in spindle bearings is presented.

Keywords: Detection, Diagnosis, Failures, Bearings, Spindles, Machining.

1. Introducción

El monitoreo de la condición de una máquina, sistema o proceso es la manera más eficiente de administrar el mantenimiento en muchas industrias, ya que los ahorros económicos pueden ser excepcionales en muchos casos, sin considerar los daños materiales (y humanos) que se pueden evitar. El mantenimiento basado en la condición de una máquina o proceso que requiere operar continuamente, demanda de aplicaciones (algoritmos computacionales) que determinen o estimen la condición interna de la maquina mientras ésta se encuentre en operación.

En el caso de los sistemas de mecanizado de alta velocidad existen dos grandes alternativas para realizar esta tarea, el análisis de vibraciones y el análisis de lubricantes; siendo el estudio de las vibraciones el de mayor interés práctico.

Un centro de maquinado aun en condiciones normales tiene un cierto nivel de vibraciones, cuando se presenta una falla,

estas vibraciones cambian de tal manera, que pueden asociarse a dicha falla.

En este trabajo se presentarán algoritmos de detección y diagnóstico de fallas para husillos en centros de mecanizado de alta velocidad; aunque existen muchos enfoques y herramientas matemáticas, el estudio se limita al uso de la *Transformada de Onduletas (WT, Wavelets Transform)*. Se conservan los términos en inglés para evitar confusiones. La Tabla 1 resume los acrónimos utilizados.

Este artículo está organizado como se indica. La *Sección 2* describe el problema, mientras que la *Sección 3* presenta una revisión bibliográfica de los trabajos más importantes que se han publicado utilizando *WT*. La *Sección 4* ejemplifica este tipo de enfoque utilizando datos experimentales. Finalmente, la *Sección 5* concluye la investigación.

Monitoreo de Husillos usando la Transformada de Onduletas ^{*}

George Batallas Moncayo, Cristina Villagómez Garzón ^{*}
Diana Hernández Alcantara, Antonio Jr Vallejo Guevara ^{*}
David Ibarra Zarate and Ruben Morales-Menendez ^{*}

^{*} *Tecnológico de Monterrey, Escuela de Ingeniería y Ciencias
Monterrey NL, México, {A01361945, A00819778, dianahalc, avallejo,
david.ibarra, rmm}@itesm.mx*

Abstract: El diagnóstico y prevención de fallas ha permitido evolucionar las estrategias de mantenimiento en las industrias, mejorando la eficiencia y optimizando los paros en la producción. En el caso de los sistemas de mecanizado, el diagnóstico oportuno de fallas evita productos fuera de especificación y/o daños extremos. Un maquinado óptimo es altamente dependiente del desempeño y condición del husillo, dentro del cual los rodamientos representan los componentes mecánicos con más probabilidad de falla. A partir de una revisión bibliográfica exhaustiva, se presentan los avances en el uso de la Transformada de Onduletas para el análisis de vibraciones mecánicas de rodamientos en husillos. Adicionalmente, se propone una metodología para detectar y diagnosticar fallas en este tipo de aplicaciones.

Keywords: Diagnóstico fallas, Vibraciones, Husillos, Rodamientos, Onduletas

1. INTRODUCCIÓN

El monitoreo de la condición de una máquina, sistema o proceso es la manera más eficiente de administrar el mantenimiento. La economía del proceso puede ser excepcional. Para llevar a cabo un mantenimiento basado en la condición de una máquina en operación continua, se requieren algoritmos eficientes que determinen el estado interno en línea, mientras está operando.

Un centro de maquinado aún en condiciones normales presenta un cierto nivel de vibraciones. Cuando ocurre una falla, estas vibraciones se modifican y en ellas se puede encontrar el motivo del desperfecto. Este análisis puede realizarse utilizando diferentes herramientas matemáticas, una de las más usadas por su capacidad de manejar señales complejas gracias a su multiresolución es la *Transformada de Onduletas* (*WT*, *Wavelet Transform*). En la Tabla 1 se muestra un resumen todos los acrónimos utilizados en este artículo, se conservarán los términos en inglés por ser muy familiares y para evitar confusiones en su traducción.

La *WT* se asemeja a la *Transformada de Fourier* (*FT*, *Fourier Transform*) al descomponer una función con base a otras preestablecidas, mientras la *FT* utiliza senos y cosenos; la *WT* maneja como funciones base distintas onduletas. La *WT* está definida como:

$$F(a, b) = \int_{-\infty}^{\infty} f(x)\psi_{(a,b)}^*(x)dx \quad (1)$$

^{*} Los autores le agradecen al *Tecnológico de Monterrey* y al *CONAcYT* por sus apoyos parciales.

donde el ^{*} representa el conjugado complejo y la función $\psi(\dots)$ se selecciona de acuerdo a ciertas reglas de diseño.

La *WT* tiene beneficios en tiempo y frecuencia debido a su ventana modificable, seleccionando el tiempo mediante traslaciones y los rangos de frecuencia por medio de dilataciones. En el procesamiento de señales no estacionarias presenta un mejor rendimiento que los análisis tradicionales, Kankar et al. (2011) y Lauro et al. (2014). Además, a diferencia de la *FT*, tiene un conjunto infinito de funciones base, lo que hace que la *WT* sea muy versátil. Entre los beneficios intrínsecos de esta transformada están la reducción de ruido, la compresión de datos, filtrado, entre otros.

Este artículo está organizado en 5 secciones. En la *Sección 2* se describe el problema y en la *Sección 3* se presenta una revisión bibliográfica de los trabajos más importantes usando *WT*. La *Sección 4* ejemplifica la metodología desarrollada para la detección de fallas, y finalmente, la *Sección 5* concluye el trabajo.

2. DESCRIPCIÓN DEL PROBLEMA

La relación entre las señales de vibración y el estado de una máquina fueron inicialmente identificadas por Rathbone (1939), concluyendo que el efecto negativo era proporcional a la amplitud de la señal de vibración. Más tarde, en 1960 se vió que el monitoreo y análisis de la vibración podía prevenir dichos daños. Posteriormente, se empezaron a analizar las señales de vibración con técnicas como la *Transformada Rápida de Fourier* (*FFT*, *Fast Fourier Transform*) para buscar relaciones más claras o explícitas en problemas más complejos. Con el desarrollo de la era digital se mejoró la velocidad y capacidad de procesamiento en el área de detección, Randall (2011).

Appendix F

Developed Programs

For the developed methodology four *Matlab* functions were developed, two for plotting the scalograms, the first one in two dimensions and the second one in three dimensions; and two for processing the signals, one for bearing faults diagnosis and the other for shaft faults diagnosis. Parameters are shown in the following code:

```
1 % Loading signal
2 load DE12k_0_007_OR_C; Signal=X130_DE_time;
3
4 % Parameters
5 Level=6; % Level for WPT
6 MW='dmey'; % Mother Wavelet
7 fs=12000; % Sampling Frequency
8 RPM=2000; % Spindle Speed
9
10 % Decomposition: WPT (Matlab Toolbox)
11 Tree=wpdec(Signal,Level,MW);
12
13 % Scalogram Plots 2D y 3D
14 figure(1)
15 ScalogramWPT2D(Tree,fs)
16 figure(2)
17 ScalogramWPT3D(Tree,fs)
18
19 % Final signal after processing for bearing fault diagnosis
20 Fsignal=MetodologiaGBCV(Signal1,fs,'OR');
21
22 % Final signal after processing for shaft fault diagnosis
23 Fsignal_2=MetodologiaGBCV_2(Signal1,fs,RPM);
```

An scalogram can be plotted for any signal, the parameters needed are: the tree of the *WPT* and the sampling frequency. The tree is easily obtained with the *Matlab Toolbox* function: *wpdec* selecting the level of decomposition and the *MW*. An example is shown in Fig. F.1, for the 2D scalogram and in Fig. F.2 for the 3D scalogram.

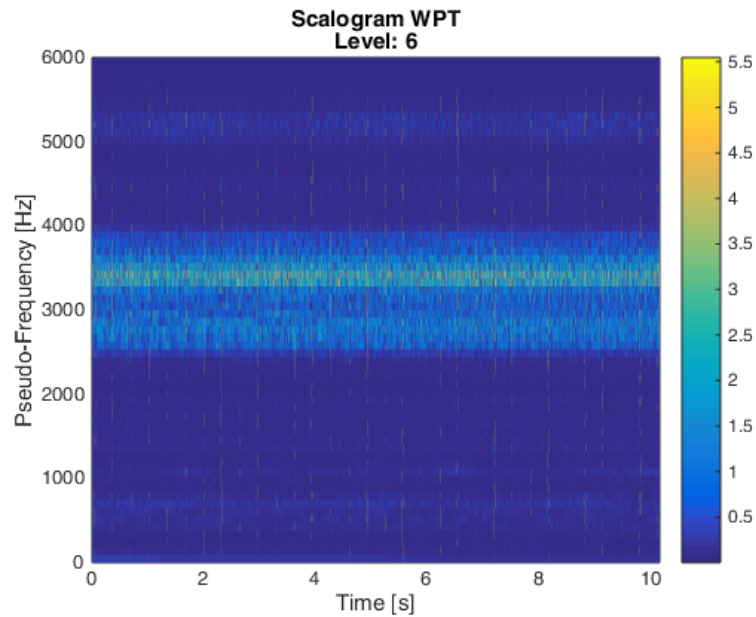


Figure F.1: *WPT* 2D scalogram function

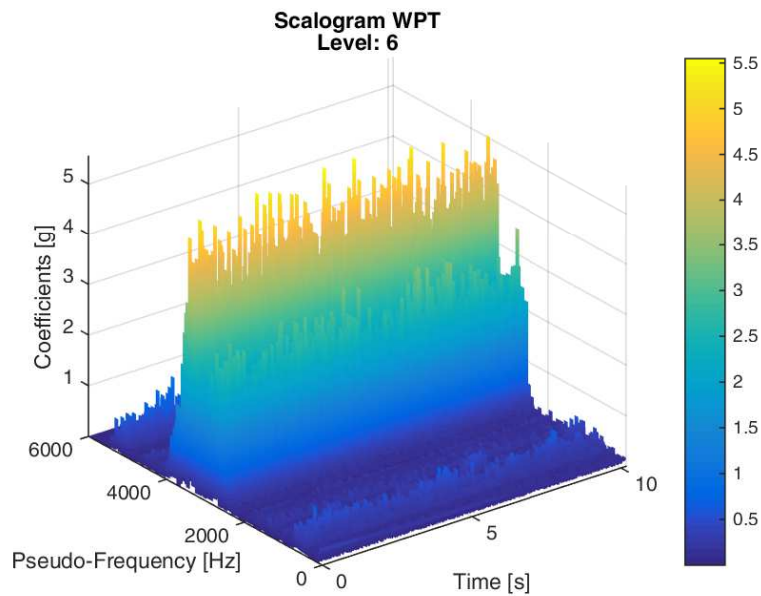


Figure F.2: *WPT* 3D scalogram function

The full development of the scalogram functions is shown below.

```

1 function ScalogramWPT2D(Tree , fs )
2 % -Tree:TreeWPT -fs:Sampling frequency
3 level=get(Tree , 'Depth' );
4 [SPEC ,TIMES ,FREQ ,TNFO] = wpspectrum(Tree , fs );
5 SPEC=flipud (SPEC);
6 FREQ1=0; SPEC1=[];
7
8 for i=1:length (FREQ)
9     FREQ1=vertcat (FREQ1,FREQ(i) );
10    FREQ1=vertcat (FREQ1,FREQ(i) );
11    SPEC1=vertcat (SPEC1,SPEC(i ,: ) );
12    SPEC1=vertcat (SPEC1,SPEC(i ,: ) );
13 end
14 FREQ1=FREQ1(1:length (FREQ)*2)';
15
16 pcolor (TIMES ,FREQ1 ,SPEC1); shading ('interp '); colorbar
17 xlabel ('Time [s] '); ylabel ('Pseudo-Frequency [Hz] '); zlabel ('Coefficients [g]')
18 title ({ 'Scalogram WPT' ;[ 'Level: ', num2str (level) ]})
19 axis tight

```

```

1 function ScalogramWPT3D(Tree , fs )
2 % -Tree:TreeWPT -fs:Sampling frequency
3 level=get(Tree , 'Depth' );
4 [SPEC ,TIMES ,FREQ ,TNFO] = wpspectrum(Tree , fs );
5 SPEC=flipud (SPEC);
6 FREQ1=0; SPEC1=[];
7
8 for i=1:length (FREQ)
9     FREQ1=vertcat (FREQ1,FREQ(i) );
10    FREQ1=vertcat (FREQ1,FREQ(i) );
11    SPEC1=vertcat (SPEC1,SPEC(i ,: ) );
12    SPEC1=vertcat (SPEC1,SPEC(i ,: ) );
13 end
14 FREQ1=FREQ1(1:length (FREQ)*2)';
15
16 surf (TIMES ,FREQ1 ,SPEC1); shading ('interp '); colorbar
17 xlabel ('Time [s] '); ylabel ('Pseudo-Frequency [Hz] '); zlabel ('Coefficients [g]')
18 title ({ 'Scalogram WPT' ;[ 'Level: ', num2str (level) ]})
19 axis tight

```

The functions developed for processing the signal based on the proposed methodology are presented below.

```

1 %% METHODOLOGY FOR BEARING FAULT DIAGNOSIS USING WPT
2 % By GEORGE BATALLAS & CRISTINA VILLAGOMEZ
3

```

```

4 function FilteredSignal = MetodologiaGBCV( Signal , fs , fault )
5 %\////////////////////////////////////
6 % Wavelet Parameters
7 %\////////////////////////////////////
8 WaveIR='db41';
9 WaveOR='dmey';
10 WaveRE='db45';
11 Nlevel=6;
12
13 %\////////////////////////////////////
14 % Signal Parameters
15 %\////////////////////////////////////
16 switch fault
17 case 'IR'
18     wavelet=WaveIR;
19 case 'OR'
20     wavelet=WaveOR;
21 case 'RE'
22     wavelet=WaveRE;
23 end
24
25 %\////////////////////////////////////
26 % Signal Preprocessing Trend Removal
27 %\////////////////////////////////////
28 time=0:1/fs :( length( Signal)-1)/ fs ;
29 fitness = fit( time , Signal , 'poly1' );
30 trend = fitness .p1*time+fitness .p2;
31 Signal=Signal-trend ;
32
33 %\////////////////////////////////////
34 % Wavelet Packet Decomposition and Best Tree
35 %\////////////////////////////////////
36 dwtmode( 'mode' );
37 T=wpdec( Signal , Nlevel , wavelet );
38 [SPEC , TIMES , FREQ] = wpspectrum( T , fs );
39 % BestTree
40 BT=besttree( T );
41 BTnodesN = leaves( BT ); BTnodesL = leaves( BT , 'dp' );
42 for i=1:length( BTnodesN )
43     FREQS( i )=BTnodesL( i , 2 )*( fs / 2 ) / ( 2 ^ BTnodesL( i , 1 ) );
44 end
45 FREQS=horzcat( FREQS( 2 : end ) , 6000 );
46
47 %\////////////////////////////////////
48 % Best Nodes Selection [ Kurtosis x RMS ]

```



```

11 %\////////////////////////////////////
12 % Shaft Speed and 5 SSHz harmonics
13 %\////////////////////////////////////
14 SSHz=RPM/60;
15 fcorte=ceil(SSHz*5);
16
17 %\////////////////////////////////////
18 % Signal Preprocessing Trend Removal
19 %\////////////////////////////////////
20 time=0:1/fs:(length(Signal)-1)/fs;
21 fitness = fit(time',Signal,'poly1');
22 trend = fitness.p1*time+fitness.p2;
23 Signal=Signal-trend';
24
25 %\////////////////////////////////////
26 % Wavelet Packet Decomposition and Cutoff Frequency
27 %\////////////////////////////////////
28 T=wpdec(Signal,Nlevel,wavelet);
29 [SPEC,TIMES,FREQ,TNFO] = wpspectrum(T,fs);
30 % Selecting first nodes 5 SSHz harmonics
31 if fcorte>FREQ(1)
32     cutF=find(FREQ<=fcorte,1,'last');
33 else
34     cutF=1;
35 end
36
37 %\////////////////////////////////////
38 % Reconstructed Signal only Low Frequencies
39 %\////////////////////////////////////
40 BSignal=0;
41 for i=1:cutF
42     BSignal=BSignal+wprcoef(T,TNFO(i));
43 end
44
45 %\////////////////////////////////////
46 % DC REMOVAL
47 %\////////////////////////////////////
48 fitness = fit(t',BSignal,'poly1');
49 trend = fitness.p1*t+fitness.p2;
50 BSignal=BSignal-trend';
51 BSignal=BSignal-mean(BSignal);
52
53 FilteredSignal=BSignal;

```

Curriculum Vitae



George Francisco Batallas Moncayo was born in Quito, Ecuador on October 4th, 1993. He received the degree of Mechatronics Engineer from the Tecnológico de Monterrey Campus Toluca, Toluca México in Dec 2015. He was part of the group of the Automotive Consortium, as member actively participated with the Bocar Group in the project named: MONITORING AND DIAGNOSIS OF *HSM* SPINDLES. He was accepted in the Master of Science in Manufacturing Systems program in the Tecnológico de Monterrey, Escuela de Ingeniería y Ciencias, Campus Monterrey.

This document was typed in using L^AT_EX by George Francisco Batallas Moncayo.